UNMANNED AERIAL REMOTE SENSING FOR ESTIMATING COTTON YIELD

A Dissertation

by

JEFFREY ALAN SIEGFRIED

Submitted to the Graduate and Professional School of
Texas A&M University
in partial fulfillment of the requirements for the degree of

DOCTOR OF PHILOSOPHY

Chair of Committee,	Nithya Rajan
Committee Members,	Curtis Adams
	Steve Hague
	Ronnie Schnell
	Robert Hardin
Head of Department,	David D Baltensperger

December 2021

Major Subject: Agronomy

ABSTRACT

Unmanned aerial systems (UAS) allow collection of imagery with unprecedented temporal, spatial, and spectral resolutions suitable for specialized purposes. Crop yield data is critical both for precision agriculture management purposes and crop breeding programs. However, collecting yield data at fine scales necessary for small plot research is labor-intensive. UAS could be leveraged to quantify yield variability while limiting labor requirements. Therefore, the objectives of this dissertation were to examine the relationship between cotton yield and derivatives from UAS multispectral and thermal infrared imagery and to determine optimal in-season timing of UAS flights for the strongest relationship with cotton yield. The experimental design was a 3x8 factorial within a completely randomized design arrangement with four repetitions and the study was conducted over four growing seasons (2017-2020). One treatment factor was three irrigation levels applied as a percentage of the estimated crop evapotranspiration (ET_c) requirement: 0%, 40%, and 80% ET replacement while the other factor was eight commercial cotton cultivars. UAS imagery was acquired at biweekly intervals to produce high resolution multispectral and thermal infrared orthomosaics. Normalized Difference Vegetation Index (NDVI), Normalized Difference Red Edge (NDRE), a pixel-based classification of cotton bolls termed Boll Area Index (BAI), and canopy temperature were derived from the orthomosaics and analyzed to determine suitability for cotton yield estimation. NDVI had a positive linear relationship with yield, which was strongest at approximately 1200 heat units (R^2 = 0.61, 0.78, 0.49, and 0.78 in 2017,

2018, 2019 and 2020, respectively). There were strong positive linear relationships between BAI and yield each year (R^2 = 0.61, 0.79, 0.67, and 0.73). Multiple linear regression using vegetation indices, boll area index, and/or canopy temperature from two flight dates produced better yield estimates (Adjusted R^2 = 0.79, 0.89, 0.84, and 0.81 for 2017, 2018, 2019 and 2020). Vegetation indices, BAI, and canopy temperature could differentiate variation among irrigation levels. Results suggest that derivatives from just two or three UAS flights presents a detailed dataset for cotton yield prediction while limiting labor, risk, requisite computational resources, and equipment wear.

ACKNOWLEDGEMENTS

I would like to thank my advisor, Dr. Rajan, for her support and the resources she provided during my graduate studies. I also appreciate the support and contributions of my committee, Drs. Curtis Adams, Steve Hague, Ronnie Schnell, and Robert Hardin.

Thank you to my friends and colleagues as well as the departmental faculty and staff for making my time at Texas A&M a good experience. I especially appreciate Bruno, Jennifer, and Philip for making these past few years of study more enjoyable.

I am very thankful for the support of my mother Patrice and my sisters Whitney and Hillary, who always offered encouragement and optimism during my studies. Without these three, none of this would have been possible.

CONTRIBUTORS AND FUNDING SOURCES

Contributors

This work was supervised by a dissertation committee consisting of Professors Nithya Rajan, Curtis Adams, Steve Hague, and Ronnie Schnell of the Department of Soil and Crop Sciences and Professor Robert Hardin of the Department of Biological and Agricultural Engineering. Data for 2017 was collected by Miles Mikeska and the Unmanned Aerial Systems team from Texas A&M Corpus Christi. Bruno Fontana assisted with field operations and data collection. All other work conducted for the dissertation was completed independently by the student.

Funding Sources

Graduate study was supported by Cotton Incorporated, a Merit Fellowship from Texas A&M University Association of Former Students, and the Mills Scholarship from Texas Water Resources Institute.

TABLE OF CONTENTS

Page

LIST OF FIGURES

Page

LIST OF TABLES

Page

1. INTRODUCTION

Seed cotton and lint yield data are valuable metrics for making management decisions in commercial cotton production, especially for precision agricultural purposes. Commercial yield monitors are the most prevalent method for quantifying variability at field scale. These yield monitors were a key advancement in precision agriculture technology because they provided fine spatial resolution yield measurements (Mulla, 2013).

However, adoption of cotton yield monitors has lagged behind adoption of grain yield monitors due to early issues in their accuracy and reliability (Vories et al., 2019). While adoption of cotton yield monitors has increased, this is primarily due to new cotton harvesting machinery sold with yield monitors as standard equipment (Nair et al., 2014). Unfortunately, farmers must purchase an unlock key to digitally enable the yield monitor. Some researchers suggest that monitors are collecting data that is never used, and it remains unclear whether farmers are leveraging it for management decisions (Ortiz & Duzy, 2016). While commercial yield monitor data in combination with fiber quality data has proven valuable for creating profit maps (Ge et al., 2011; Wanjura et al., 2015), they require careful cultivar-specific calibration (Vories et al., 2019). Regardless, yield monitor data is collected at the end of the growing season when it is only useful for the following season. Unmanned aerial systems (UAS) could uncover in-field spatial and temporal variability during the growing season and the data could be used in

combination with variable rate technology for in-season adjustment of crop inputs such as fertilizer, irrigation, plant growth regulators, and pesticides.

For crop breeders endeavoring to improve field performance of crops, yield data is useful for evaluating experimental lines in pedigree selection programs. This is especially true for early generations, where poor performing lines could be eliminated before costly harvesting and boll sampling. Yield estimates derived from UAS could potentially provide yield estimates for eliminating the worst performing lines, but accuracy may not be adequate for screening advanced lines. UAS are a cost-effective alternative to proximal systems which generally slowly collect datasets for high-throughput phenotyping purposes and increase field traffic.

UAS are now much more affordable for farmers (Sugiura et al., 2005) and they allow exceptional flexibility to choose ideal spatial, temporal, and spectral resolution based specifically on research or management objectives (Shi et al., 2016). These advantages have stimulated considerable interest in research for agronomy purposes. However, recent efforts related to UAS cotton yield estimation methods generally focus on segmenting techniques to isolate bolls in inexpensive red, green, and blue orthomosaics for quantifying yield after defoliation. These methodologies are not useful for in-season purposes, and the literature lacks thorough studies (i.e. across several growing seasons) into using high quality narrowband multispectral imagery to quantify yield during the growing season. Furthermore, very few researchers investigated yield estimation by including image products from both multispectral and thermal infrared cameras.

Therefore, this dissertation was divided into three chapters with the following objectives. For Chapter Two, the objectives were to 1) examine the relationship between in-season UAS-derived narrowband vegetation indices and cotton yield across irrigation regimes and time and 2) determine if heat unit accumulation can provide a physiological basis for optimizing the timing of UAS flights for in-season yield prediction. For Chapter Three, the objectives were to 1) determine the efficacy of a pixel-based multispectral image classification technique for cotton yield estimation and 2) develop a multiple linear regression model to enhance the accuracy of cotton yield estimates. Finally, the objectives for Chapter Four were to 1) evaluate infrared thermography for detecting differences in crop water stress across irrigation regimes and cotton cultivars 2) explore the relationship between UAS-derived canopy temperature and cotton yield across irrigation regimes, and 3) examine the relationship between soil moisture and UAS-derived canopy temperature.

1.1. References

Ge, Y., Thomasson, J. A., & Sui, R. (2011). Wireless-and-GPS system for cotton fiber-quality mapping. *Precision Agriculture*, 13(1), 90-103. https://doi.org/10.1007/s11119-011-9225-6

Mulla, D. J. (2013). Twenty five years of remote sensing in precision agriculture: Key advances and remaining knowledge gaps. *Biosystems Engineering*, 114(4), 358-371. https://doi.org/10.1016/j.biosystemseng.2012.08.009

Nair, S., Wang, C., Segarra, E., Wang, Y., & Johnson, J. (2014, January 6-8). Precision Agriculture Adoption by Texas Cotton Producers: Trends and Drivers. *Beltwide Cotton Conferences*, New Orleans, Louisiana.

Ortiz, B. V., & Duzy, L. M. (2016). Adoption of precision agriculture technology in the Southeastern United States. *Crops & Soils*, 49(6), 4-9.

Shi, Y., Thomasson, J. A., Murray, S. C., Pugh, N. A., Rooney, W. L., Shafian, S., Rajan, N., Rouze, G., Morgan, C. L., Neely, H. L., Rana, A., Bagavathiannan, M. V., Henrickson, J., Bowden, E., Valasek, J., Olsenholler, J., Bishop, M. P., Sheridan, R., Putman, E. B., Popescu, S., Burks, T., Cope, D., Ibrahim, A., McCutchen, B. F., Baltensperger, D. D., Avant, R. V., Jr., Vidrine, M., & Yang, C. (2016). Unmanned Aerial Vehicles for High-Throughput Phenotyping and Agronomic Research. *PLoS One*, 11(7), e0159781. https://doi.org/10.1371/journal.pone.0159781

Sugiura, R., Noguchi, N., & Ishii, K. (2005). Remote-sensing Technology for Vegetation Monitoring using an Unmanned Helicopter. *Biosystems Engineering*, 90(4), 369-379. https://doi.org/10.1016/j.biosystemseng.2004.12.011

Vories, E. D., Jones, A. S., Meeks, C. D., & Stevens, W. E. (2019). Variety Effects on Cotton Yield Monitor Calibration. *Applied Engineering in Agriculture*, 35(3), 345-354. https://doi.org/10.13031/aea.13144

Wanjura, J. D., Barnes, E. M., Kelley, M. S., & Boman, R. K. (2015). Harvesting. In *Cotton* (pp. 571-608). https://doi.org/10.2134/agronmonogr57.2013.0047

2. UAS-DERIVED VEGETATION INDICES FOR IN-SEASON COTTON YIELD PREDICTION

2.1. Introduction

Yield data is an important metric for plant breeding to assess genetic diversity and traits that contribute to improving field performance of experimental genotypes. Collecting yield data along with fiber samples from machine harvesters is labor-intensive for cotton breeding programs where many small plots are harvested, weighed, and ginned individually. UAS could increase the efficiency of cotton breeding through rapid phenotyping of secondary traits (Maja et al., 2016; Pabuayon et al., 2019; Rutkoski et al., 2016; Sun et al., 2018; Thompson et al., 2020). UAS facilitate quick collection of dense datasets, especially when compared to proximal systems used for high-throughput phenotyping that take almost three hours to collect one hectare of data (Thompson et al., 2018). Accurate in-season yield estimates made using remote sensing, such as from an unmanned aerial systems (UAS) platform, could also reveal spatiotemporal yield variability during the growing season for precision agriculture management to optimize crop production through more efficient distribution of irrigation water, fertilizer, plant growth regulators, and other inputs.

Researchers have explored methods for estimating cotton yield with remote sensing for over twenty years. Early efforts began with proximal measurements from handheld sensors (Ansari et al., 1999), while recent efforts have focused on using high spatial resolution imagery captured with UAS. Leon et al. (2003) found correlations

between cotton yield and common vegetation indices derived from aerial multispectral imagery. In their study, correlation coefficients (R) between Normalized Difference Vegetation Index (NDVI) and lint yield ranged from 0.23 to 0.87 across two sites in 1999 and 2000, while the best model coefficient of determination ($R^2 = 0.76$) selected by stepwise regression was at 105 days after planting. They identified the better timing for determining variability in cotton growth as between first bloom and first open boll, but this was based on only two image acquisition dates from each site-year for the yield analysis. More flights would be necessary to determine optimal timing. Leon et al. (2003) also noted that correlations were not consistent over multiple dates within each growing season. Huang et al. (2013) observed similar correlations ($R^2 = 0.47$) between yield and Ratio Vegetation Index (RVI) calculated from manned airborne multispectral imagery of a cotton field with irrigation and nitrogen treatments. The highest correlations with lint yield were at peak bloom and soil electrical conductivity measurements improved yield estimation ($R^2 = 0.53$), but measures of error were not reported. Read et al. (2003) concluded that plant height, leaf area index, and lint yield were closely related to NDVI maps and near infrared reflectance acquired from either aircraft or proximal sensors.

Yang et al. (2004) investigated the relationship between airborne hyperspectral imagery captured at maximum canopy cover and cotton yield data generated from an optical yield monitor installed on a four-row cotton picker. The hyperspectral system had 128 bands between 457 to 922 nm, a bandwidth of 3.63 nm, and the resulting image had a spatial resolution of 1.3 m. They observed that narrowband vegetation indices

explained yield variability better than broadband indices and individual bands. Correlation coefficients between yield monitor data and the narrowband indices ranged from 0.32 to 0.68 over the two cotton fields in the one-year study. Zarco-Tejada et al. (2005) used hyperspectral data from an airborne flight to estimate cotton yield using narrowband vegetation indices, which performed slightly better than broadband NDVI. They also observed that vegetation indices related to leaf-area index and canopy structure, such as Renormalized Difference Vegetation Index (RDVI) and Optimized Soil-Adjusted Vegetation Index (OSAVI), had the strongest relationships with yield earlier in the growing season. At later growth stages (i.e. closer to harvest) the best relationships were from hyperspectral indices closely related to crop physiological status, such as Modified Chlorophyll Absorption Index (MCARI) which was designed to maximize sensitivity to chlorophyll concentration while limiting the effects of soil reflectance and non-photosynthetic materials (Daughtry et al., 2000). The aforementioned studies were generally limited by the technology of their time. Coarse spatial resolution and a limited number of flights were inadequate for exploring vegetation indices as potential tools for cotton breeding and precision agriculture.

Recent efforts related to remote sensing for yield estimation have focused on using high spatial resolution imagery captured with UAS. Researchers explored segmentation and classification techniques to isolate open cotton bolls in imagery from inexpensive red, green, and blue (RGB) cameras to estimate cotton yield (Feng et al., 2018; Huang et al., 2016; Maja et al., 2016; Yeom et al., 2018). The model R^2 values ranged from 0.78 to 0.83 for these techniques that produced imagery with 0.6 to 3.4 cm

ground sampling distance (GSD). The authors noted some problems with accuracy caused by variable lighting conditions such as clouds, shadows, and bright soil but the root mean squared error ranged from about eight percent to 19 percent. These methodologies require imagery captured after defoliation and are not useful for in-season management.

Researchers then began investigating cotton yield estimation using imagery from two or more cameras. Feng et al. (2020) used a modified RGB camera to capture near-infrared, red, and green images with bandwidths of 80, 80, and 50 nm, respectively, and a GSD of 1.6 cm. They also collected imagery using an unmodified RGB camera (2.6 cm GSD) and thermal camera (6.8 cm GSD) for modeling crop yield with multiple image-derived features. The models had R^2 values up to 0.94 and RMSE ranged from 164 to 362 kg ha^{-1} (7 - 14%). While adjusted R^2 was not reported, Akaike's Information Criterion (AIC) was used to evaluate model complexity. The seed cotton yield estimation model they suggested was optimal based on accuracy (RMSE = 194 kg ha^{-1}) and cost included both plant height and the a* channel from the CIE 1976 L*a*b* (CIE-Lab) color space. Plant height estimates were calculated from the digital surface model (DSM) of the canopy and the closest bare soil surface within each plot. While this requires only one flight, a major disadvantage of this methodology is that it requires visible bare soil within the plot boundary or region of interest, which is not available when the canopy closes. Otherwise, interpolation methods to estimate the soil surface become an additional source of error. As an alternative, a digital terrain model (DTM) could be generated from an additional flight immediately following planting to obtain a

baseline surface to later subtract from the DSM to estimate plant height, but this requires an additional flight during a busy time. This method relies on accurate, repeatable 3D georeferencing, which is not always available. Feng et al. (2020) also noted that cotton yield estimation may be affected by growth stage.

Ashapure et al. (2020) used a combination of canopy features derived from RGB and multispectral UAS imagery to determine how early in the growing season a machine learning model could accurately predict cotton yield with canopy volume, Excess Green Index, and irrigation status as the input variables. They found that an artificial neural network model had reasonable accuracy as early as 70 days after planting ($R^2 = 0.72$). While the authors included many flights for analysis, these 30 flights were collected from only one growing season. Furthermore, the multispectral camera had very large bandwidths of 100, 300, and 160 nm for the green, red, and near-infrared channels, respectively.

Remote sensing studies using UAS for in-season cotton yield estimation generally have not included multispectral imagery from higher quality narrowband cameras with discrete sensors, global shutters, and irradiance sensors that can be used to correct for variable lighting conditions (e.g. clouds). Furthermore, information about cotton yield estimation using in-season imagery alone and associated ideal timing for UAS flights is sparse. While researchers previously established the link between narrowband vegetation indices and cotton yield, they were limited to proximal sensing or a small number of manned flights within a growing season. Very few explored vegetation indices for agronomic treatment comparisons, and the literature lacks more

thorough investigations using imagery with the fine spatial resolution achievable with UAS. Therefore, the objectives of this study were to 1) examine the relationship between in-season UAS-derived narrowband vegetation indices and cotton yield across irrigation regimes and time and 2) determine if heat unit accumulation can provide a physiological basis for optimizing the timing of UAS flights for in-season yield prediction.

2.2. Materials and Methods

2.2.1. Study Site

This experiment was conducted over the 2017, 2018, 2019, and 2020 cotton growing seasons in a 3 ha field at the Texas A&M University research farm near College Station, Texas (30.550° N, 96.436° W). The field has been managed with conventional tillage and subsurface drip irrigation for more than 10 years. The predominant soil series at the site is Belk clay, which is classified as a fine, mixed, active, thermic Entic Hapluderts (Soil Survey Staff, 2021) and has a slope of less than one percent. The climate is humid subtropical with an average annual precipitation of about 1018 mm and temperature of 20.6˚C (Menefee et al., 2020). Weather data was logged at 15-minute intervals from a station installed adjacent to the study site and daily averages were used for subsequent analysis.

2.2.2. Experimental Design and Cultural Practices

For all four growing seasons, the experimental design was a 3x8 factorial arranged within a completely randomized design and had four repetitions. There were three irrigation levels, which were applied as a percentage of the estimated crop evapotranspiration (ETc) requirement at 80% (irrigated), 40% (deficit irrigated), and 0%

(dryland). The only exception was 2017, during which irrigation was applied at 90%, 45%, and 0% of the ETc requirement. Crop evapotranspiration was estimated based on the FAO Penman-Monteith method using weather data from the study site and crop coefficients for upland cotton in Texas. For details on the methodology for calculating crop water requirements, see Allen et al. (1998). There were eight commercial cotton cultivars planted per season (Table 2.1). Raised beds with 1 m spacing were prepared in December or January, and cotton was planted in April on beds into four-row plots. Each plot was 12 meters in length.

Table 2.1. Cotton cultivars planted in 2017 to 2020. Maturity between Early to Full refers to least determinate growth to most indeterminate growth habit, respectively.

Year	Cultivar	Maturity
2017, 2018	Deltapine 1549 B2XF	Medium-Full
2017 - 2020	Deltapine 1646 B2XF	Medium-Full
2017, 2018	FiberMax 1900 GLT	Early-Medium
2017, 2018	FiberMax 2484 B2F	Medium
2017, 2018	NexGen 1511 B2RF	Medium
2017, 2018	Phytogen 333 WRF	Early
2017, 2018	Phytogen 499 WRF	Medium
2017, 2018	Stoneville 4946 GLB2	Early-Medium
2019	Deltapine 1835 B3XF	Medium
2019, 2020	Deltapine 1845 B3XF	Medium-Full
2019, 2020	FiberMax 2398 GLTP	Medium
2019	Phytogen 350 W3FE	Early-Medium
2019	Phytogen 480 W3FE	Medium
2019, 2020	Phytogen 580 W3FE	Full
2019, 2020	Stoneville 4550 GLTP	Early-Medium
2020	NexGen 4936 B3XF	Medium
2020	NexGen 5711 B3XF	Medium-Full
2020	Phytogen 400 B3XF	Medium

Cultural practices varied slightly in each growing season. Table 2.2 includes information about nitrogen fertilizer, plant growth regulator, and defoliant applications along with planting and harvest dates. Weed control included pre-emergence herbicides and over-the-top glyphosate applications when necessary. Urea-ammonium nitrate fertilizer (32-0-0) was knifed-in either prior to planting or shortly after at rates based on yield potential and composite soil sampling. Mepiquat chloride was applied at labeled rates when needed to limit rank growth, and irrigation was suspended when cutout was reached in the 80% ET_c treatment. Chemical defoliants were applied when the irrigated treatment reached at least 60% open boll. To mitigate potential edge effects, only the two interior rows of each four-row subplot were harvested using a 2-row spindle picker retrofitted with an onboard scale to measure seed cotton yield by mass. Cotton stalks were shredded after harvest each year and residue was incorporated via vertical tillage.

Table 2.2. Summary of cultural practices and timing for each cotton growing season.

Year	Planting	Nitrogen (kg ha^{-1})	Plant Growth Regulator	Defoliation	Harvest
2017	April 28	112 on 3/30 112 on 6/20	6/15 7/16	10/2	10/26
2018	April 12	112 on 5/22	6/27	9/6	9/18
2019	April 24	112 on 5/29	7/11	9/24	10/3
2020	April 16	112 on 4/9	---	9/29	10/5

2.2.3. Unmanned Aerial System and Image Acquisition

A MicaSense RedEdge-3 (MicaSense, Seattle, Washington) multispectral camera was fixed to a DJI Matrice 100 quadcopter (SZ DJI Technology Company Limited, Shenzhen, China) with a pitched mount to maintain nadir view during forward flight.

Camera specifications are presented in Table 2.3. The quadcopter was upgraded with a dual battery compartment to ensure it could cover the entire study area in a single flight (Figure 2.1). Using UgCS flight control software (SPH Engineering, Riga, Latvia), photogrammetry missions were flown about every two weeks at 30 m above ground level (AGL) to produce a 2 cm ground sampling distance (GSD) for all image dates except for 2017, which were ~1.3 cm from about 20 m AGL. Optimal weather, such as sunny conditions and minimal wind between around 12:30 - 14:30 (near solar noon), were prioritized to ensure quality image capture. Direct georeferencing was used in 2017 and 2018, but permanent ground control points were installed in 2019 and surveyed using a Reach RS+ Global Navigation Satellite System receiver (Emlid Limited, Hong Kong, China) with Trimble VRS real-time kinematic corrections (Trimble Navigation Limited, Sunnyvale, USA).

Table 2.3. Sensor characteristics for the MicaSense RedEdge-3 multispectral camera.

Band Name	Center Wavelength (nm)	Bandwidth/FWHM (nm)
Blue	475	20
Green	560	20
Red	668	10
Red Edge	717	10
Near Infrared	840	40

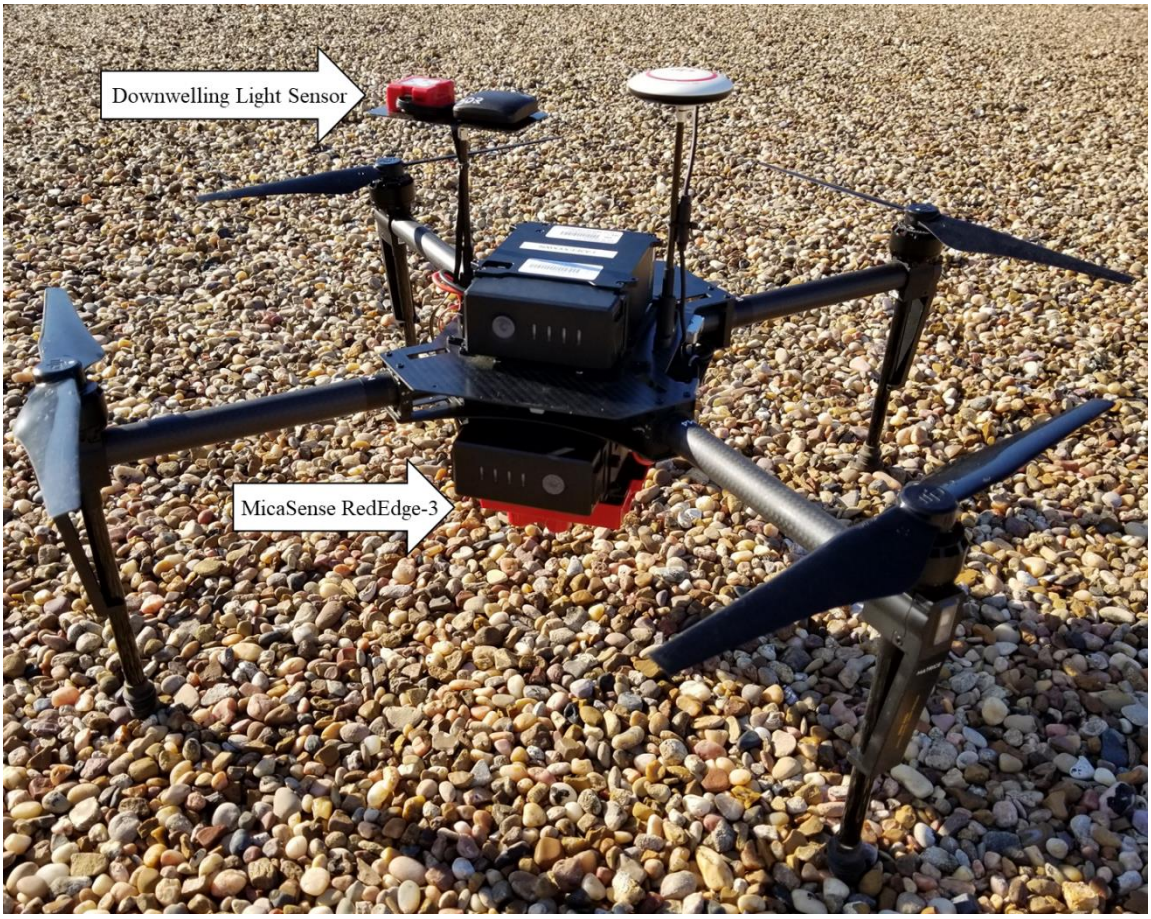

Figure 2.1. MicaSense RedEdge-3 multispectral camera payload attached via fixed mount to the DJI Matric 100 quadcopter. The Downwelling Light Sensor is attached above the aircraft on a mast.

2.2.4. Image Processing and Analysis

Figure 2.2 includes detailed information on flight parameters and the image processing workflow used in this study. Radiometric 16-bit TIFF imagery from the MicaSense RedEdge-3 was processed using structure from motion photogrammetry in Pix4Dmapper software (Pix4D S.A., Prilly, Switzerland) to generate orthomosaics. These orthomosaics were then calibrated to reflectance using the MicaSense calibration target, a panel with known reflectance values for which images were captured prior to and following each flight. NDVI and Normalized Difference Red Edge (NDRE) were calculated with the following equations:

$$NDVI = \frac{NIR - Red}{NIR + Red} \qquad \text{Equation 1}$$

$$NDRE = \frac{NIR - Red\ Edge}{NIR + Red\ Edge} \qquad \text{Equation 2}$$

Finally, average vegetation indices per plot were calculated using vector boundaries digitized in ArcMap (ESRI, Redlands, USA). Figure 2.3 shows an example NDVI orthomosaic and corresponding 2 row subplots from which averages were calculated. Solely to compare vegetation index values graphically for each season, all plots were averaged per treatment for all image dates and used to form line graphs similar to growth curves.

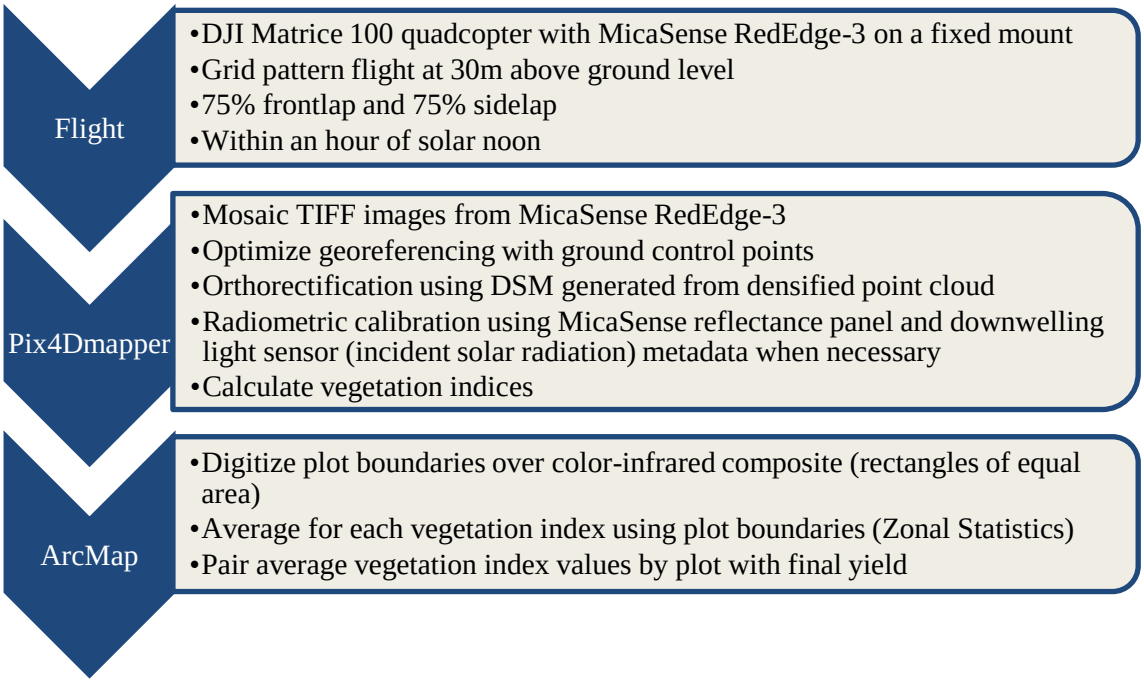

Figure 2.2. Flow chart summarizing the flight parameters and steps in the multispectral image processing workflow.

Analysis of variance (ANOVA) and linear regression analysis was conducted in R Studio (R Core Team, 2021) to examine treatment effects and the relationship between yield and vegetation indices for 28 UAS flight dates over 4 years. Tukey's Honest Significant Difference (HSD) tests were used for pairwise mean comparisons. Image acquisition dates were analyzed separately by year and separately by irrigation level to identify optimal in-season timing at which UAS-derived vegetation indices had the strongest linear relationship with seed cotton yield. Linear models were evaluated using R^2, root mean squared error (RMSE) and normalized RMSE (NRMSE). NRMSE was calculated by dividing RMSE by mean yield and multiplying by 100. Models were validated using the R caret package for k-fold cross validation with 10 folds repeated 10 times (Kuhn, 2021). To account for seasonal weather variation and to provide a more

universal and physiological basis for analysis, the data was plotted against heat units accumulated after planting rather than by time using R packages ggplot2 and ggpubr for graphics (Kassambara, 2021; Wickham, 2009). Daily heat units were calculated using on-site ambient temperature and the development threshold temperature of 15.6°C (Oosterhuis, 1990) as in the following equation:

$$Heat\ Units = \frac{Max\ Ambient\ Temperature\ °C\ -\ Min\ Ambient\ Temperature\ °C}{2} - 15.6°C$$

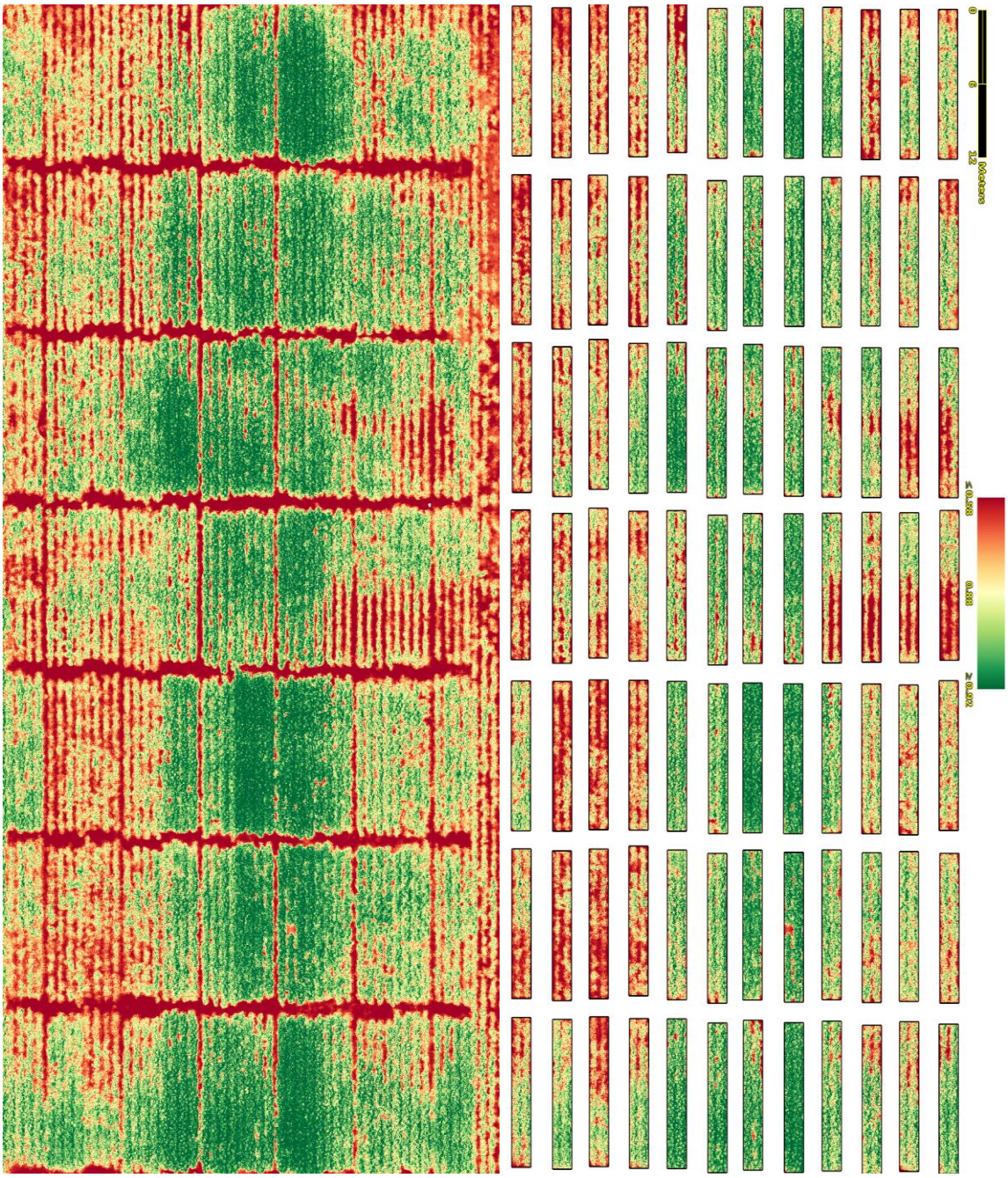

Figure 2.3. Normalized Difference Vegetation Index mosaic (left) and 2 row cotton subplots (right) from which averages were calculated for analysis. Of a total of 96 plots, 70 are shown in these images. Subplots are approximately 2 x 12 m.

2.3. Results

2.3.1. Seasonal rainfall and accumulated heat units

The most notable difference among growing seasons was rainfall, with rain events occurring earlier in 2017 and 2019, and 2018 and 2020 being relatively dry throughout most of the growing season (Figure 2.4). The driest growing season was 2018 with 323 mm of rain, and 2017 had the most rainfall with 1087 mm. Rainfall during 2019 and 2020 growing seasons was 528 mm and 395 mm, respectively. Much of the rain in 2017 and 2020 occurred after maturation. The cumulative estimated crop evapotranspiration requirement (ET_c) varied each year and ranged from about 365 to 615 mm (Table 2.4). Much of the total of 400 mm irrigation in 2019 was applied near the end of the growing season as precipitation diminished, while the 334 mm of irrigation required in 2018 was distributed more evenly over time.

Ambient temperature trends were similar for 2019 and 2020, which is evident in the accumulated heat unit curves presented in Figure 2.4. Average ambient temperature during the 2019 growing season was about 2.5% higher than 2018 at 27.6 °C and 26.9 °C. Average ambient temperature for 2017 and 2020 were 26.7 °C, and both years also had tropical weather towards the end of the season.

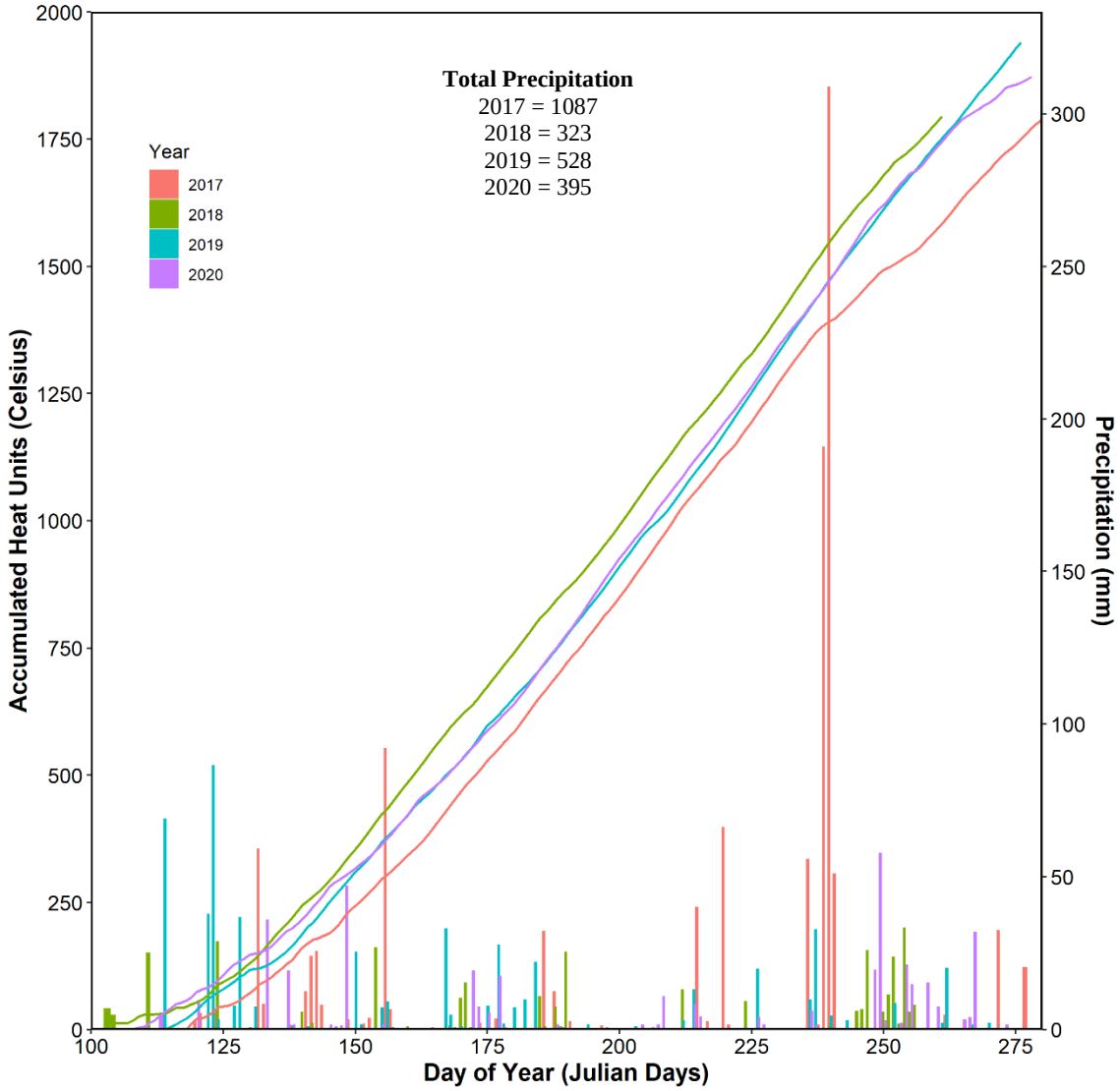

Figure 2.4. Daily rainfall represented by colored bars and accumulated heat units (15.6˚C development threshold) represented by lines during each cotton growing season at the Texas A&M Research Farm in Burleson County, Texas from 2017 to 2020.

Table 2.4. Weekly cumulative cotton crop evapotranspiration requirements, rainfall, and irrigation treatment amounts during the irrigation period for the 2018 – 2020 growing seasons.

Weeks After Emergence	Cumulative ETc (mm)				Rain (mm)			
	2017	2018	2019	2020	2017	2018	2019	2020
1	13.5	25.4	7.9	15.9	51.8	0.0	52.1	54.9
2	24.2	50.8	25.1	34.6	0.0	5.6	1.0	1.5
3	43.5	75.4	51.8	54.1	0.0	2.5	1.0	50.0
4	69.8	110.3	75.6	77.3	7.9	26.7	26.7	1.8
5	94.1	148.8	100.3	111.0	0.0	0.8	16.3	0.0
6	120.6	193.5	131.1	148.4	47.0	1.0	37.3	19.1
7	147.7	229.9	166.9	171.5	66.3	26.4	8.6	30.5
8	183.9	284.4	196.8	212.1	8.4	0.0	45.7	0.0
9	212.8	326.0	234.6	255.8	121.2	19.6	21.8	2.3
10	259.4	374.5	282.6	313.8	1.0	25.1	1.5	0.0
11	310.9	444.2	335.2	362.2	0.0	0.0	0.8	3.3
12	356.2	505.3	389.6	-	3.3	0.0	0.0	-
13	416.9	562.7	434.6	-	6.6	13.0	15.7	-
14	473.6	614.7	491.8	-	0.0	9.4	0.0	-
15	524.6	-	547.9	-	0.0	-	19.6	-
16	588.2	-	-	-	0.0	-	-	-
Total:	588.2	614.7	547.9	362.2	313.4	130.0	248.2	163.3
Weeks After Emergence	**Irrigation 80% (mm)**				**Irrigation 40% (mm)**			
	2017*	2018	2019	2020	2017*	2018	2019	2020
1	0.0	0.0	0.0	0.0	0.0	0.0	0.0	0.0
2	0.0	0.0	0.0	0.0	0.0	0.0	0.0	0.0
3	0.0	8.4	60.8	0.0	0.0	4.2	57.4	0.0
4	12.7	14.3	0.0	0.0	12.7	7.1	0.0	0.0
5	25.4	0.0	0.0	11.5	25.4	0.0	0.0	0.0
6	0.0	0.0	0.0	19.3	0.0	0.0	111.5	21.7
7	0.0	35.3	0.0	0.0	0.0	10.6	0.0	0.0
8	0.0	49.7	0.0	8.9	0.0	26.5	0.0	0.0
9	0.0	18.3	0.0	27.9	0.0	10.7	0.0	22.2
10	14.1	35.4	0.0	60.7	6.9	8.4	0.0	9.4
11	13.7	63.5	0.0	17.8	8.1	2.4	0.0	9.5
12	20.0	48.9	36.6	-	11.8	33.3	0.0	-
13	18.6	40.1	72.9	-	11.0	10.2	0.0	-
14	19.3	19.7	105.9	-	11.3	18.1	0.0	-
15	32.1	-	123.6	-	18.5	-	31.5	-
16	44.3	-	-	-	26.0	-	-	-
Total:	200.2	333.5	399.8	146.1	131.6	131.7	200.4	62.8

*2017 Irrigation was replaced at 90% and 45% of ET_c.

2.3.2. Seed Cotton Yield

Irrigation level had a significant effect on seed cotton yield for each study year (Figure 2.5; Table 2.5). The highest and lowest seed cotton yield for each year were observed in the 80% ET_c and dryland treatments, respectively. Irrigation at 80% ET_c increased seed cotton yield by 106, 98, 44, and 99% compared to dryland cotton in 2017, 2018, 2019, and 2020, respectively. Average seed cotton yield for 40% ET_c (deficit irrigated) was highest (mean yield of 2830 kg ha^{-1}) in 2018, ranging from 1752 to 3897 kg ha^{-1} and lowest (mean yield of 1183 kg ha^{-1}) in 2020, ranging from 769 to 1963 kg ha^{-1} (Table 2.6, Figure 2.5). In 2019, deficit irrigation yielded 480 kg ha^{-1} more than the dryland treatment. In 2017, the average seed cotton yield of deficit irrigation was 1004 kg ha^{-1} more than observed in the dryland cotton. In addition to irrigation level, seed cotton yield was affected by cotton cultivar: 2017 ($P < 0.0001$), 2018 ($P = 0.044$), and 2019 ($P < 0.0001$). There was no difference in seed cotton yield among cultivars in 2020 ($P = 0.144$). There was no interaction between irrigation level and cotton cultivar for seed cotton yield for any year (Table 2.5).

Similar to seed cotton yield, irrigation level had a significant effect on NDVI for all years (Table 2.5). Mean NDVI of 80% ET_c irrigation was 13 and 11% greater than dryland cotton mean NDVI in 2017 and 2019, respectively (Table 2.6). In 2020, average NDVI was 40% higher in the 80% ET_c irrigated cotton than in the dryland cotton (Table 2.6). Variation in NDVI was observed among cotton cultivars for all study years (Table 2.5). There was significant irrigation by cultivar interaction in 2017 ($P = 0.037$), but not in any other year (Table 2.5). Pairwise irrigation treatment comparisons for NDVI and

NDRE generally matched those for yield (Table 2.6). As shown in Table 2.7, pairwise comparisons for cultivar yield in 2017 were similar to those for NDVI. The top three yielding cultivars were ranked the same using NDVI, but Deltapine 1549 had unusually high NDVI and NDRE with a low mean yield relative to other cultivars. In Cultivar NDRE means were ranked similarly to NDVI, except in 2019 when NDRE groups matched yield better than NDVI.

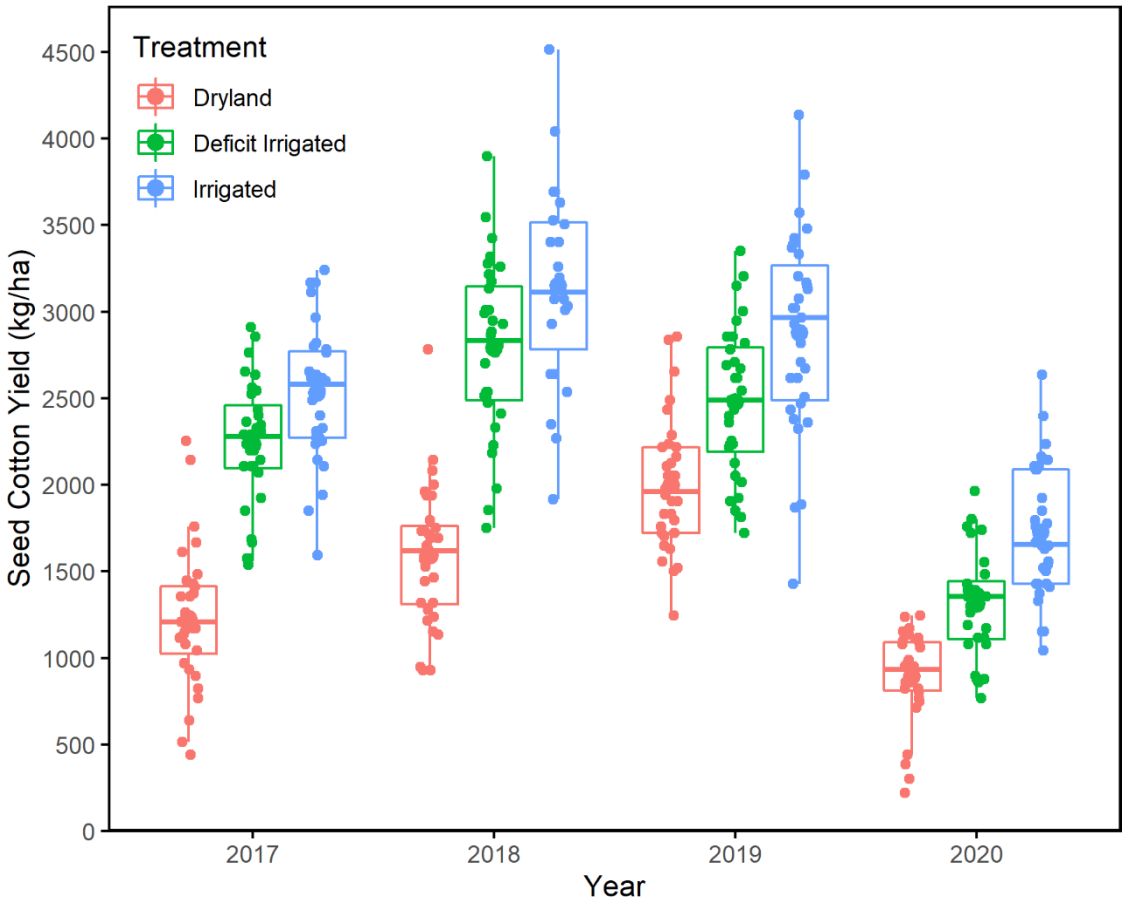

Figure 2.5. Box and whisker plot of seed cotton yield separated by irrigation treatment for all four years in the study.

Table 2.5. Analysis of variance for cotton yield and corresponding NDVI during the same year for all years in the study.

Source of Variation	DF	F-value	Pr > F	F-value	Pr > F	F-value	Pr > F
		2017 Yield		**NDVI 1239 Heat Units**		**NDRE 1239 Heat Units**	
Irrigation	2	146.668	< 0.0001	147.773	< 0.0001	81.446	< 0.0001
Cultivar	7	6.034	< 0.0001	6.787	< 0.0001	5.455	< 0.0001
Irrigation x Cultivar	14	1.508	0.13	1.923	0.0377	1.349	0.201
		2018 Yield		**NDVI 1108 Heat Units**		**NDRE 1108 Heat Units**	
Irrigation	2	90.379	< 0.0001	128.512	< 0.0001	109.562	< 0.0001
Cultivar	7	2.217	0.0444	3.195	0.00585	4.397	< 0.001
Irrigation x Cultivar	14	1.201	0.2975	0.406	0.96795	0.276	0.995
		2019 Yield		**NDVI 1237 heat units**		**NDRE 1237 Heat Units**	
Irrigation	2	41.171	< 0.0001	21.157	< 0.0001	9.511	< 0.001
Cultivar	7	8.236	< 0.0001	2.771	0.0131	4.228	< 0.001
Irrigation x Cultivar	14	0.682	0.785	1.167	0.3187	0.911	0.551
		2020 Yield		**NDVI 1154 Heat Units**		**NDRE 1154 Heat Units**	
Irrigation	2	42.33	< 0.0001	26.734	< 0.0001	25.858	< 0.0001
Cultivar	7	1.619	0.144	3.267	0.00454	3.729	0.002
Irrigation x Cultivar	14	0.8	0.666	0.352	0.98347	0.356	0.983

Table 2.6. Irrigation treatment means comparisons of cotton yield data and NDVI at corresponding heat units during the same year.

Treatment	Average Yield (kg ha^{-1})	NDVI	NDRE
	2017	**1239 Heat Units**	**1239 Heat Units**
Irrigated	2530 a	0.9047 a	0.5322 a
Deficit Irrigated	2232 b	0.8919 a	0.5302 a
Dryland	1228 c	0.8046 b	0.4580 b
	2018	**1108 Heat Units**	**1108 Heat Units**
Irrigated	3196 a	0.8383 a	0.4631 a
Deficit Irrigated	2830 b	0.7752 b	0.4382 b
Dryland	1614 c	0.6565 c	0.3730 c
	2019	**1237 Heat Units**	**1237 Heat Units**
Irrigated	2879 a	0.8366 a	0.5358 a
Deficit Irrigated	2479 b	0.8535 a	0.5229 a
Dryland	1999 c	0.7943 b	0.5030 b
	2020	**1154 Heat Units**	**1154 Heat Units**
Irrigated	1724 a	0.6798 a	0.3330 a
Deficit Irrigated	1183 b	0.5849 b	0.2923 b
Dryland	866 c	0.4859 c	0.2385 c

Table 2.7. Cultivar mean comparisons of cotton yield data and NDVI during the same year at corresponding heat units.

Cultivar	Mean Yield (kg ha^{-1})	NDVI	NDRE
2017		**1239 Heat Units**	**1239 Heat Units**
Phytogen 499	2275 a	0.8955 a	0.5264 a
Phytogen 333	2140 ab	0.8749 ab	0.5237 a
Stoneville 4946	2125 ab	0.8692 ab	0.5101 ab
DeltaPine 1646	2123 ab	0.8408 b	0.4826 b
FiberMax 1900	2116 ab	0.8674 ab	0.4974 ab
NexGen 1511	1751 b	0.8595 ab	0.4881 b
FiberMax 2484	1735 b	0.8433 b	0.4979 ab
DeltaPine 1549	1707 b	0.8860 a	0.5280 a

2018		1108 Heat Units	1108 Heat Units
Stoneville 4946	2727	0.7735	0.4125 abc
Phytogen 499	2722	0.7732	0.4226 abc
DeltaPine 1646	2634	0.7471	0.4005 c
NexGen 1511	2537	0.7655	0.4260 abc
FiberMax 1900	2457	0.7498	0.4204 abc
DeltaPine 1549	2347	0.7419	0.4435 a
FiberMax 2484	2210	0.7195	0.4358 ab
Phytogen 333	2185	0.7175	0.4070 bc
2019		**1237 Heat Units**	**1237 Heat Units**
Phytogen 580	2931 a	0.8813 a	0.5479 a
Phytogen 480	2707 ab	0.8504 ab	0.5292 ab
DeltaPine 1845	2607 ab	0.8272 ab	0.5287 ab
Phytogen 350	2576 abc	0.8303 ab	0.5287 ab
DeltaPine 1646	2382 bcd	0.8076 b	0.5114 abc
Deltapine 1835	2319 bcd	0.8202 b	0.5066 bc
Stoneville 4550	2090 cd	0.8505 ab	0.5234 abc
FiberMax 2398	1985 d	0.8366 ab	0.4886 c
2020		**1154 Heat Units**	**1154 Heat Units**
Phytogen 400	1469	0.6084 ab	0.3015 ab
Phytogen 580	1456	0.6878 a	0.3395 a
NexGen 5711	1265	0.5906 ab	0.2697 b
Stoneville 4550	1256	0.6012 ab	0.2914 ab
DeltaPine 1845	1185	0.5928 ab	0.3049 ab
NexGen 4936	1182	0.5501 b	0.2892 ab
FiberMax 2398	1170	0.5207 b	0.2431 b
DeltaPine 1646	1080	0.5171 b	0.2643 b

2.3.3. Relationship Between Vegetation Indices and Yield

There were significant positive linear relationships between vegetation indices and seed cotton yield for all irrigation levels and cultivars in 2017 (Figure 2.6, Table 2.8). Correlation (R^2 = 0.61) between NDVI and seed cotton yield reached a maximum

during the bloom period with similar R^2 values and error (NRMSE of about 21%) between 1028 to 1328 heat units or 85 - 107 DAE. NDVI accounted for more yield variation than NDRE (R^2 = 0.54) at 101 DAE and 6 out of 8 flight dates.

Table 2.8. Coefficient of Determination (R^2) and Root Mean Squared Error (RMSE) for linear regression of seed cotton yield on UAS-derived vegetation indices for all flight dates.

Date	DAE	Heat Units	NDVI			NDRE		
			R^2	RMSE	Signif.	R^2	RMSE	Signif.
6/14/17	38	399.7	0.30	568.1	***	0.13	633.3	***
7/13/17	67	770.9	0.42	519.2	***	0.06	659.5	*
7/31/17	85	1028.4	0.60	431.0	***	0.53	467.9	***
8/10/17	95	1151.6	0.60	431.6	***	0.54	462.7	***
8/16/17	101	1239	0.61	425.8	***	0.54	462.1	***
8/22/17	107	1326.8	0.59	433.5	***	0.49	485.9	***
9/8/17	124	1498.2	0.04	665.6	*	0.09	648.1	**
10/20/17	166	1872.2	0.004	679.1	NS	0.04	667.8	NS
6/28/18	68	727.5	0.04	829.5	NS	0.03	829.9	NS
7/27/18	97	1108	0.78	392.8	***	0.67	482.9	***
8/9/18	110	1278.7	0.76	413.9	***	0.60	533.9	***
8/17/18	118	1385.73	0.73	441.7	***	0.59	541.7	***
8/28/18	129	1551.8	0.69	466.7	***	0.53	581.7	***
9/6/18	138	1666	0.65	501.8	***	0.52	585.7	***
9/18/18	150	1794.8	0.26	724.6	***	0.22	744.3	***
6/1/19	29	330	0.02	588.4	NS	0.02	587.6	NS
7/9/19	67	774	0.10	562.4	**	0.19	534.6	***
7/25/19	83	988.8	0.29	499.0	***	0.40	461.1	***
8/12/19	101	1236.8	0.49	426.3	***	0.56	395.8	***
8/22/19	111	1390	0.48	426.4	***	0.62	366.9	***
10/3/19	153	1940.6	0.45	441.4	**	0.34	483.5	**
6/5/20	42	386.6	0.06	461.3	***	0.02	469.4	**
6/12/20	49	469	0.11	446.7	***	0.12	445.9	***
7/3/20	70	709.3	0.48	343.4	***	0.44	356.6	***
7/16/20	83	896.8	0.73	248.5	***	0.69	266.0	***
8/4/20	102	1154.1	0.73	248.6	***	0.67	272.9	***
8/18/20	116	1355.5	0.61	297.3	***	0.55	319.4	***
10/4/20	167	1872.8	0.04	464.1	*	0.12	445.9	***

RMSE units = seed cotton yield kg ha^{-1}
0.001 (***) 0.01 (**) 0.05 (*)

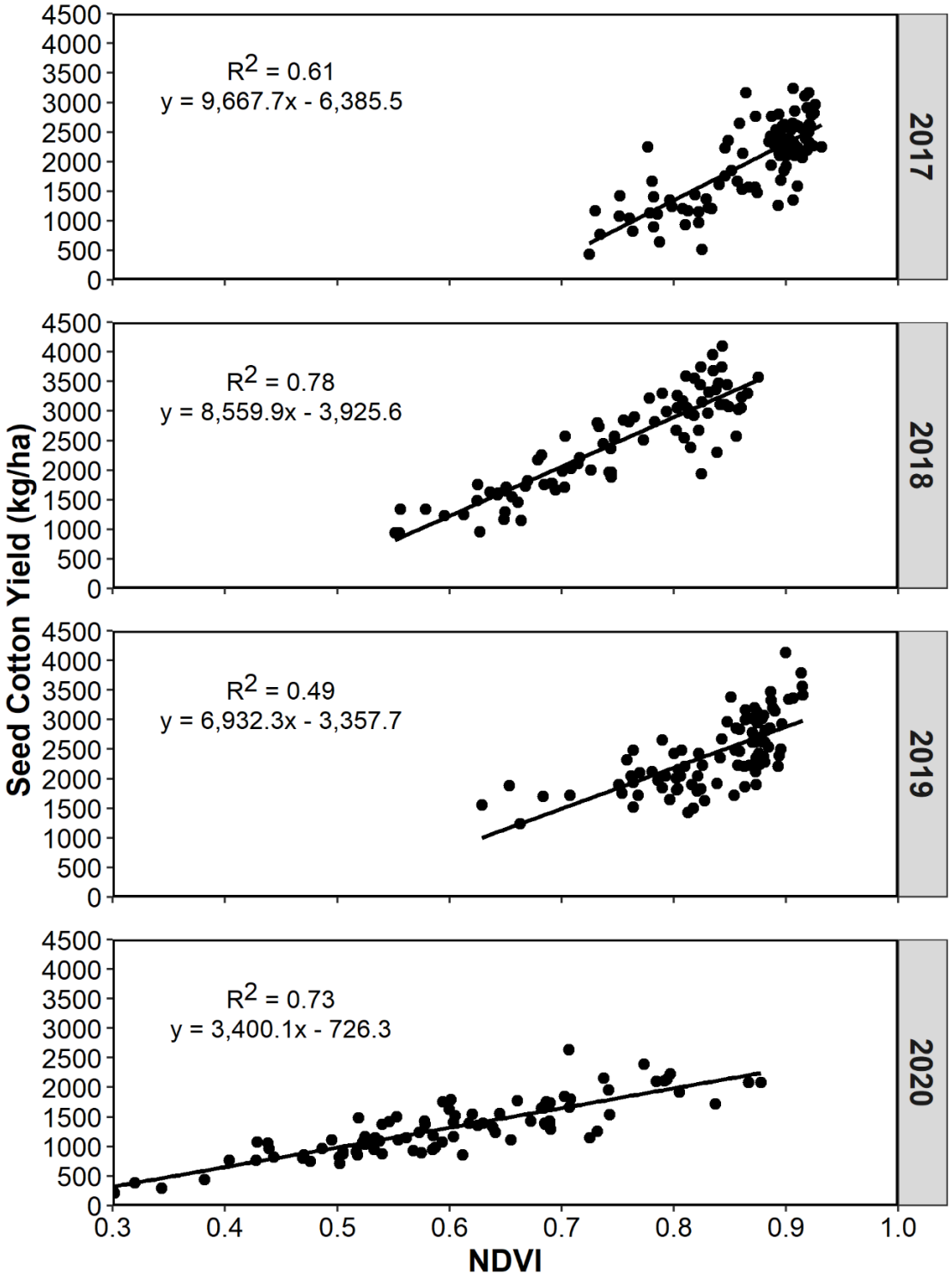

Figure 2.6. Positive linear relationship between seed cotton yield and NDVI in 2017 at 1239 heat units or 101 DAE (August 16, 2017); on July 27, 2018 at 1108 heat units or 97 DAE; on August 12, 2019 at 1237 heat units or 101 DAE; on August 4, 2020 at 1154 heat units or 97 DAE.

In 2018, NDVI had the highest relationship (R^2 = 0.78) with seed cotton yield and the lowest RMSE of 392.8 kg ha^{-1} (NRMSE = 15.8%) at 1,108 heat units or 97 DAE during bloom. Higher yielding cotton (generally irrigated) contributed to greater variation in yield prediction error. The model underestimated the highest yielding irrigated plot in the experiment (4515 kg ha^{-1}). Weeds in a few irrigated plots contributed to greater variation in NDVI values while some irrigated plots reached maximum average NDVI. Cultivar differences in canopy structure contributed to differences in NDVI which did not necessarily affect seed cotton yield.

In contrast with other years, 2019 NDRE provided better correlations with seed cotton yield than NDVI. NDRE explained more yield variation in 2019 at peak bloom (Figure 2.7) with an R^2 of 0.62 at 1,390 heat units (111 DAE) and NRMSE of 15%. Variation in yield of irrigated cotton was observed due to early season weed competition exacerbated by excessive rainfall. Presence of weeds affected yield and mean vegetation indices. Yields were above average for dryland cotton. The strongest relationship (R^2 = 0.49) between NDVI and seed cotton yield occurred at 1,236 heat units or 101 DAE, which aligned with the timing of other years. Although the relationships were weaker (lower R^2 values) than other years, the NRMSE was 17.4% for the 2019 linear model at 101 DAE and was comparable to the NRMSE of the best linear models for other years.

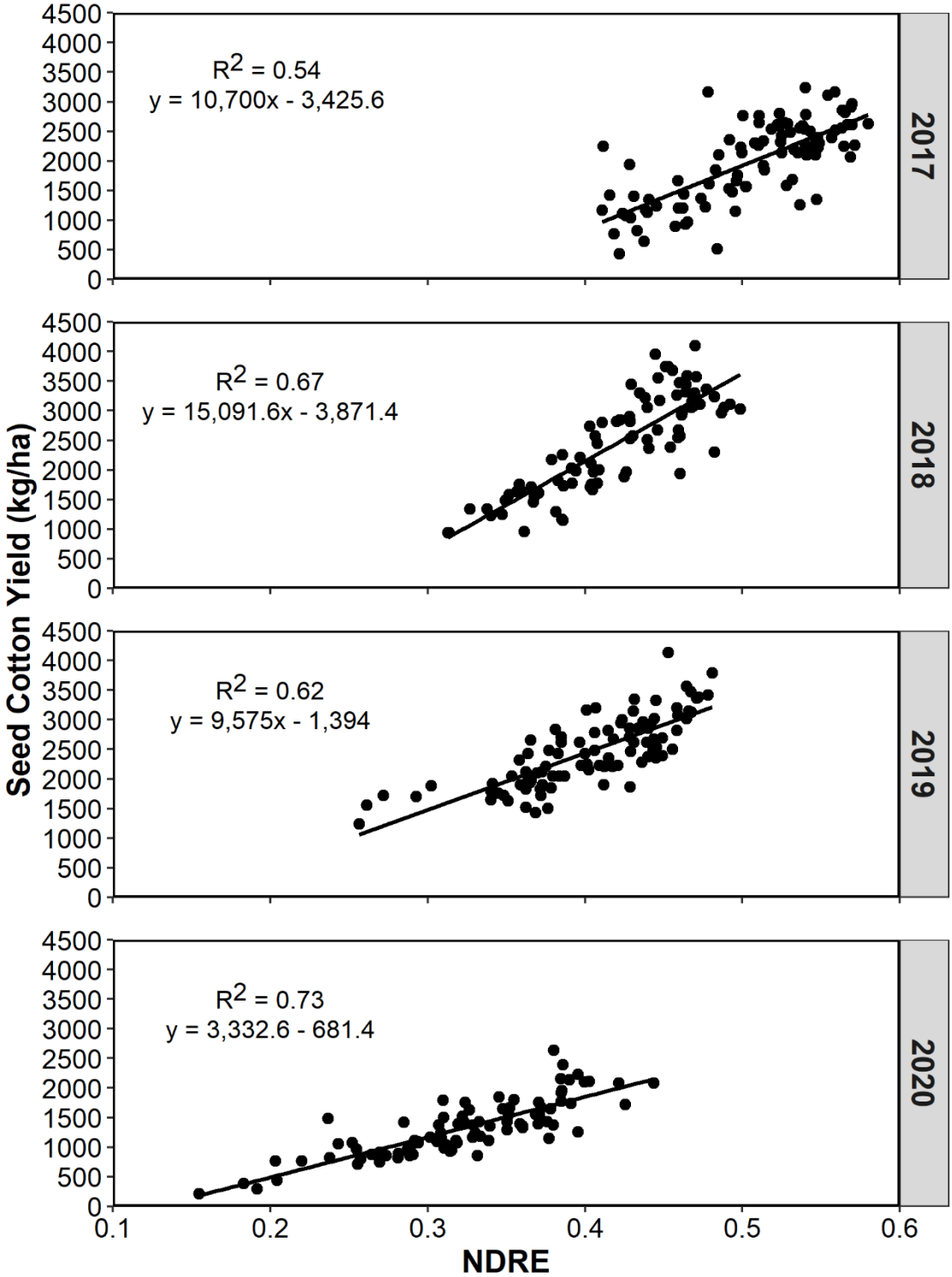

Figure 2.7. Positive linear relationship between seed cotton yield and NDRE in 2017 at 1239 heat units or 101 DAE (August 16, 2017); on July 27, 2018 at 1108 heat units or 97 DAE; on August 22, 2019 at 1390 heat units or 111 DAE; and on July 16, 2020 at 897 heat units or 83 DAE.

Despite lower seed cotton yields in 2020 relative to previous study years, vegetation indices provided good correlations with cotton yield. The strongest relationship (R^2 = 0.73) between NDVI and yield occurred at 1154 heat units or 97 DAE (Figure 2.6). RMSE was minimized on the same day at 244 kg ha^{-1} (NRMSE = 19.4%). While NDVI models consistently outperformed NDRE with higher R^2 and lower RMSE, NDRE also had strong relationships with yield (highest R^2 = 0.69 with RMSE = 266 kg ha^{-1}).

The best NDVI yield estimation models were within the bloom period, particular between about 1100 to 1300 heat units (Table 2.8). Strong relationships began as early as first flower or about 900 heat units (85 DAE), became strongest during the bloom period, and deteriorated closer to harvest and especially after defoliation. While timing and R^2 of the linear models varied by year (Figure 2.8), both NDVI and NDRE generally followed this seasonal trend. The higher yielding cotton had greater error in yield estimation using NDVI or NDRE. With seed cotton yield increasing with increasing irrigation levels (80% and 40% ET_c), models for yield estimation using vegetation indices should be developed independently for contrasting irrigation management.

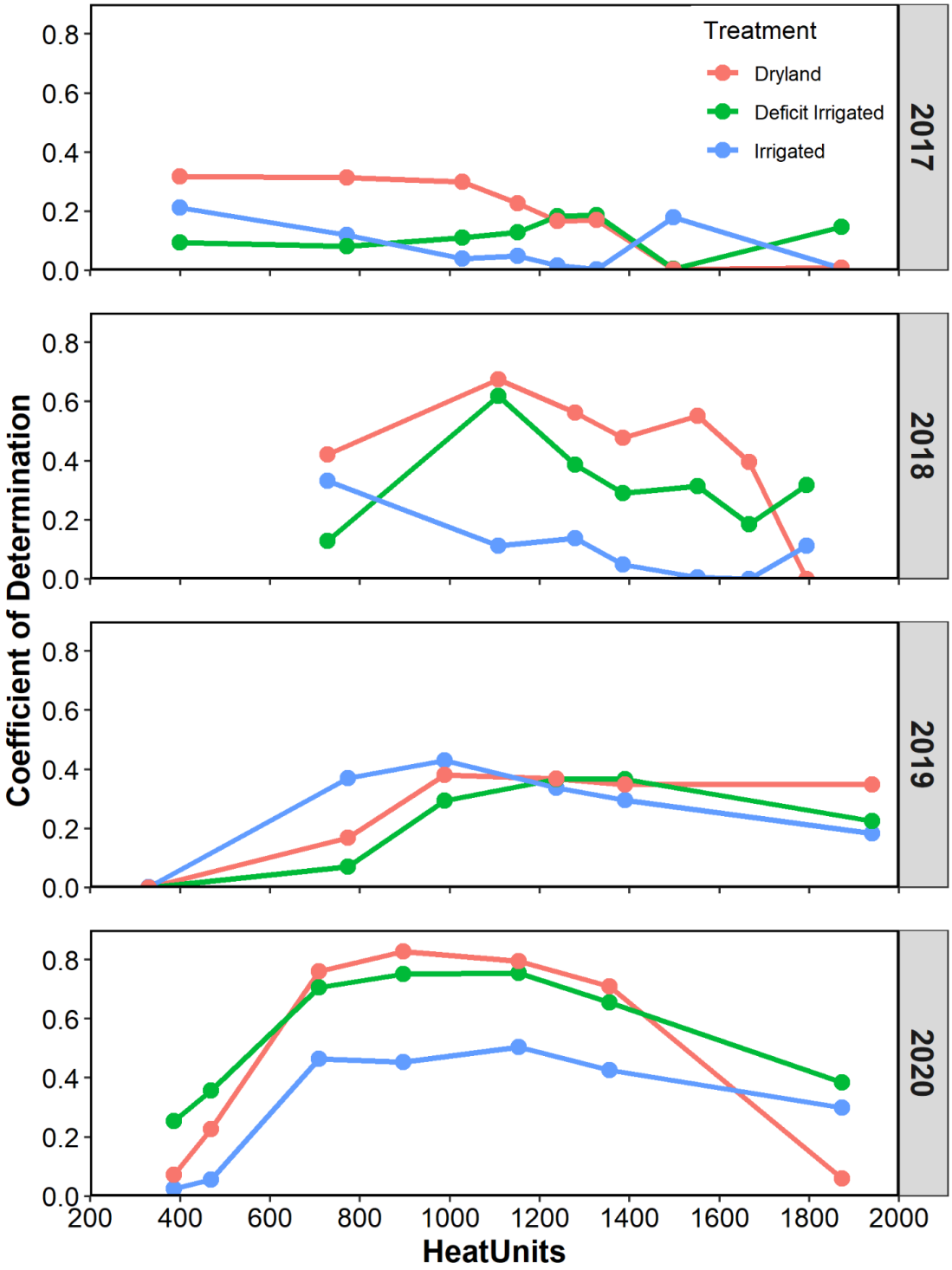

Figure 2.8. In-season Normalized Difference Vegetation Index (NDVI) yield estimation model coefficient of determination by accumulated heat units and separated by treatment. Each dot represents a flight date during each year for a total of 28 multispectral flights over 4 years.

Cross-validations of linear models were conducted for each irrigation level using all years of seed cotton yield as the dependent variable and NDVI measured closest to peak bloom (~1200 heat units). Significant linear models were found for all irrigation levels with R^2 ranging from 0.38 to 0.42 (Table 2.9). The 2017 data was excluded because the image GSD was different than the other years. Doing so increased the strength of the relationships and excluding 2017 from cross validation increased the dryland R^2 from 0.38 to 0.83. Irrigated cotton results improved ($R^2 > 0.58$) relative to models using all years. Using the 2018-2019 dryland model (Figure 2.9 A), 2020 dryland yield could be predicted with reasonable accuracy (RMSE = 151 kg ha^{-1}, NRMSE = 17%) as shown in Figure 2.9 B. Predicting 2020 yield across irrigation levels from the 2018 – 2019 model (Figure 2.10) produced over 10% higher error (RMSE = 368.5 kg ha^{-1}, NRMSE = 28%).

Table 2.9. Model parameters for linear regression of NDVI and seed cotton yield across growing seasons by irrigation level (left) and corresponding repeated k-fold cross validation results (right).

Treatment	Model Parameters (all years)					Cross Validation		
	Slope	Intercept	R^2	RMSE	NRMSE	R^2	RMSE	MAE
Irrigated	4417.1	-1091.2	0.42	559.2	22.1	0.44	548.13	439.15
Deficit Irrigated	3707.6	-689.5	0.40	532.7	23.8	0.42	523.94	440.54
Dryland	2442.5	-245.9	0.38	435.2	30.3	0.41	428.14	341.27
Treatment	**2018 - 2020**					**Cross Validation**		
	Slope	Intercept	R^2	RMSE	NRMSE	R^2	RMSE	MAE
Irrigated	5809.1	-2050.1	0.59	529.9	20.9	0.63	516.65	408.74
Deficit Irrigated	5056.6	-1574.5	0.58	499.4	22.2	0.61	489.46	415.62
Dryland	3749.9	-930.1	0.81	254.9	16.9	0.83	248.46	191.58

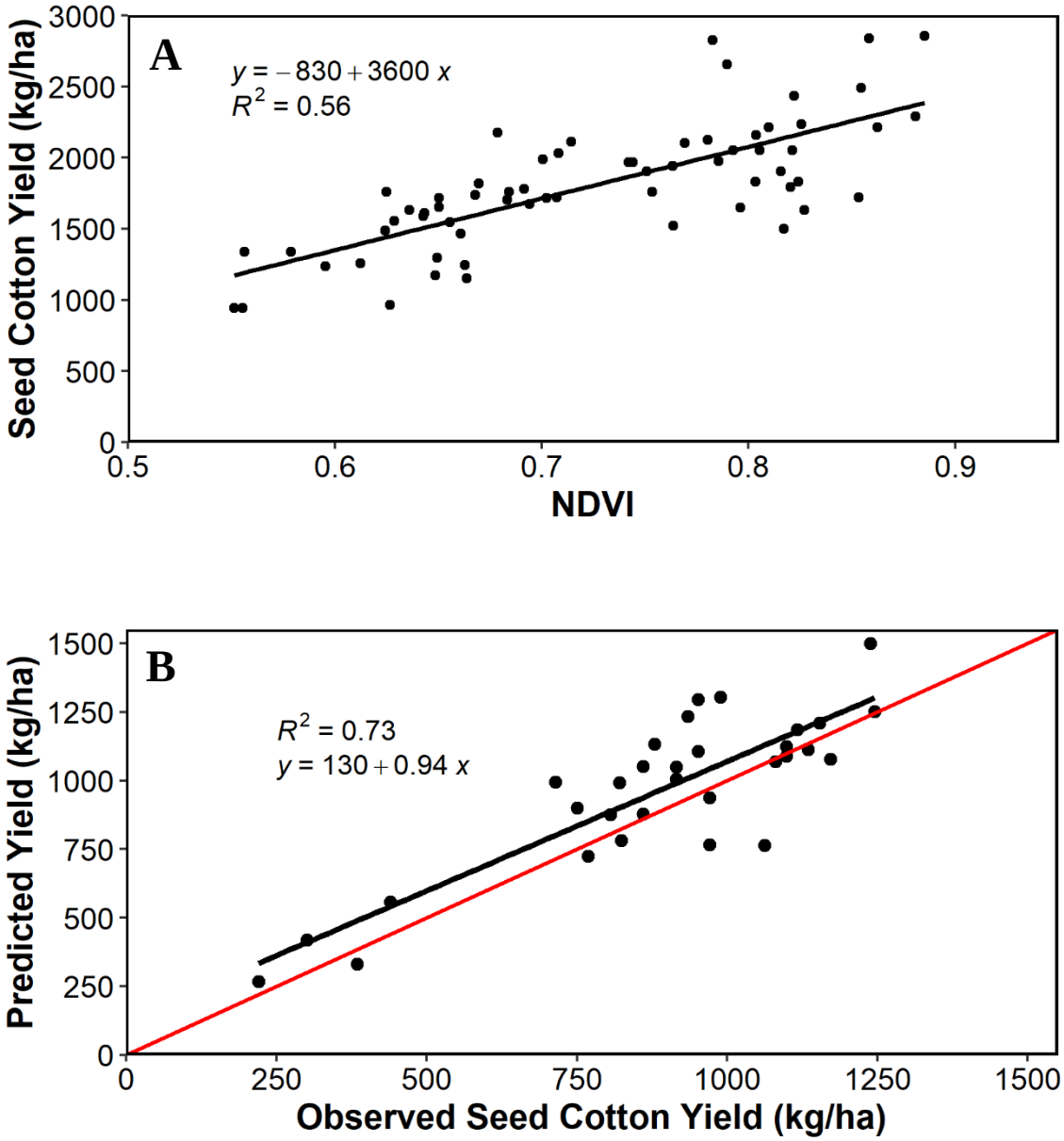

Figure 2.9. (A) Dryland Seed Cotton Yield as a function of NDVI for 2018 - 2019 and (B) 2020 observed vs. predicted yield regression line compared with a line that has a slope of one (red).

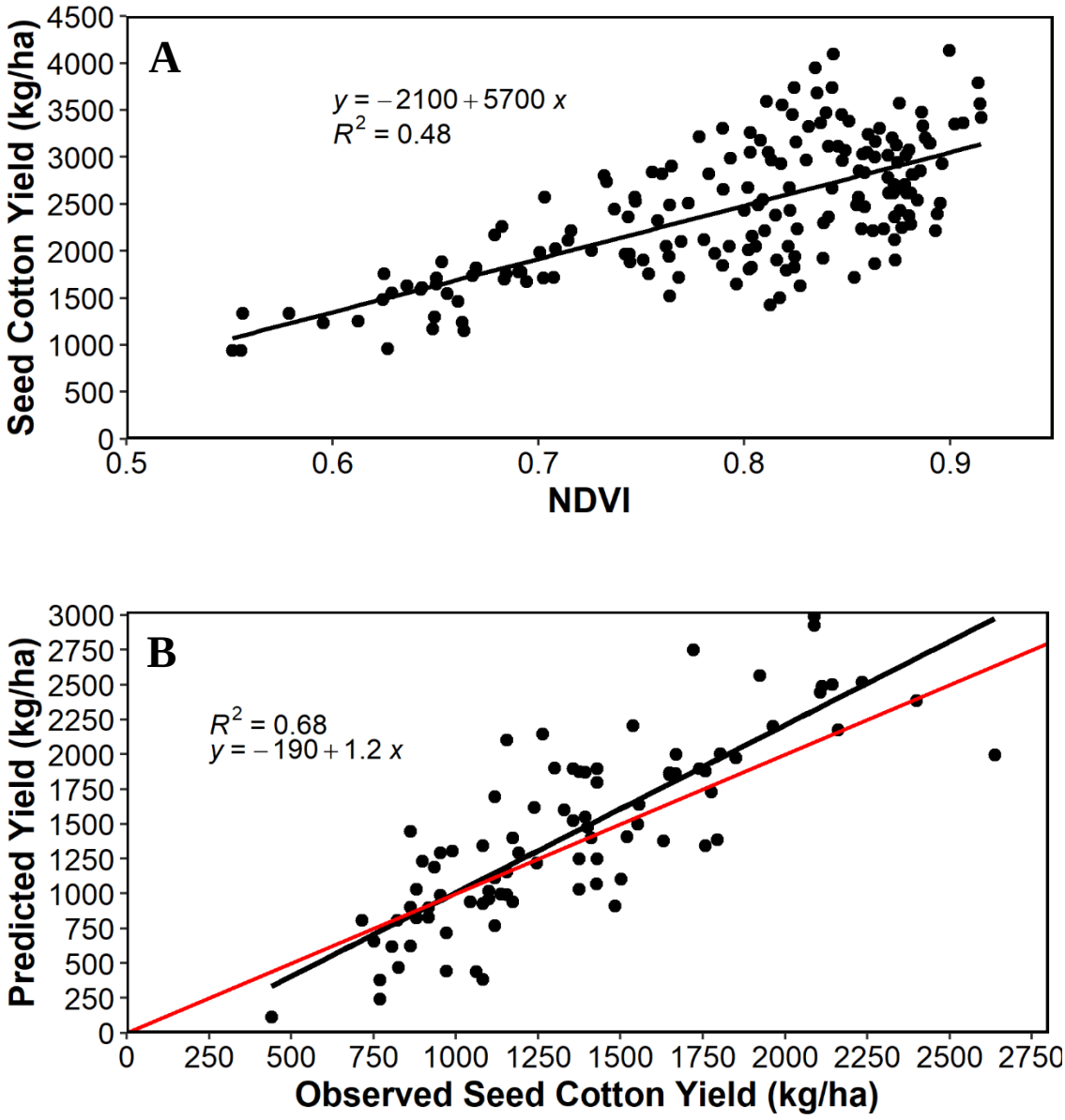

Figure 2.10. (A) Seed Cotton Yield as a function of NDVI for all irrigation treatments in 2018 - 2019 and (B) 2020 observed vs. predicted yield regression line compared with a line that has a slope of one (red).

2.4. Discussion

NDVI was effective for irrigation treatment mean comparisons, producing similar statistical results to observed yield. Variation in seed cotton yield among increasing levels of irrigation was accurately predicted with in-season vegetation indices. Huang et al. (2013) also noted that NDVI values for irrigation treatments were significantly different in cotton. The strength of relationships between in-season vegetation indices and seed cotton yield ranged from moderate to strong within each growing season but were generally weaker when split by irrigation level. Adams et. al (2021) observed this same trend in subsurface drip irrigated cotton using a proximal phenotyping system. The linear regression models performed poorly across growing seasons except in dryland, for which 2020 yield was estimated from the previous 2 years NDVI with reasonable accuracy. This suggests that the methodology is best suited for dryland production systems, but more robust methodologies should be investigated for irrigated production. Vegetation indices could be useful for relative or potential dryland cotton yield estimates based on historical yield data for research or insurance claim purposes in situations where the crop is lost or cannot be harvested.

While high yielding cultivars often had greater NDVI values and more significant differences among cultivars were found, differences in NDVI were likely due to variations in canopy architecture and were not necessarily directly related to observed yield. Thompson et al. (2018) also found NDVI measurements from a proximal sensing cart were significantly different between cotton breeding lines and broad-sense heritability estimates for NDVI ranged from 0.28 to 0.49. UAS flights timed during

bloom are generally suitable and the average ideal timing across all treatments (1185 heat units) aligned closely with previous work that also found maximum correlations with yield around this time during bloom (Feng et al., 2020; Gutierrez et al., 2012; Leon et al., 2003; Satir & Berberoglu, 2016; Yang et al., 2004; Zarco-Tejada et al., 2005). NDVI could be useful as a phenotyping tool for cotton breeders during the early stages of pedigree selection to eliminate only the worst performing lines prior to investing labor resources for boll sampling and harvesting hundreds of small plots. However, this methodology is not accurate enough for screening advanced lines later in the selection process. Rutkoski et al. (2016) observed that secondary traits such as NDVI improved the accuracy of pedigree and genomic prediction for wheat grain yield and could improve breeding selection particularly during the early stages. Thompson et al. (2020) also found that a multispectral vegetation index (NDRE) from a single proximal measurement around peak bloom provided good cotton yield predictions (R^2 up to 0.71) which is comparable to the results of this study.

Vegetation indices accounted for much of the yield variability early enough in the growing season to inform nutrient, irrigation, growth regulator, and pest management decisions. Results suggest that it could potentially be used for in-season management purposes such as defoliation timing, plant growth regulator timing, scouting, disease tracking, and to update management zones for variable rate application of inputs such as fertilizer. At a minimum, the methodology should be suitable for spatially targeted sampling, for example using GNSS positioning to navigate in the field to extreme locations (i.e. unexpectedly low or high NDVI) for investigating and collecting any

necessary ground reference data (e.g. tissue samples, soil cores, soil moisture, plant height, pest incidence). Model parameters differ for each year, which may be partially attributed to cotton cultivar differences and environmental variation, but results suggest that NDVI yield estimation models are unlikely to be consistent across years except in dryland conditions.

Contrary to all other years, NDRE explained more yield variability than NDVI across all image acquisition dates in 2019. The crop canopy closed earlier in 2019 than other years due to frequent rainfall early in the growing season. This led to some plot NDVI averages exceeding 0.9 as early as 83 DAE or ~1000 heat units and most likely caused NDVI to underperform because it was less sensitive due to saturation. Weaker relationships between vegetation indices and cotton yield when the crop canopy closed early and/or grew to suboptimal heights suggests that some adjustment to the methodology may be necessary in these situations as NDVI tends to become less sensitive. This along with lower harvest index may also explain why relationships with yield were usually weaker in the 80% ET_c irrigated cotton than in deficit irrigated and dryland cotton. Feng et al. (2020) similarly observed saturated NDVI values in higher yielding cotton and higher canopy cover. While NDRE is likely a better choice than NDVI to address this issue as it is not susceptible to saturation (Adams et. al, 2021). The methodology is probably more suitable in low or average yielding cotton characteristic of dryland or deficit irrigated production systems.

While the accuracy of this methodology would be affected by presence of weeds, areas with major weed pressure could be excluded from analysis by visually inspecting

suspected problem areas in the orthomosaics or those areas could be excluded via image classification methods. It is important to note that the multispectral camera used for this methodology is high-quality with discrete sensors, global shutters, and relatively narrow wavebands, so relationships with yield may be different when cheaper equipment such as modified RGB cameras with rolling shutters and broadband filters are used (Deng et. al, 2018). This methodology could limit equipment wear, risk, and field traffic relative to phenotyping rovers.

Increasing the flight height AGL (i.e. coarser GSD) should produce similar results, but more investigation is warranted to determine an ideal GSD for research and production purposes. More complicated methodologies, such as image classification/segmentation, negative buffers, and data fusion may be necessary to enhance results in irrigated cotton. These are important topics for future research to improve absolute yield prediction accuracy.

2.5. Conclusions

Vegetation indices are among the simplest tools for agronomists and researchers to make use of multispectral imagery. Irrigation and cotton cultivar have a significant effect on vegetation indices measured during bloom. NDVI was effective for irrigation treatment comparisons, producing similar statistical results to observed yield. UAS-derived narrowband vegetation indices from a single flight around 1200 accumulated heat units (bloom period) have the strongest relationship with cotton yield during the growing season. Planning UAS flights around the optimal in-season timing produces a powerful dataset while minimizing labor and requisite computational resources. This

presents a simple methodology accessible to a wider range of analysts working in research than more advanced methodologies that require many flights or imagery collected after defoliation. NDVI produced better linear regression models than NDRE for all years except 2019, which suggests that NDVI is better suited for this task in cotton. Except for the dryland treatment, for which 2020 yield was estimated with fair accuracy using the previous two years of NDVI data acquired closest to 1200 heat units, models were weaker when split by irrigation level across years. This demonstrates with greater confidence that narrowband vegetation indices derived from a single, properly timed UAS flight have value for cotton yield estimation and therefore should be considered as part of broader high-throughput phenotyping endeavors, particularly in dryland production systems.

2.6. References

Adams, C. B., Ritchie, G. L., & Rajan, N. (2021). *Cotton phenotyping and physiology monitoring with a proximal remote sensing system*. Crop science, 61(2), 1317-1327. https://doi.org/https://doi.org/10.1002/csc2.20434

Allen, R. G., Pereira, L. S., Raes, D., & Smith, M. (1998). Crop evapotranspiration-Guidelines for computing crop water requirements. *FAO Irrigation and drainage paper 56*.

Ansari, M. S., Mahey, R., & Sidhu, S. (1999). Cotton yield prediction through spectral parameters. *Journal of the Indian Society of Remote Sensing*, 27(4), 185.

Ashapure, A., Jung, J., Chang, A., Oh, S., Yeom, J., Maeda, M., Maeda, A., Dube, N., Landivar, J., Hague, S., & Smith, W. (2020). Developing a machine learning based cotton yield estimation framework using multi-temporal UAS data. *ISPRS Journal of Photogrammetry and Remote Sensing*, 169, 180-194. https://doi.org/https://doi.org/10.1016/j.isprsjprs.2020.09.015

Daughtry, C. S. T., Walthall, C. L., Kim, M. S., de Colstoun, E. B., & McMurtrey, J. E. (2000). Estimating Corn Leaf Chlorophyll Concentration from Leaf and Canopy Reflectance. *Remote sensing of environment*, 74(2), 229-239. https://doi.org/https://doi.org/10.1016/S0034-4257(00)00113-9

Deng, L., Mao, Z., Li, X., Hu, Z., Duan, F., & Yan, Y. (2018). UAV-based multispectral remote sensing for precision agriculture: A comparison between different cameras. ISPRS Journal of Photogrammetry and Remote Sensing, 146, 124-136. https://doi.org/https://doi.org/10.1016/j.isprsjprs.2018.09.008

Feng, A., Sudduth, K., Vories, E., Zhang, M., & Zhou, J. (2018). Cotton Yield Estimation based on Plant Height From UAV-based Imagery Data. 2018 ASABE Annual International Meeting,

Feng, A., Zhou, J., Vories, E. D., Sudduth, K. A., & Zhang, M. (2020). Yield estimation in cotton using UAV-based multi-sensor imagery. *Biosystems Engineering*, 193, 101-114. https://doi.org/10.1016/j.biosystemseng.2020.02.014

Gutierrez, M., Norton, R., Thorp, K. R., & Wang, G. (2012). Association of spectral reflectance indices with plant growth and lint yield in upland cotton. *Crop science*, 52(2), 849-857.

Huang, Y., Brand, H. J., Sui, R., Thomson, S. J., Furukawa, T., & Ebelhar, M. W. (2016). Cotton yield estimation using very high-resolution digital images acquired with a low-cost small unmanned aerial vehicle. Transactions of the ASABE, 59(6), 1563-1574.

Huang, Y., Sui, R., Thomson, S. J., & Fisher, D. K. (2013). Estimation of cotton yield with varied irrigation and nitrogen treatments using aerial multispectral imagery. *International Journal of Agricultural and Biological Engineering*, 6(2), 37-41.

Kassambara, A. (2021). *ggpubr: 'ggplot2' Based Publication Ready Plots*. In https://CRAN.R-project.org/package=ggpubr

Kuhn, M. (2021). *Misc functions for training and plotting classification and regression models*. In https://cran.r-project.org/package=caret

Leon, C. T., Shaw, D. R., Cox, M. S., Abshire, M. J., Ward, B., Wardlaw, M. C., & Watson, C. (2003). Utility of remote sensing in predicting crop and soil characteristics. *Precision Agriculture*, 4(4), 359-384.

Maja, J. M. J., Campbell, T., Neto, J. C., & Astillo, P. (2016). Predicting cotton yield of small field plots in a cotton breeding program using UAV imagery data. *Autonomous Air and Ground Sensing Systems for Agricultural Optimization and Phenotyping*.

Menefee, D., Rajan, N., Cui, S., Bagavathiannan, M., Schnell, R., & West, J. (2020). Carbon exchange of a dryland cotton field and its relationship with PlanetScope remote sensing data. *Agricultural and Forest Meteorology*, 294. https://doi.org/10.1016/j.agrformet.2020.108130

Oosterhuis, D. M. (1990). Growth and Development of a Cotton Plant (W. N. Miley & D. M. Oosterhuis, Eds.). https://doi.org/https://doi.org/10.2134/1990.nitrogennutritionofcotton.c1

Pabuayon, I. L. B., Sun, Y., Guo, W., & Ritchie, G. L. (2019). High-throughput phenotyping in cotton: a review. *Journal of Cotton Research*, 2(1). https://doi.org/10.1186/s42397-019-0035-0

R Core Team. (2021). R: A Language and Environment for Statistical Computing. In R Foundation for Statistical Computing. https://www.R-project.org/

Read, J. J., Iqbal, J., Thomasson, J. A., Willers, J. L., & Jenkins, J. N. (2003). Remote sensing in dryland cotton: relation to yield potential and soil properties.

Ecosystems' Dynamics, Agricultural Remote Sensing and Modeling, and Site-Specific Agriculture,

Rutkoski, J., Poland, J., Mondal, S., Autrique, E., Pérez, L. G., Crossa, J., Reynolds, M., & Singh, R. (2016). Canopy Temperature and Vegetation Indices from High-Throughput Phenotyping Improve Accuracy of Pedigree and Genomic Selection for Grain Yield in Wheat. *G3: Genes|Genomes|Genetics*, *6*(9), 2799-2808.

Satir, O., & Berberoglu, S. (2016). Crop yield prediction under soil salinity using satellite derived vegetation indices. *Field crops research*, 192, 134-143.

Soil Survey Staff. (2021). Soil Survey Geographic (SSURGO) Database. Natural Resources Conservation Service, United States Department of Agriculture.

Sun, S., Li, C., Paterson, A. H., Jiang, Y., Xu, R., Robertson, J. S., Snider, J. L., & Chee, P. W. (2018). In-field High Throughput Phenotyping and Cotton Plant Growth Analysis Using LiDAR. *Frontiers in Plant Science*, 9, 16. https://doi.org/10.3389/fpls.2018.00016

Thompson, A. L., Thorp, K. R., Conley, M., Andrade-Sanchez, P., Heun, J. T., Dyer, J. M., & White, J. W. (2018). Deploying a Proximal Sensing Cart to Identify Drought-Adaptive Traits in Upland Cotton for High-Throughput Phenotyping. *Frontiers in Plant Science*, *9*(507). https://doi.org/10.3389/fpls.2018.00507

Thompson, C. N., Mills, C., Pabuayon, I. L. B., & Ritchie, G. L. (2020). Time-based remote sensing yield estimates of cotton in water-limiting environments. *Agronomy Journal*, 112(2), 975-984. https://doi.org/10.1002/agj2.20126

Wickham, H. (2009). ggplot2: Elegant Graphics for Data Analysis. In Springer-Verlag New York. http://ggplot2.org

Yang, C., Everitt, J. H., Bradford, J. M., & Murden, D. (2004). Airborne Hyperspectral Imagery and Yield Monitor Data for Mapping Cotton Yield Variability. *Precision Agriculture*, 5(5), 445-461. https://doi.org/https://doi.org/10.1007/s11119-004-5319-8

Yeom, J., Jung, J., Chang, A., Maeda, M., & Landivar, J. (2018). Automated Open Cotton Boll Detection for Yield Estimation Using Unmanned Aircraft Vehicle (UAV) Data. *Remote Sensing*, 10(12), 1895.

Zarco-Tejada, P. J., Ustin, S. L., & Whiting, M. (2005). Temporal and spatial relationships between within-field yield variability in cotton and high-spatial hyperspectral remote sensing imagery. *Agronomy Journal*, 97(3), 641-653.

3. COMBINING UNMANNED AERIAL MULTISPECTRAL AND THERMAL IMAGERY FOR COTTON YIELD ESTIMATION

3.1. Introduction

Precision agriculture technology was recognized over a decade ago as a top ten agricultural revolution (Crookston, 2006). Precision agriculture continues to benefit from technological advances that enable collection of more frequent and finer spatial resolution datasets. Analysis of these large datasets can account for spatiotemporal variability to improve sustainability of agricultural production (ISPA, 2021). Remote sensing has long provided rich datasets for such purposes, and the spatial resolution of spaceborne and airborne remote sensing imagery has improved over the last few decades from coarse resolutions of hundreds of meters to submeter resolutions (Mulla, 2013). The temporal resolution or revisit time has concurrently improved from weeks to daily global coverage (Menefee et al., 2020). While these advancements have increased the utility of those platforms, the advent of unmanned aerial systems (UAS) allows unprecedented flexibility to choose suitable temporal, spatial, and spectral resolution for specialized purposes (Shi et al., 2016). Along with many improvements to the reliability of UAS, cost has decreased from prices comparable to 100 kW tractors in 2005 (Sugiura et al., 2005) to affordable systems now more attainable for farmers.

The many advantages of UAS have inspired much interest from agricultural researchers. Quantifying yield using UAS remains a primary goal for high-throughput phenotyping for crop breeding programs and precision agriculture analytics. Recent

efforts to estimate cotton yield with UAS imagery focus mainly on segmentation or classification techniques to isolate open cotton bolls in imagery from inexpensive red, green, and blue (RGB) cameras. Huang et al. (2016) captured UAS imagery at a ground sampling distance (GSD) of 2.7cm and investigated two different methods for yield estimation. The 3D point cloud was used to derive plant height, which was related to cotton yield (R^2 = 0.43), but did not improve upon the correlation of manually measured plant height and yield. Their second method involved image segmentation to isolate cotton bolls from the background of the imagery and form a "cotton unit coverage" by dividing lint pixel area by plot pixel area (i.e. pixel counts multiplied by GSD). Although some outliers needed to be removed, the results were much better (R^2 0.83) than the plant height method they investigated.

Maja et al. (2016) calculated percent cotton area using images collected from an RGB camera. They employed a Gaussian blur followed by an unsupervised classification to isolate the cotton pixels. Dividing the cotton pixels by the total area of the plot produced the percent cotton area, which had a strong relationship with yield (R^2 = 0.78). Feng et al. (2018) also used an inexpensive RGB camera for in-season yield estimation. The authors generated a canopy height model from the imagery and conducted a correlation analysis with yield. Pearson correlation coefficients ranged between 0.66 to 0.96, and root mean squared error was less than ten percent. Feng et al. (2020) used a modified RGB camera to capture near-infrared, red, and green images along with unmodified RGB and thermal images (canopy temperature) for modeling crop yield with multiple image-derived features. The models had R^2 values up to 0.94

when features from two cameras were used, but they noted that cotton yield estimation may be affected by growth stage. While Akaike's Information Criterion (AIC) was used to evaluate the models, the corresponding R^2 values reported do not appear to be adjusted for the number of predictors. Canopy temperature was often selected as a predictor in the best two and three variable multiple regression models.

Canopy temperature is driven by transpiration, as water evaporation from the leaf surface helps cool the plant (Taiz et al., 2015). Researchers found it was correlated with cotton lint and grain yield as well as important traits such as water use efficiency and leaf water potential (Bai et al., 2016; Colaizzi et al., 2012; O'Shaughnessy et al., 2011). However, the influence of bare soil background was early recognized as a key limitation for accurately estimating canopy temperature with infrared thermography (Cohen et al., 2005; Heilman et al., 1981; Sullivan et al., 2007; Wanjura et al., 1984).

Using a classification technique to identify open cotton bolls in high spatial resolution UAS images, Yeom et al. (2018) calculated cotton boll area for yield estimation. Their algorithm involved initial seed points for which spatial features (e.g. size and shape) were calculated to identify potential cotton bolls. These potential areas were then classified as cotton bolls using the Otsu threshold method (Otsu, 1979). The resultant cotton boll area from this methodology had a strong positive correlation with cotton yield ($R = 0.80$). Jung et al. (2018) classified cotton bolls using a threshold value on the red band from DJI Phantom 2 camera. Boll pixels were clustered into individual cotton bolls then mapped and analyzed using patch analysis. The data were used for a cultivar selection process which improved average lint yield by about 10 percent.

Recent UAS studies such as these focused mostly on RGB cameras and did not leverage high quality narrowband multispectral imagery to incorporate in-season measurements of the cotton canopy into the yield estimation models. Furthermore, information about cotton yield estimation using multispectral pixel-based image classification and especially a combination of in-season vegetation indices and post-defoliation imagery is sparse. These efforts also tend to be limited to imagery from only one camera and one growing season.

UAS have been used to collect RGB and multispectral imagery for modeling yield in other crops (Galli et al., 2020). Except for biomass yield, multispectral features tend to be more closely related to crop yield than features such as plant height generated from RGB imagery (Herrero-Huerta et al., 2020). Most authors endeavored to directly model structural characteristics such as plant height in cotton and other crops, or even to detect sorghum panicles (De Souza et al., 2017; Malambo et al., 2019; Malambo et al., 2018; Pugh et al., 2018). The literature currently lacks thorough investigations in cotton across several growing seasons using multiple image products from UAS multispectral imagery along with other advanced sensors such as thermal infrared cameras. Therefore, the objectives of this study were to 1) determine the efficacy of a pixel-based multispectral image classification technique for cotton yield estimation and 2) develop a multiple linear regression model to enhance the accuracy of cotton yield estimates.

3.2. Materials and Methods

3.2.1. Study Site and Experimental Design

This experiment was conducted from 2017 to 2020 at the Texas A&M University research farm near College Station, Texas (30.550° N, 96.436° W). The field was managed with conventional tillage and subsurface drip irrigation throughout the study period. Belk clay is the prevalent soil series and is classified as fine, mixed, active, thermic Entic Hapluderts. It is very deep, well drained, and very slowly permeable (Soil Survey Staff, 2021). The slope is less than one percent and the climate is classified as humid subtropical. Average annual precipitation is about 100 cm (National Weather Service, 2021) with nearly half of the rainfall typically occurring between April to September during the cotton growing season.

The experiment was a 3x8 factorial design with four repetitions arranged within a completely randomized design. Irrigation rate was the main treatment factor. Irrigation amounts were determined as percent crop evapotranspiration (ET_c) replacement: 80% (full irrigation), 40% (deficit irrigation), and 0% (dryland). In 2017, ET_c was managed at 90%, 45%, and 0%. ETc was estimated using the FAO-56 method described in detail by Allen et al. (1998) and data from a weather station adjacent to the field. The second treatment factor was commercial cotton cultivar. For each season, eight commercial cultivars were planted using a 4-row planter on raised beds at 1 m row spacing. Plots were 12 m long and only the center 2 rows of each plot were measured and harvested for a final plot size of 12 x 2 m.

3.2.2. Cultural Methods

Cotton was planted on April 28 in 2017, April 12 in 2018, April 24 in 2019, and April 16 in 2020. Weed control included pendimethalin as Prowl® H2O (BASF, Ludwigshafen, Germany) pre-emergence herbicide and over-the-top glyphosate applications when necessary. Liquid urea-ammonium nitrate fertilizer (32-0-0) was injected at 112 kg ha^{-1} prior to planting in 2017 and 2020 and at first square in 2018 and 2019. The 2019 cotton received an additional 112 kg ha^{-1} at first white bloom. In 2017, 2018, and 2019, mepiquat chloride was applied at the labeled rate in June or July to limit rank growth, but growth regulator was not necessary in 2020. Chemical defoliants were applied when the irrigated treatment reached 60% open boll. Only the two interior rows of each four-row subplot were harvested using a 2-row spindle picker retrofitted with an onboard scale to measure seed cotton yield by mass. Harvest was in September or early October for 2018 – 2020 but was delayed until October 26th in 2017 due to inclement weather. Residual cotton stalks were shredded following the completion of harvest each year and residue was incorporated via vertical tillage. Raised beds were then prepared in December or January for the next growing season.

3.2.3. Unmanned Aerial Systems and Image Acquisition

The multispectral camera used for the study was a MicaSense RedEdge-3 (MicaSense, Seattle, Washington), which was attached via a fixed-mount on a Matrice 100 quadcopter (SZ DJI Technology Company Limited, Shenzhen, China). The RedEdge-3 has 5 discrete sensors with global shutters and narrow spectral bands (Table 3.1). The thermal camera was an ICI 8640p (Infrared Cameras Incorporated, Beaumont,

Texas). It was attached to an H3 gimbal (Gremsy, Ho Chi Minh City, Vietnam) on a DJI Matrice 600 Pro (Figure 3.1). The ICI 8640P has a 640 x 512 radiometric imager and requires less than 1 watt of power. The sensor was an uncooled microbolometer with a sensitivity of 0.02 °C at 30 °C and produces 14-bit thermal images for the spectral range between 7 – 14 micrometers. The attached lens was a 12.5 mm manual focus lens with 50° by 37.5° field of view.

Figure 3.1. DJI Matrice 600 Pro (left) and Matrice 100 (right) with the Infrared Cameras Incorporated 8640P thermal camera and MicaSense RedEdge-3 multispectral camera onboard, respectively.

Table 3.1. Sensor specifications for the multispectral MicaSense RedEdge-3 camera.

Band Name	Center Wavelength (nm)	Bandwidth/FWHM (nm)
Blue	475	20
Green	560	20
Red	668	10
Red Edge	717	10
Near Infrared	840	40

Flights for both systems were controlled using the UgCS software (UgCS Integrated Systems, Riga, Latvia) photogrammetry tool about every two weeks. Flight

height above ground level (AGL) was at 30m to produce a 2 cm ground sampling distance (GSD) for multispectral imagery at 40m AGL to produce a 5 cm GSD for thermal infrared imagery. Flights were consistently scheduled around solar noon (about 12:30 – 14:30 Central Standard Time) during sunny conditions with minimal wind to ensure adequate image quality. Direct georeferencing (i.e. image metadata alone) was used for image processing in 2017 and 2018, but permanent ground control points (GCP's) were installed into small concrete footings in 2019 and used again in 2020 for extremely consistent placement of reversible photogrammetric targets 0.36 m^2 in size (Figure 3.2). One side was painted matte black and grey for identification in the multispectral imagery to prevent image overexposure in sunny conditions. Low emissivity aluminum tape was applied to the reverse side to ensure a stark contrast for easy target identification. A small hole was drilled in the center of each target to align it over threaded rod in permanent concrete footers. This ensured repeatable georeferencing over time and precise alignment of thermal infrared and multispectral mosaics. GCP's were surveyed using a Reach RS+ GNSS receiver (Emlid Limited, Hong Kong, China) configured for Real Time Kinematic (RTK) corrections from Trimble VRS (Trimble Navigation Limited, Sunnyvale, USA).

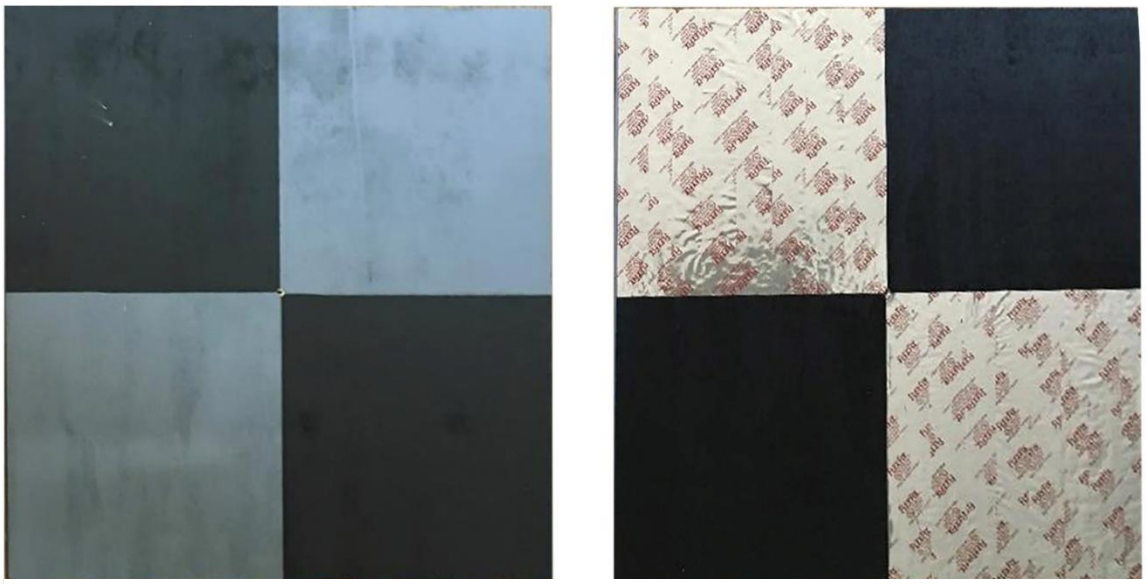

Figure 3.2. Reversible photogrammetric targets were used to ensure precise alignment of multispectral and thermal infrared orthomosaics.

3.2.4. Image Processing and Analysis

Radiometric 16-bit TIFF imagery captured with the MicaSense RedEdge-3 (Table 1) was imported into Pix4Dmapper software (Pix4D S.A., Prilly, Switzerland) and processed using structure from motion (SfM) photogrammetry to produce orthomosaics. The orthomosaics were calibrated to reflectance using image captures of the MicaSense calibration target (a white panel with known reflectance) before and after each flight. Normalized Difference Vegetation Index (NDVI), Normalized Difference Red Edge (NDRE), and Optimized Soil Adjusted Vegetation Index (OSAVI) were calculated from reflectance using the equations shown below:

$$NDVI = \frac{NIR - Red}{NIR + Red} \qquad \text{Equation 1}$$

$$NDRE = \frac{NIR - Red\ Edge}{NIR + Red\ Edge} \qquad \text{Equation 2}$$

$$OSAVI = \frac{NIR - Red}{NIR + Red + 0.16}$$ Equation 3

To isolate image pixels corresponding to bolls, the multispectral orthomosaic from the day of harvest was classified using the supervised Mahalanobis-distance algorithm (Richards, 1999) in ENVI software (Exelis Visual Information Solutions, Boulder, Colorado). Training classes for cotton bolls, soil, and vegetation were selected in random locations throughout the scene to train the Mahalanobis-distance classifier to recognize each cover type. A count of the pixels classified as cotton bolls within each plot was generated using vector boundaries and Zonal Statistics in ArcMap software (ESRI, Redlands, USA). Boll Area Index (BAI) was then calculated by multiplying the cotton pixels counted as bolls within each plot by the image GSD to produce the final area measured in m^2. Finally, average vegetation indices per plot were calculated in ArcMap with the same boundaries. Plot boundaries were adjusted slightly for 2017 and 2018 when they did not perfectly surround the plots due to inaccuracies in georeferencing. However, the same plot boundaries for 2019 and 2020 were used for all spatial analysis due to the high accuracy of the georeferencing in those years where GCP's were used.

Thermal infrared images were converted to radiometric 16-bit TIFF images using proprietary IRFlash software from ICI and processed using Pix4Dmapper. The orthomosaics were calibrated to surface temperature using equations generated from at least four ground reference temperatures captured in the scene during each flight. Pixels from each reference were sampled and averaged using ENVI, paired with the corresponding thermocouple-measured ground reference temperature, and then a linear regression model was built and applied to the orthomosaics in ENVI. This procedure for

calibrating the thermal images to surface temperature is described in detail by Han et al. (2020).

Soil background was removed from the thermal imagery using a temperature threshold determined by looking at the bimodal distribution of canopy and soil temperature. All pixels above the threshold temperature (i.e. soil background) were set to null values to ensure they were ignored in subsequent steps. The remaining canopy was compared visually with a natural-color composite to ensure canopy was accurately separated from bare soil. Finally, average canopy temperatures per plot were calculated using the vector boundaries. See Figure 3.3 for more detailed information on the image processing workflow.

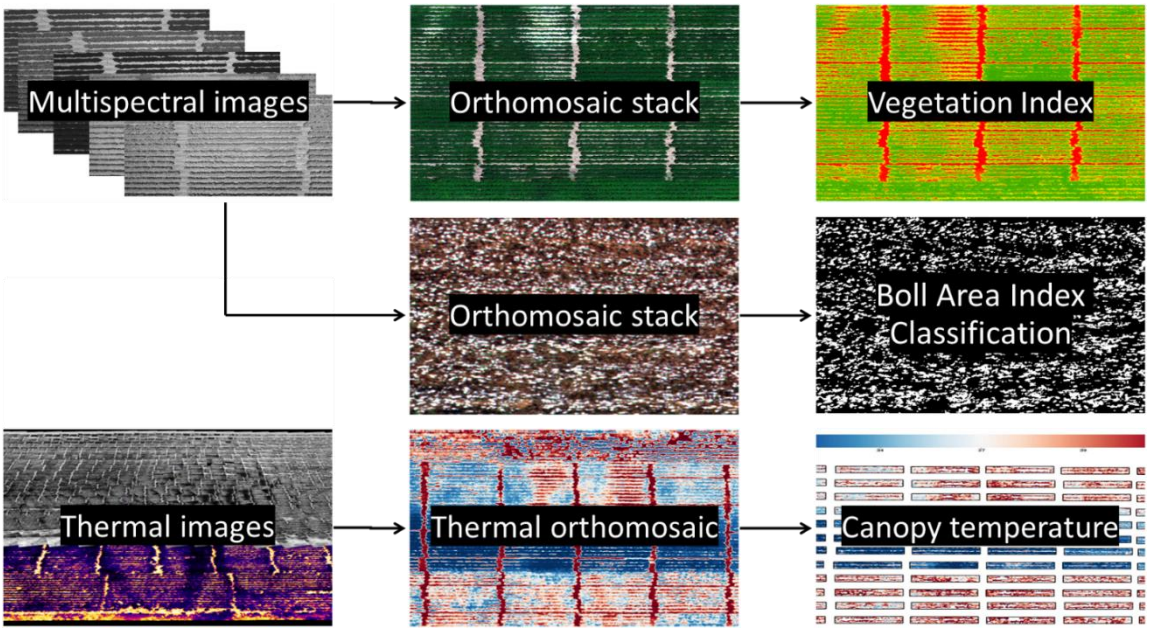

Figure 3.3. Flow chart summarizing steps in the multispectral and thermal image processing workflow.

3.2.5. Data Analysis

Irrigation treatments and cultivars were compared using analysis of variance in R Studio (R Core Team, 2021). Significant differences indicated by ANOVA were then followed with Tukey's Honest Significant Difference (HSD) post-hoc means tests. Multiple linear regression analysis was conducted to examine the relationship between cotton yield and UAS-derived vegetation indices, canopy temperature, and boll area index over four years. Available predictors were evaluated by finding the best multiple regression using the leaps package (Lumley & Miller, 2020) in R Studio. The leaps package returns the most explanatory linear regression model up to a specified number of independent variables using an exhaustive search technique (i.e. all possible subsets) of all the provided variables. Leaps was configured to provide the best subsets model up to four predictors from all image products produced from all flights during each growing season, which included NDVI, NDRE, BAI, and canopy temperature for 2019 and 2020 only. Multiple regression models were further evaluated using the Bayesian Information Criterion (BIC) and Mallow's C_p along with coefficient of determination (R^2), adjusted R^2, root mean squared error (RMSE) and normalized RMSE (NRMSE). NRMSE was calculated by dividing the mean yield from RMSE and then multiplying by 100. The R caret package was used for repeated k-fold cross validation, which was configured for 10 folds repeated 10 times (Kuhn, 2021). Plots of the data (Kassambara, 2021; Wickham, 2009) were generated using heat units accumulated since planting, rather than calendar date, for more universal results linked to crop physiology and seasonal weather variation. Daily heat units were calculated with ambient temperature from an on-site

weather station. The development threshold of 15.6°C (Oosterhuis, 1990) was used in the formula:

$$Heat\ Units = \frac{Max\ Ambient\ Temperature\ °C\ -\ Min\ Ambient\ Temperature\ °C}{2} - 15.6°C$$

3.3. Results and Discussion

3.3.1. Treatment Comparisons Using Boll Area Index

The range of seed cotton yields varied for each growing season and irrigation level (Figure 3.4). Average yield for the dryland treatments ranged from 891 kg ha^{-1} in 2020 to 1,525 kg ha^{-1} in 2018. Mean yield for the deficit irrigated treatments ranged from 1,310 kg ha^{-1} in 2020 to 2,830 kg ha^{-1} in 2018. The irrigated treatments mean yield ranged from 1,724 kg ha^{-1} in 2020 up to 3,195 kg ha^{-1} in 2018. Cetin and Bilgel (2002) observed similar seed cotton yields in subsurface drip irrigated cotton. Overall annual mean yields were 1,997 kg ha^{-1} in 2017, 2,545 kg ha^{-1} in 2018, 2,452 kg ha^{-1} in 2019, and 1,313 kg ha^{-1} in 2020. Yields were lowest in 2020 due to weather complications from nearby hurricane activity that interfered with defoliation and harvest timing. Furthermore, the growing season was shorter in 2020 because of delayed germination caused by cool, dry weather immediately following planting.

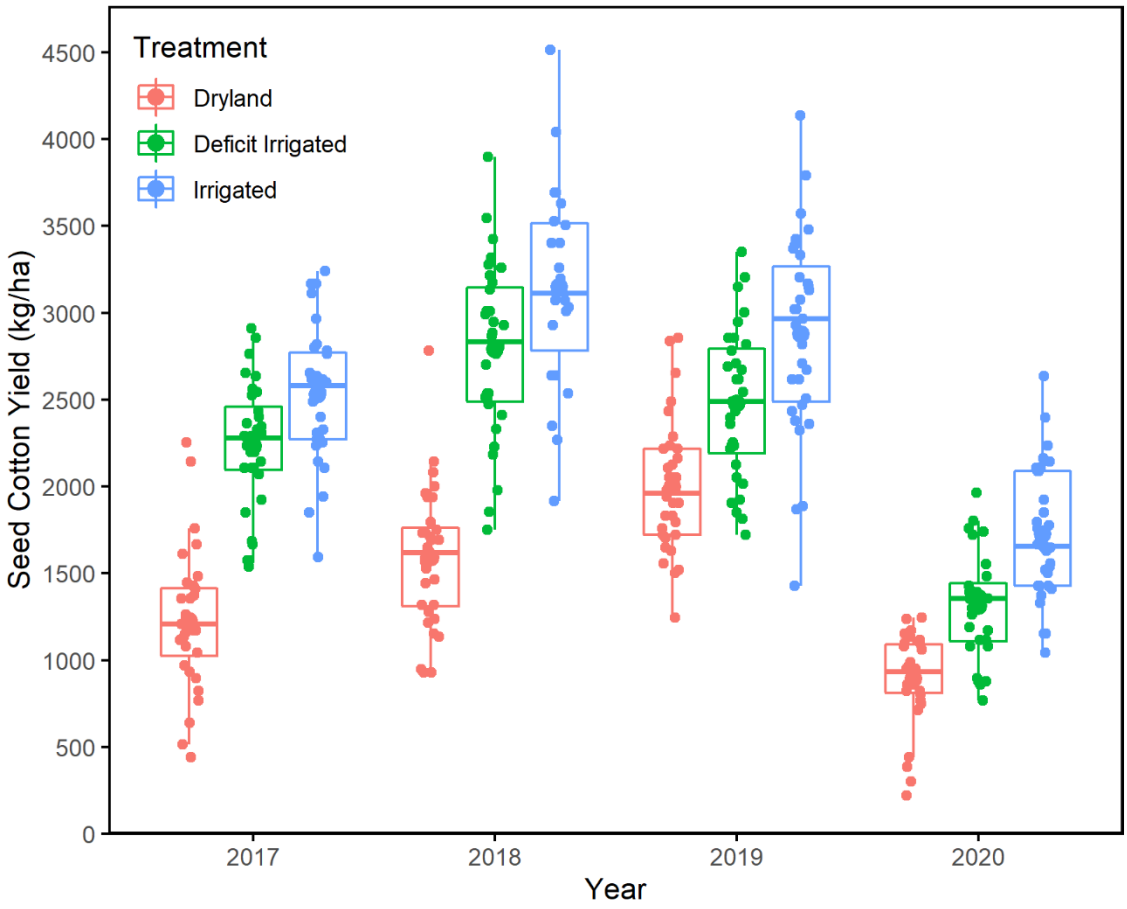

Figure 3.4. Bar plot of seed cotton yield separated by irrigation treatment for all four years in the study.

There were significant differences between the yield of irrigation treatments for all four years of the study. Similarly, BAI indicated significant differences among irrigation levels for each year (Table 3.2). Cotton irrigated at 80% ET_c had greater seed cotton yield than at 40% ET_c irrigation in all years of the study. In contrast, BAI indicated that cotton irrigated at 80% ET was greater than 40% ET in only 1 of the 4 growing seasons. The inability to differentiate irrigation levels with estimation of BAI compared to direct yield measurements could be due to several issues. One is the

propensity of irrigated cotton both to set bolls higher in the canopy (Dube et al., 2020; Pettigrew, 2004) and produce larger bolls which could cause the difference between mean BAI for irrigated and deficit irrigated treatments to be more subtle. In addition to boll size and position, drip irrigated cotton produces higher yields than other irrigation methods at lower irrigation levels by increasing the number of bolls produced per plant (Cetin & Bilgel, 2002). Plant height also increases with the amount of irrigation applied (DeTar, 2008). This makes it more likely that bolls were at least partially occluded by stems or other bolls in the imagery, and therefore the increase in BAI with increasing cotton yield may be limited. Although the GSD of the imagery used to derive BAI was fine (1.2 to 2 cm), it is possible that a smaller GSD would better capture these differences.

Table 3.2. Analysis of variance for cotton yield and corresponding Boll Area Index (BAI) during the same year for all years in the study.

Source of Variation	DF	F-value	Pr > F	F-value	Pr > F
		2017 Yield		**2017 BAI**	
Irrigation	2	146.668	< 0.0001	66.336	< 0.0001
Cultivar	7	6.034	< 0.0001	4.433	0.000383
Irrigation x Cultivar	14	1.508	0.13	2.467	0.006624
		2018 Yield		**2018 BAI**	
Irrigation	2	90.379	< 0.0001	59.233	< 0.0001
Cultivar	7	2.217	0.0444	3.289	0.00481
Irrigation x Cultivar	14	1.201	0.2975	0.846	0.61819
		2019 Yield		**2019 BAI**	
Irrigation	2	41.171	< 0.0001	22.23	< 0.0001
Cultivar	7	8.236	< 0.0001	19.009	< 0.0001
Irrigation x Cultivar	14	0.682	0.785	0.486	0.934

		2020 Yield		2020 BAI	
Irrigation	2	42.33	< 0.0001	118.495	< 0.0001
Cultivar	7	1.619	0.144	7.137	< 0.0001
Treatment x Cultivar	14	0.8	0.666	1.395	0.178

In 2020, all irrigation levels were different both by yield and BAI (Table 3.3). There were significant differences in BAI among cultivars even when there were not for yield (Table 3.4), but cultivar ranked by BAI did not match rank by yield in any case. This suggests that although BAI may indicate differences between cultivars, BAI should not be used for cultivar comparisons without ancillary data. Further investigation is warranted to determine the cause of these cultivar differences, such as plant architecture along with previously mentioned factors like bolls distributed higher or lower in the canopy.

Table 3.3. Treatment means comparisons of cotton yield data and Boll Area Index (BAI) during the same year.

Treatment	Mean Yield (kg ha^{-1})	BAI
	2017	
Irrigated	2530 a	1.343 a
Deficit Irrigated	2232 b	1.328 a
Dryland	1228 c	0.758 b
	2018	
Irrigated	3196 a	2.727 a
Deficit Irrigated	2830 b	2.579 a
Dryland	1614 c	1.127 b
	2019	
Irrigated	2879 a	4.241 a
Deficit Irrigated	2479 b	3.929 a
Dryland	1999 c	3.123 b

	2020	
Irrigated	1724 a	1.644 a
Deficit Irrigated	1183 b	0.899 b
Dryland	866 c	0.295 c

Table 3.4. Cultivar mean comparisons of cotton yield data and Boll Area Index (BAI) during the same year.

Cultivar	Mean Yield (kg ha^{-1})	Mean BAI
2017		
Phytogen 499	2275 a	1.384 a
Phytogen 333	2140 ab	1.171 ab
Stoneville 4946	2125 ab	1.249 ab
DeltaPine 1646	2123 ab	1.231 ab
FiberMax 1900	2116 ab	0.974 b
NexGen 1511	1751 b	0.996 b
FiberMax 2484	1735 b	1.070 ab
DeltaPine 1549	1707 b	1.068 ab
2018		
Stoneville 4946	2727	2.023 ab
Phytogen 499	2722	2.724 a
DeltaPine 1646	2634	2.324 ab
NexGen 1511	2537	2.182 ab
FiberMax 1900	2457	1.910 ab
DeltaPine 1549	2347	2.073 ab
FiberMax 2484	2210	1.873 b
Phytogen 333	2185	1.567 b
2019		
Phytogen 580	2931 a	5.410 a
Phytogen 480	2707 ab	4.075 b
DeltaPine 1845	2607 ab	3.447 bcd
Phytogen 350	2576 abc	4.145 b
DeltaPine 1646	2382 bcd	3.633 bc
Deltapine 1835	2319 bcd	3.969 b

Stoneville 4550	2090 cd	2.629 d
FiberMax 2398	1985 d	2.806 cd
2020		
Phytogen 400	1469	1.051 abc
Phytogen 580	1456	1.445 a
NexGen 5711	1265	0.674 c
Stoneville 4550	1256	1.003 abc
DeltaPine 1845	1185	0.690 c
NexGen 4936	1182	1.156 ab
FiberMax 2398	1170	0.842 bc
DeltaPine 1646	1080	0.709 bc

3.3.2. Relationship between Boll Area Index and Yield

There was a positive linear relationship between Boll Area Index (BAI) and yield in 2017 (R^2 = 0.57, Figure 3.5). As the area classified as cotton bolls increased, there was a corresponding increase in yield. In-season NDVI at 1239 heat units or 101 DAE had a stronger relationship with yield (R^2 = 0.61) than BAI. Since the cotton in 2017 was taller than the other three years, a likely explanation is that cotton bolls lower in the canopy were occluded by those closer to the top. This was the only year in which NDVI outperformed BAI. Vegetation indices should be explored as a second predictor in growing seasons during which managing plant height is more difficult.

In 2018, BAI had a strong relationship with yield (R^2 = 0.79). This result is comparable to the NDVI model at 1108 heat units, which had an R^2 of 0.78 and similar RMSE. BAI also explained much of the yield variation in 2019 (Figure 3.5) with an R^2 of 0.67 and RMSE of 366.9 kg ha^{-1} (NRMSE = 15%) that outperformed the best vegetation index model (NDRE) during that year. In 2020, repeated rain events and wind

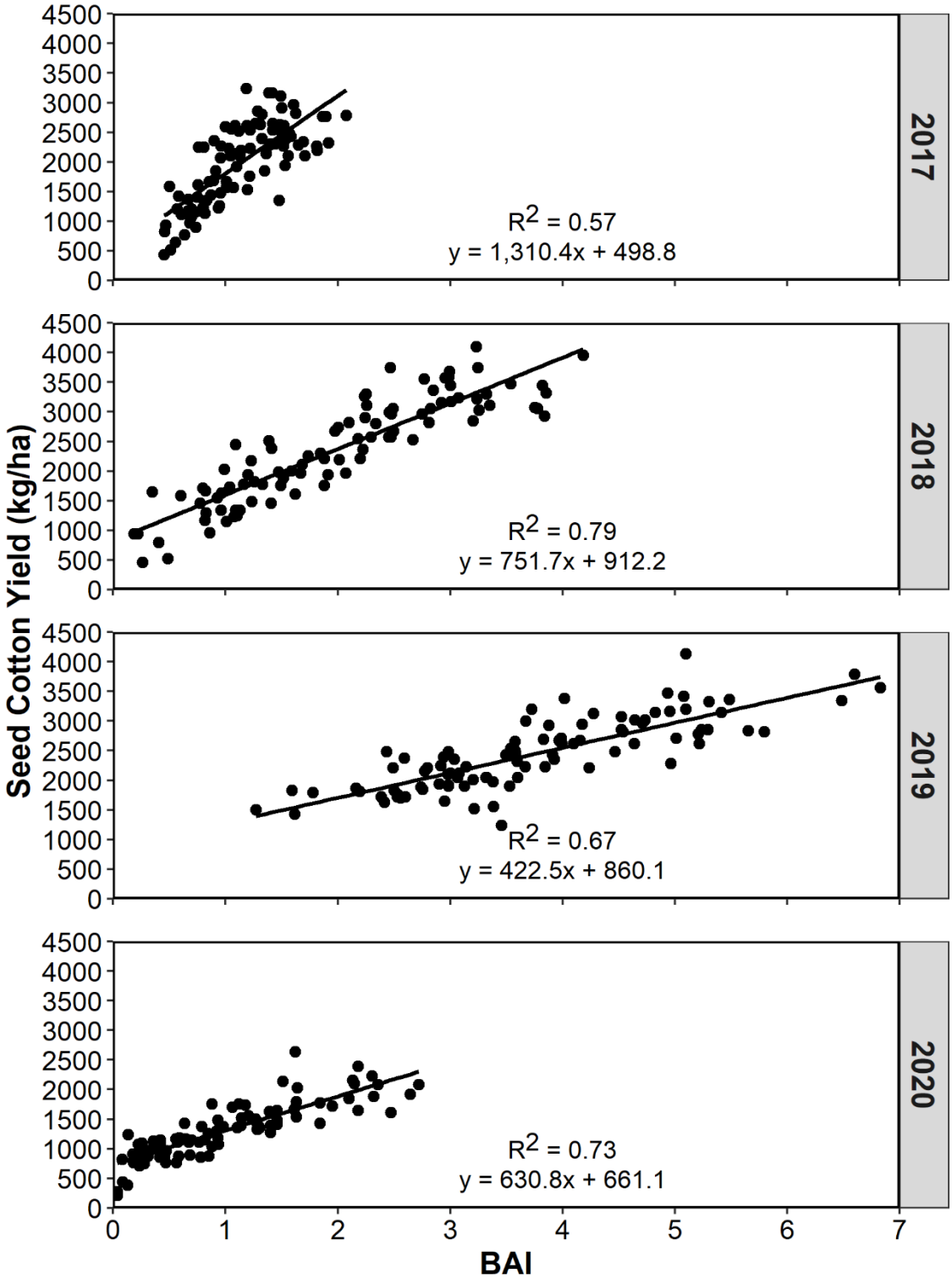

Figure 3.5. Positive linear relationship between boll area index (BAI) and seed cotton yield for the four cotton growing seasons between 2017-2020.

(tropical weather) after physiological maturity reduced seed cotton recovered by the picker and thus decreased observed yield. Despite this, BAI had a strong relationship with yield (R^2 = 0.73, RMSE = 245.2). BAI alone provided only slightly better estimates than in-season NDVI alone at 1154 heat units or 102 DAE: R^2 for both models was 0.73, but RMSE was 3.4 kg ha^{-1} higher for NDVI.

BAI had stronger relationships with yield in the irrigated and deficit irrigated treatments than the dryland treatment for all years except 2017 (Table 3.5). This is likely due to bolls distributed lower in the canopy, decreased boll size, and increased presence of soil background in the dryland treatments. All of these could increase the difficulty for accurately classifying cotton bolls in the imagery. This is especially true for low quality imagery from cheaper cameras, but classifications for this study were accurate. Furthermore, irrigated cotton plants tend to set bolls higher in the canopy, closer to the top of the plant where they would be more easily identified in nadir imagery (Dube et al., 2020; Pettigrew, 2004). Boll area index consistently had strong relationships with seed cotton yield and generally had higher R^2 values and lower RMSE than vegetation indices.

Table 3.5. Linear regression results for relationships between boll area index (BAI) and seed cotton yield separated by treatment for the cotton growing seasons between 2017-2020.

Irrigation Treatment	Coefficient of Determination (R^2)			
	2017	2018	2019	2020
Irrigated	0.14	0.58	0.76	0.42
Deficit Irrigated	0.23	0.65	0.68	0.56
Dryland	0.37	0.46	0.38	0.37

3.3.3. Multiple Regression Models for Cotton Yield Estimation

To develop more robust models for cotton yield prediction, multiple regression models were evaluated. BAI, NDVI, NDRE, OSAVI, and canopy temperature were all included as potential predictors. The strongest multiple regression model included BAI along with both NDVI and NDRE at 400 heat units. Including the vegetation indices improved the Adjusted R^2 to 0.79 from 0.57 using BAI alone and reduced the RMSE to 321.6 kg ha^{-1} (NRMSE = 16%). Aside from incorporating early season crop vigor into the regression, it is unclear why the vegetation indices at 400 heat units were selected as part of this model. Imagery from early in the growing season was not generally selected otherwise. The best model with two predictors (Adjusted R^2 = 0.7) consisted of BAI and NDVI at 1327 heat units. Both multiple linear regression models required only two UAS flights: one during the growing season and one just prior to harvest, after defoliation. The model with three variables (BAI, NDVI, and NDRE) was optimal based on minimizing BIC and C_p (Table 3.6). OSAVI produced similar results but did not improve upon multiple regressions selected by the best subsets algorithm.

In 2018, the best multiple regression model with two predictors included BAI and NDVI at 1108 heat units for an Adjusted R^2 of 0.87 and RMSE of 306.6 kg ha^{-1}. Adding NDRE as the third predictor increased the Adjusted R^2 slightly to 0.89 and reduced the RMSE to 283 kg ha^{-1} (NRMSE = 11.9%). This model with three variables (BAI, NDVI, and NDRE) was optimal based on the lowest BIC value (Table 3.6). Both models had considerably less error (80 - 103 kg ha^{-1}) than vegetation indices or BAI alone. This was the best multiple regression model by BIC out of the study and suggests

Table 3.6 Multiple linear regression results using the best subset of all possible combinations with Adjusted R^2, Root Mean Squared Error (RMSE), Bayesian Information Criterion (BIC), and Mallow's C_p.

2017					Selected Variables
Variables	Adj. R^2	RMSE	BIC	C_p	
1	0.61	425.8	-80.9	114.7	NDVI (1239)
2	0.70	373.4	-102.6	67.3	BAI + NDVI (1327)
3	0.79	312.6	-133.2	21.1	BAI + NDVI (400) + NDRE (400)
4	0.80	305.8	-133.9	17.1	BAI + NDVI (400) + NDRE (400) + NDVI (1327)
2018					
Variables	Adj. R^2	RMSE	BIC	C_p	**Selected Variables**
1	0.79	383.3	-128.6	98.0	BAI
2	0.87	306.6	-163.9	33.5	BAI + NDVI (1108)
3	0.89	283.0	-174.5	17.4	BAI + NDVI (1108) + NDRE (1108)
4	0.89	281.8	-171.8	17.4	BAI + NDVI (1108) + NDRE (1108) + NDVI (1279)
2019					**Selected Variables**
Variables	Adj. R^2	RMSE	BIC	C_p	
1	0.67	343.4	-95.1	143.0	BAI
2	0.82	249.8	-152.0	33.4	BAI + NDRE (1390)
3	0.84	233.0	-161.7	18.4	BAI + NDRE (1390) + TIR (1237)
4	0.85	227.7	-162.6	14.6	BAI + NDRE (330) + NDRE (1237) + TIR (1237)
2020					**Selected Variables**
Variables	Adj. R^2	RMSE	BIC	C_p	
1	0.73	245.2	-111.1	47.5	BAI
2	0.80	212.2	-134.0	14.6	BAI + NDVI (897)
3	0.81	204.7	-137.0	8.6	BAI + NDVI (709) + TIR (897)
4	0.82	202.1	-135.9	7.3	BAI + NDVI (469) + NDVI (1154) + TIR (897)

The number in parenthesis following each variable corresponds to heat units accumulated on the flight date. BAI = Boll Area Index, NDVI = Normalized Difference Vegetation Index, NDRE = Normalized Difference Red Edge, TIR = Thermal Infrared (canopy temperature).

that the accuracy of yield estimates could be adequate for some purposes with multiple products (e.g. NDVI, BAI) from the same multispectral camera. These results are comparable to Feng et. al (2020), who observed NRMSE around 10% or lower for

cotton yield models derived from UAS imagery from two or more cameras. OSAVI was not selected for any of the best subset models.

For 2019, adding NDRE at 1390 heat units as the second predictor increased the Adjusted R^2 to 0.82 and reduced the RMSE to 250 kg ha^{-1} (NRMSE = 10.2%). Further including canopy temperature at 1237 heat units in the multiple linear regression increased the Adjusted R^2 slightly to 0.84 and reduced the RMSE to 233 kg ha^{-1} (NRMSE = 9.5%). This multiple regression model with BAI, NDRE, and canopy temperature had a slightly higher BIC and C_p (Table 3.6) than the model with four predictors, but BIC difference was marginal. OSAVI had slightly better model R^2 than NDVI in 2019, but neither were selected in a best subset because NDRE performed better. The best in-season model from a single day, i.e. a multispectral flight followed immediately by a thermal infrared flight, included NDRE at 1237 heat units or about 100 DAE (Adjusted R^2 = 0.67). The NDRE regression model alone had an R^2 of 0.56 and canopy temperature alone had an R^2 of 0.38. Herrero-Huerta et al. (2020) similarly observed improved soybean yield predictions by fusing data from multiple sensors for machine learning modeling approaches. The eXtreme Gradient Boosting and Random Forest regressions had lower R^2 values (0.38 – 0.42) than observed for cotton in this study.

Including 2020 BAI with NDVI at 897 heat units as the second predictor increased Adjusted R^2 to 0.80 and reduced the RMSE to 211.5 kg ha^{-1} (NRMSE = 16.1%). Including canopy temperature from the same day resulted in minimal improvements. The best in-season model from a single day occurred at 897 heat units or

about 83 DAE. At this point, NDVI and canopy temperature together had an Adjusted R^2 of 0.76 while reducing the RMSE by about 15 kg ha^{-1} from the NDVI alone, which provided more accurate in-season predictions (84 days prior to harvest) that rival post-season predictions. OSAVI (R^2 = 0.73) performed similarly to NDVI but was not selected for either multiple regression model. See Table 3.6 for a summary of the best regression subsets.

Although BAI alone did not always provide the best yield estimates, incorporating it into multiple regression models with vegetation indices or canopy temperature always reduced error. For this reason, it should be considered for endeavors to estimate cotton yield after defoliation is complete or around harvest time. Canopy temperature from thermal imagery improved in-season yield estimation models and should be considered as part of in-season efforts. However, it provided minimal improvement as a third predictor for post-defoliation estimates because multiple regressions of NDVI and BAI already had quite strong relationships with yield (R^2 = 0.7 to 0.87). Three predictors were optimal for multiple linear regression models with one year of data because BIC improved only marginally with a fourth predictor. This differs from findings in other crops, such as those of Galli et al. (2020), who found that the best results for predicting grain yield in sorghum required only a single flight date and vegetation index with the same multispectral camera used in this study.

3.3.4. Multi-year Yield Estimation with Boll Area Index

A multiple linear regression of all four years BAI with NDVI (at ~1200 heat units) for yield estimation resulted in an Adjusted R^2 of 0.68 and moderate error (RMSE

= 461 kg ha^{-1}, NRMSE = 22.6%). Cross validation produced similar results even when split by treatment, although NRMSE decreased for the irrigated and deficit irrigated models (Table 3.7). Including NDVI in the models potentially compensates for year-to-year variations of vegetative growth or vertical distribution of cotton bolls in the canopy, which varies with irrigation and genotype (Dube et al., 2020; Pettigrew, 2004).

A multiple linear regression model built from 2018 – 2019 BAI and NDVI data could predict 2020 cotton yield with reasonable accuracy (RMSE = 216.1 kg ha^{-1}, NRMSE = 16.5%) and has a slope of approximately one (Figure 3.7), which suggests that the model is well calibrated. The data from 2017 was excluded because image GSD was different than all other years. A model such as this built from historical data could therefore enhance the early stages of pedigree selection (Rutkoski et al., 2016) by helping to eliminate the worst performing lines prior to harvesting numerous small plots to ensure labor intensive data collection efforts are not wasted on lines that would be eliminated anyways. There is likely too much error for this methodology to be useful later in the crop improvement process.

Table 3.7. Cross validation results for multiple regression models of Boll Area Index and NDVI on seed cotton yield.

Treatments	R^2	RMSE (kg ha^{-1})	NRMSE	MAE (kg ha^{-1})
Irrigated	0.64	445.3	18.1	349.5
Deficit Irrigated	0.62	432.1	19.3	361.9
Dryland	0.68	319.9	22.3	247.4
All	0.68	441.5	21.6	359.6
2018 - 2019	0.51	507.9	21.0	407.0

R^2 = Coefficient of Determination, RMSE = Root Mean Squared Error, NRMSE = Normalized RMSE, MAE = Mean Absolute Error

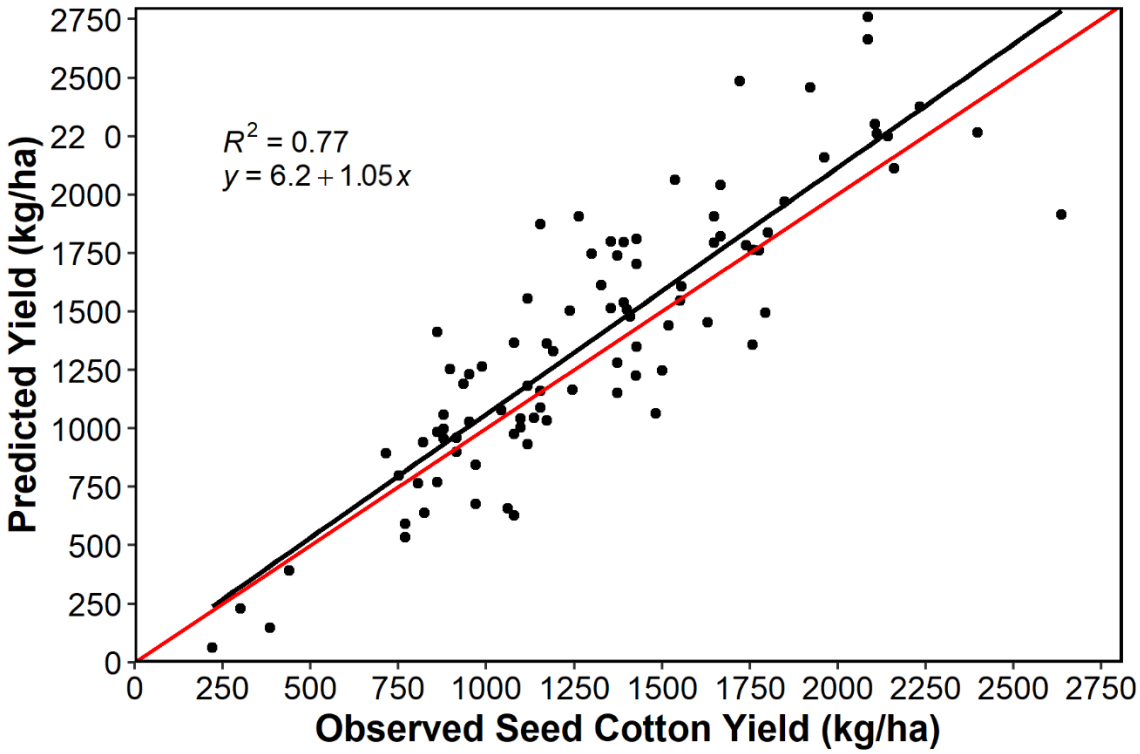

Figure 3.6. Observed yield vs. 2020 predicted yield from the multiple regression model built from 2018 – 2019 BAI and NDVI. The validation regression is the black line and the line with a slope of one is red in color.

Multiple regression with a second image product (e.g. vegetation index or canopy temperature) or more advanced machine learning techniques should be strongly considered to limit error. A subset of the plots could be harvested for calibrating the BAI-yield model each year to help reduce labor and machinery costs. An advantage of BAI over vegetation indices is that weeds are easily classified out and therefore do not adversely impact the methodology as long as weeds are not occluding harvested bolls from the imagery. Feng et al. (2020) similarly found that two image features (i.e. two predictors) are adequate to estimate cotton yield while keeping image processing and model complexity to a minimum. Canopy temperature from thermal imagery most often increased the efficacy of in-season multiple regression models (R^2 increased by up to 0.14), so cameras or payloads with both optical and thermal sensors are ideal for in-season estimation endeavors but not necessary near harvest or after defoliation. Regardless, boll area index can reduce cotton yield estimation error and should be considered as part of high-throughput phenotyping methodologies.

3.4. Conclusions

Irrigation and cotton cultivar have a significant effect on boll area index, which was derived using a pixel-based multispectral image classification methodology. BAI was not reliable for comparison of irrigated and deficit irrigated treatment means, providing statistical results comparable to cotton yield only in 2020. While vegetation indices provide a simple means of estimating cotton yield in-season, after defoliation BAI had stronger relationships with seed cotton yield in all years but 2017. BAI has potential to substantially reduce error with a modest increase in image processing

requirements and only one additional flight after defoliation. Including NDVI acquired during the bloom period optimally at around 1200 heat units with BAI for multiple linear regression models reduced error substantially, and 2020 yield was estimated with reasonable accuracy using the model built from data collected in 2018 – 2019. Focusing UAS image collection efforts on just two or three flight dates per growing season delivers a robust dataset while striving to efficiently utilize labor and computational resources. This suggests that the methodology could be useful for cotton breeders to enhance efficiency during the early stages of pedigree selection by identifying the worst performing lines prior to labor-intensive harvest and related data collection efforts from which these poor performing lines could be excluded. However, the methodology may not be adequate for screening advanced lines later in the process when accuracy is more critical.

3.5. References

Allen, R. G., Pereira, L. S., Raes, D., & Smith, M. (1998). Crop evapotranspiration-Guidelines for computing crop water requirements-FAO Irrigation and drainage paper 56.

Bai, G., Ge, Y., Hussain, W., Baenziger, P. S., & Graef, G. (2016). A multi-sensor system for high throughput field phenotyping in soybean and wheat breeding. *Computers and Electronics in Agriculture*, 128, 181-192.

Cetin, O., & Bilgel, L. (2002). Effects of different irrigation methods on shedding and yield of cotton. *Agricultural Water Management*, *54*(1), 1-15. https://doi.org/https://doi.org/10.1016/S0378-3774(01)00138-X

Cohen, Y., Alchanatis, V., Meron, M., Saranga, Y., & Tsipris, J. (2005). Estimation of leaf water potential by thermal imagery and spatial analysis. *J Exp Bot*, 56(417), 1843-1852. https://doi.org/10.1093/jxb/eri174

Colaizzi, P. D., O'Shaughnessy, S. A., Evett, S. R., & Howell, T. A. (2012). Using canopy temperature to improve irrigated crop management. Publications from USDA-ARS / UNL Faculty. https://digitalcommons.unl.edu/usdaarsfacpub/1820

Crookston, R. K. (2006). A Top 10 List of Developments and Issues Impacting Crop Management and Ecology During the Past 50 Years. *Crop science*, *46*(5), 2253-2262. https://doi.org/10.2135/cropsci2005.11.0416gas

De Souza, C. H. W., Lamparelli, R. A. C., Rocha, J. V., & Magalhães, P. S. G. (2017). Height estimation of sugarcane using an unmanned aerial system (UAS) based on

structure from motion (SfM) point clouds. *International Journal of Remote Sensing*, *38*(8-10), 2218-2230. https://doi.org/10.1080/01431161.2017.1285082

DeTar, W. R. (2008). Yield and growth characteristics for cotton under various irrigation regimes on sandy soil. *Agricultural Water Management*, *95*(1), 69-76. https://doi.org/https://doi.org/10.1016/j.agwat.2007.08.009

Dube, N., Bryant, B., Sari-Sarraf, H., & Ritchie, G. L. (2020). Cotton boll distribution and yield estimation using three-dimensional point cloud data. *Agronomy Journal*, *112*(6), 4976-4989. https://doi.org/10.1002/agj2.20412

Feng, A., Sudduth, K., Vories, E., Zhang, M., & Zhou, J. (2018). Cotton Yield Estimation based on Plant Height From UAV-based Imagery Data. 2018 ASABE Annual International Meeting,

Feng, A., Zhou, J., Vories, E. D., Sudduth, K. A., & Zhang, M. (2020). Yield estimation in cotton using UAV-based multi-sensor imagery. *Biosystems Engineering*, *193*, 101-114. https://doi.org/10.1016/j.biosystemseng.2020.02.014

Galli, G., Horne, D. W., Collins, S. D., Jung, J., Chang, A., Fritsche-Neto, R., & Rooney, W. L. (2020). Optimization of UAS-based high-throughput phenotyping to estimate plant health and grain yield in sorghum. *The Plant Phenome Journal*, *3*(1). https://doi.org/10.1002/ppj2.20010

Han, X., Thomasson, J. A., Swaminathan, V., Wang, T., Siegfried, J., Raman, R., Rajan, N., & Neely, H. (2020). Field-Based Calibration of Unmanned Aerial Vehicle Thermal Infrared Imagery with Temperature-Controlled References. *Sensors*, *20*(24), 7098. https://www.mdpi.com/1424-8220/20/24/7098

Heilman, J., Heilman, W., & Moore, D. (1981). Remote Sensing of Canopy Temperature at Incomplete Cover. *Agronomy Journal*, 73(3), 403-406.

Herrero-Huerta, M., Rodriguez-Gonzalvez, P., & Rainey, K. M. (2020). Yield prediction by machine learning from UAS-based mulit-sensor data fusion in soybean. *Plant Methods*, *16*, 78. https://doi.org/10.1186/s13007-020-00620-6

Huang, Y., Brand, H. J., Sui, R., Thomson, S. J., Furukawa, T., & Ebelhar, M. W. (2016). Cotton yield estimation using very high-resolution digital images acquired with a low-cost small unmanned aerial vehicle. *Transactions of the ASABE*, *59*(6), 1563-1574.

ISPA. (2021). *Precision Ag Definition*. International Society of Precision Agriculture. https://www.ispag.org/about/definition

Jung, J., Maeda, M., Chang, A., Landivar, J., Yeom, J., & McGinty, J. (2018). Unmanned aerial system assisted framework for the selection of high yielding cotton genotypes. *Computers and Electronics in Agriculture*, *152*, 74-81. https://doi.org/10.1016/j.compag.2018.06.051

Kassambara, A. (2021). ggpubr: 'ggplot2' Based Publication Ready Plots. In https://CRAN.R-project.org/package=ggpubr

Kuhn, M. (2021). Misc functions for training and plotting classification and regression models. In https://cran.r-project.org/package=caret

Lumley, T., & Miller, A. (2020). *leaps: Regression Subset Selection*. In https://CRAN.R-project.org/package=leaps

Maja, J. M. J., Campbell, T., Neto, J. C., & Astillo, P. (2016). Predicting cotton yield of small field plots in a cotton breeding program using UAV imagery data. Autonomous Air and Ground Sensing Systems for Agricultural Optimization and Phenotyping,

Malambo, L., Popescu, S. C., Horne, D. W., Pugh, N. A., & Rooney, W. L. (2019). Automated detection and measurement of individual sorghum panicles using density-based clustering of terrestrial lidar data. *ISPRS Journal of Photogrammetry and Remote Sensing*, *149*, 1-13. https://doi.org/10.1016/j.isprsjprs.2018.12.015

Malambo, L., Popescu, S. C., Murray, S. C., Putman, E., Pugh, N. A., Horne, D. W., Richardson, G., Sheridan, R., Rooney, W. L., Avant, R., Vidrine, M., McCutchen, B., Baltensperger, D., & Bishop, M. (2018). Multitemporal field-based plant height estimation using 3D point clouds generated from small unmanned aerial systems high-resolution imagery. *International Journal of Applied Earth Observation and Geoinformation*, *64*, 31-42. https://doi.org/10.1016/j.jag.2017.08.014

Menefee, D., Rajan, N., Cui, S., Bagavathiannan, M., Schnell, R., & West, J. (2020). Carbon exchange of a dryland cotton field and its relationship with PlanetScope remote sensing data. *Agricultural and Forest Meteorology, 294*. https://doi.org/10.1016/j.agrformet.2020.108130

Mulla, D. J. (2013). Twenty five years of remote sensing in precision agriculture: Key advances and remaining knowledge gaps. *Biosystems Engineering*, *114*(4), 358-371. https://doi.org/10.1016/j.biosystemseng.2012.08.009

National Weather Service. (2021). *College Station Extremes, Normals, and Annual Summaries* https://www.weather.gov/hgx/climate_cll_normals_summary

Oosterhuis, D. M. (1990). *Growth and Development of a Cotton Plant* (W. N. Miley & D. M. Oosterhuis, Eds.). https://doi.org/https://doi.org/10.2134/1990.nitrogennutritionofcotton.c1

O'Shaughnessy, S. A., Evett, S. R., Colaizzi, P. D., & Howell, T. A. (2011). Using radiation thermography and thermometry to evaluate crop water stress in soybean and cotton. *Agricultural Water Management*, 98(10), 1523-1535. https://doi.org/10.1016/j.agwat.2011.05.005

Otsu, N. (1979). A threshold selection method from gray-level histograms. *IEEE transactions on systems, man, and cybernetics*, *9*(1), 62-66.

Pettigrew, W. T. (2004). Moisture Deficit Effects on Cotton Lint Yield, Yield Components, and Boll Distribution. *Agronomy Journal*, *96*(2), 377-383. https://doi.org/https://doi.org/10.2134/agronj2004.3770

Pugh, N. A., Horne, D. W., Murray, S. C., Carvalho, G., Malambo, L., Jung, J., Chang, A., Maeda, M., Popescu, S., Chu, T., Starek, M. J., Brewer, M. J., Richardson, G., & Rooney, W. L. (2018). Temporal Estimates of Crop Growth in Sorghum and Maize Breeding Enabled by Unmanned Aerial Systems. *The Plant Phenome Journal*, *1*(1), 1-10. https://doi.org/10.2135/tppj2017.08.0006

R Core Team. (2021). *R: A Language and Environment for Statistical Computing*. In R Foundation for Statistical Computing. https://www.R-project.org/

Richards, J. A. (1999). *Remote sensing digital image analysis* (Vol. 3). Springer.

Rutkoski, J., Poland, J., Mondal, S., Autrique, E., Pérez, L. G., Crossa, J., Reynolds, M., & Singh, R. (2016). Canopy Temperature and Vegetation Indices from High-Throughput Phenotyping Improve Accuracy of Pedigree and Genomic Selection for Grain Yield in Wheat. *G3: Genes|Genomes|Genetics*, 6(9), 2799-2808. https://doi.org/10.1534/g3.116.032888

Shi, Y., Thomasson, J. A., Murray, S. C., Pugh, N. A., Rooney, W. L., Shafian, S., Rajan, N., Rouze, G., Morgan, C. L., Neely, H. L., Rana, A., Bagavathiannan, M. V., Henrickson, J., Bowden, E., Valasek, J., Olsenholler, J., Bishop, M. P., Sheridan, R., Putman, E. B., Popescu, S., Burks, T., Cope, D., Ibrahim, A., McCutchen, B. F., Baltensperger, D. D., Avant, R. V., Jr., Vidrine, M., & Yang, C. (2016). Unmanned Aerial Vehicles for High-Throughput Phenotyping and Agronomic Research. *PLoS One*, *11*(7), e0159781. https://doi.org/10.1371/journal.pone.0159781

Soil Survey Staff. (2021). *Soil Survey Geographic (SSURGO) Database*. Natural Resources Conservation Service, United States Department of Agriculture.

Sugiura, R., Noguchi, N., & Ishii, K. (2005). Remote-sensing Technology for Vegetation Monitoring using an Unmanned Helicopter. *Biosystems Engineering*, *90*(4), 369-379. https://doi.org/10.1016/j.biosystemseng.2004.12.011

Sullivan, D., Fulton, J., Shaw, J., & Bland, G. (2007). Evaluating the sensitivity of an unmanned thermal infrared aerial system to detect water stress in a cotton canopy. *Transactions of the ASABE*, 50(6), 1963-1969.

Taiz, L., Zeiger, E., Moller, I. M., & Murphy, A. (2015). Plant Physiology and Development (6 ed.). Sinauer Associates, Inc.

Wanjura, D., Kelly, C., Wendt, C., & Hatfield, J. (1984). Canopy temperature and water stress of cotton crops with complete and partial ground cover. *Irrigation Science*, 5(1), 37-46.

Wickham, H. (2009). *ggplot2: Elegant Graphics for Data Analysis*. In Springer-Verlag New York. http://ggplot2.org

Yeom, J., Jung, J., Chang, A., Maeda, M., & Landivar, J. (2018). Automated Open Cotton Boll Detection for Yield Estimation Using Unmanned Aircraft Vehicle (UAV) Data. *Remote Sensing*, *10*(12), 1895.

4. UAS-DERIVED CANOPY TEMPERATURE FOR ASSESSING COTTON YIELD AND IRRIGATION TREATMENTS

4.1. Introduction

Water use efficiency and drought tolerance are key traits for crop improvement programs, especially as pressure on available water resources continues to increase and the climate becomes more unpredictable. Climate projections for Texas indicate that conditions in the second half of the 21st century will be drier than the most arid times in the last millennium (Nielsen-Gammon et al., 2020). Increasing irrigation efficiency and leveraging data to improve irrigation management decisions is similarly important, but it is necessary to account for both spatial and temporal variability in soil moisture caused by factors such as soil texture and uneven irrigation application. While mapping soil physical characteristics has become simpler through technologies such as electromagnetic induction sensing (Huang et al., 2016; McBratney et al., 2005; Sudduth et al., 2001), mapping soil moisture at both fine spatial and temporal resolutions during the growing season is less practical. However, canopy temperature is closely related to both crop and soil water status (Jackson et al., 1981) and advances in technology have made it possible to map canopy temperature using thermal cameras onboard unmanned aerial systems (UAS) at fine spatiotemporal resolution.

The main crop physiological process that drives variability in canopy temperature is transpiration. Water is pulled from the xylem into the leaf mesophyll, evaporates into the air spaces, and then diffuses out of the leaf through the stomatal

pores (Taiz et al., 2015). For uptake of water through the roots and transport through the xylem to leaves, plants must maintain a water potential gradient and turgor pressure through transpiration. Transpiration provides a cooling effect for plants via the evaporation of water from the leaf surfaces. Water deficit stress induces stomatal closure, which inhibits transpiration and limits evaporative cooling (Burke & Upchurch, 1989). This causes leaf temperatures, and thus canopy temperature, to increase relative to an unstressed, actively transpiring plant that can better regulate its temperature. Water stress and heat stress together can increase canopy temperature by several degrees Celsius, which can cause many adverse reactions in the plant (Taiz et al., 2015).

Scientists have shown that infrared thermography can be useful for precision agriculture and more specifically for precision irrigation management (Colaizzi et al., 2012). Spatial variability of canopy temperature is closely related to irrigation management practices, irrigation application uniformity, and more directly to water deficit within the effective rooting zone of plants (Padhi et al., 2012; Pinter et al., 2003). Infrared thermography also has potential advantages over gas-exchange measurements in plant phenotyping studies where stomatal responses are important (Ishimwe et al., 2014), as canopy temperature measurements are not labor intensive (Ihuoma & Madramootoo, 2017). Canopy temperature has performed similarly to multispectral vegetation indices for grain and lint yield estimation (Bai et al., 2016; O'Shaughnessy et al., 2011) and is strongly correlated to traits such as water use efficiency, leaf water potential, as well as derived water stress detection indices such as Crop Water Stress Index (Colaizzi et al., 2012). Thermal imagery could also be applied for disease detection, mapping soil

properties, tillage mapping, drainage tile mapping, crop maturity mapping, and leaf water potential mapping (Cohen et al., 2005; Khanal et al., 2017).

However, limitations remain for using available data for precision agriculture purposes. While thermal data from satellite platforms such as Landsat is freely available, the spatial and temporal resolutions (e.g. 100 meters and 16 days for Landsat 8) are currently too coarse for use in irrigated agriculture at commercial scales (Pinter et al., 2003). Scientists have endeavored to capture canopy temperature more frequently by placing infrared thermometers (IRT's) in the field or mounting them onto center pivot and linear irrigation systems (Colaizzi et al., 2017; O'Shaughnessy & Evett, 2010; O'Shaughnessy et al., 2012). However, the irrigation systems must be in operation to map canopy temperature, and the measurements are susceptible to the effects of soil background prior to canopy closure. Andrade-Sanchez et al. (2014) used two IRT's with different orientations to help separate canopy temperature from bare soil on a phenotyping rover. One sensor was pointed downward at nadir while the other had an oblique view facing forward down the row. An IRT can only capture single point measurements in the sensor field of view and lack the spatial detail that thermal cameras provide.

Scientists early identified the adverse impact of bare soil background as one of the major limitations of using infrared thermography for detecting canopy stress. This is especially true during early growth when canopy cover is low, in dryland production systems, and in semi-arid regions where the canopy does not completely cover the ground (Cohen et al., 2005; Heilman et al., 1981; Sullivan et al., 2007; Wanjura et al.,

1984). Canopy temperature and indices derived from thermal imagery can overestimate water stress due to much warmer soil temperatures combining with cool crop temperatures (Pinter et al., 2003). Researchers have previously tried to address this issue by including a multispectral vegetation index to account for canopy cover in modeling endeavors (Bai et al., 2017; Clarke, 1997; Clarke et al., 2001; Gan et al., 2018; Moran et al., 1994). While this improved water deficit stress detection with thermal imagery, removing soil background altogether was identified early as the ideal solution (Jackson et al., 1981). Scientists have begun investigating machine learning for leveraging rich datasets captured from UAS, but few researchers use techniques such as support vector machines or random forests to detect crop water stress (Virnodkar et al., 2020).

More recently, scientists have similarly endeavored to use ancillary RGB imagery to limit the influence of soil background (Ge et al., 2016). Drew et al. (2019) developed a method to isolate crop canopy from thermal images by using a visible camera to distinguish between soil background and crop canopy. While this technique may be useful for cameras such as the FLIR Duo ® Pro R (FLIR Systems Incorporated, Wilsonville, USA) that have an integrated color camera, more expensive thermal infrared cameras with dedicated sensors alone are typically more sensitive to subtle variations in temperature.

While UAS now enable the collection of thermal imagery at unprecedented spatial resolutions that are fine enough to allow removal of soil background, few scientists have explored techniques to accomplish this in row-cropping systems without ancillary data sources. Literature exploring cotton yield estimation with thermal imagery

is also sparse. Therefore, the objectives of this study were to 1) evaluate unmanned aerial infrared thermography for detecting differences in crop water stress across irrigation regimes and cotton cultivars 2) explore the relationship between UAS-derived canopy temperature and cotton yield across irrigation regimes, and 3) examine the relationship between soil moisture and UAS-derived canopy temperature.

4.2. Materials and Methods

4.2.1. Study Site

This experiment was conducted in 2019 and 2020 in a subsurface drip irrigated field at the Texas A&M University research farm near College Station, Texas (30.550° N, 96.436° W). The field was managed with conventional tillage during this period and for more than 10 years prior to beginning the project. Belk clay, which is a fine, mixed, active, thermic Entic Hapluderts, is the prevailing soil type at the site (Soil Survey Staff, 2021). The slope of the field is less than 1 percent. The Koppen climate classification is humid subtropical, and average annual precipitation is 1018 mm (Menefee et al., 2020). Weather data was collected on-site from a station built directly adjacent to the study field. Daily averages were used in subsequent calculations.

4.2.2. Experimental Design and Cultural Practices

The experiment was a 3x8 factorial design within a completely randomized design arrangement and had four repetitions. The first factor was irrigation rate as a percentage of estimated crop evapotranspiration (ET_c) requirement with three levels at 80% (irrigated), 40% (deficit), and 0% (dryland). Data logged by the on-site weather station was used to estimate ET_c requirements based on the FAO-56 method described

by Allen et al. (1998). Commercial cotton cultivar was the second factor. Eight cultivars were planted per growing season in April into four-row plots which were 12 meters in length. Seedbeds with 1 meter row spacing were prepared in December or January for the subsequent season.

Cultural practices were similar between the two growing seasons. Weed control strategies included pre-emergence herbicide and glyphosate applied over-the-top when needed. Urea-ammonium nitrate fertilizer (32-0-0) was band applied via knives at squaring in 2019 and prior to planting in 2020. To limit rank growth in 2019, mepiquat chloride was applied at the labeled rate. Chemical defoliants were applied at the end of September when the irrigated treatments reached approximately 60% open boll. During the first week of October, the two center rows of the four-row plots were harvested with a 2-row spindle picker. The picker was retrofitted with a scale inside the basket to measure seed cotton yield mass. Cotton stalks were destroyed with a flail shredder following harvest, and the residue was later incorporated by means of vertical tillage.

4.2.3. Soil Volumetric Water Content

Soil moisture data (volumetric water content) was collected continuously with time domain reflectometry sensors (Model CS655, Campbell Scientific, Logan, UT) placed near the center of 6 subplots at 15 cm and 30 cm depths across the same cotton cultivar and in each irrigation treatment with two replications: 6 locations and 12 sensors total. These sensors were installed on June 7 in 2019 and June 8 in 2020 and connected to a Campbell CR1000x datalogger with a 1-minute scan interval and 15-minute

average. The VWC measurements logged during each UAS flight were averaged for analysis. The sensors were removed prior to chemical defoliation.

4.2.4. Unmanned Aerial System and Image Acquisition

An ICI 8640P (Infrared Cameras Incorporated, Beaumont, USA) thermal infrared camera was used in the study (Figure 4.1). The thermal camera was attached to a DJI Matrice 600 Pro hexacopter (SZ DJI Technology Company Limited, Shenzhen, China) on a Gremsy H3 gimbal (Gremsy, Ho Chi Minh City, Vietnam) to maintain nadir view during flight. The ICI 8640P camera has a 640 x 512 radiometric imager that produces 14-bit thermal imagery for the spectral range between 7 – 14 μm. The sensor is a microbolometer with a sensitivity of 0.02 °C at 30 °C and requires less than a watt of operating power. The camera, which has a 12.5 mm manual focus lens with 50° by 37.5° field of view, was focused by hand on the ground using a laser rangefinder to position a photogrammetric target at the appropriate distance (40m). The focusing ring was permanently marked to ensure the camera was correctly focused prior to each flight. Using UgCS flight control software (UgCS Integrated Systems, Riga, Latvia), photogrammetry missions were flown at approximately 40m above ground level (AGL) to produce a 5 cm ground sampling distance (GSD). Four flights were conducted in 2019 on July 9, July 25, August 12, and August 22. Four flights were conducted in 2020 on July 3, July 16, August 4, and August 18.

Temperature-controlled reference targets made of aluminum plates about 60 x 60 cm were prepared in the scene before each flight for calibration purposes (Han et al.,

2020). One reference target was heated for the high temperature reference (50°C) while the other was cooled to serve as the low temperature reference (20°C). Temperature was measured with 9 thermistors distributed evenly across each reference plate and average temperatures during the flight were used for calibration. Optimal weather, such as sunny conditions and minimal wind between about 12:30 - 14:30 (near solar noon), were prioritized to ensure quality image capture. Permanent ground control points (Figure 4.2) were installed with concrete footings and surveyed using a Reach RS+ Global Navigation Satellite System receiver (Emlid Limited, Hong Kong, China) with Trimble VRS real-time kinematic corrections (Trimble Navigation Limited, Sunnyvale, USA).

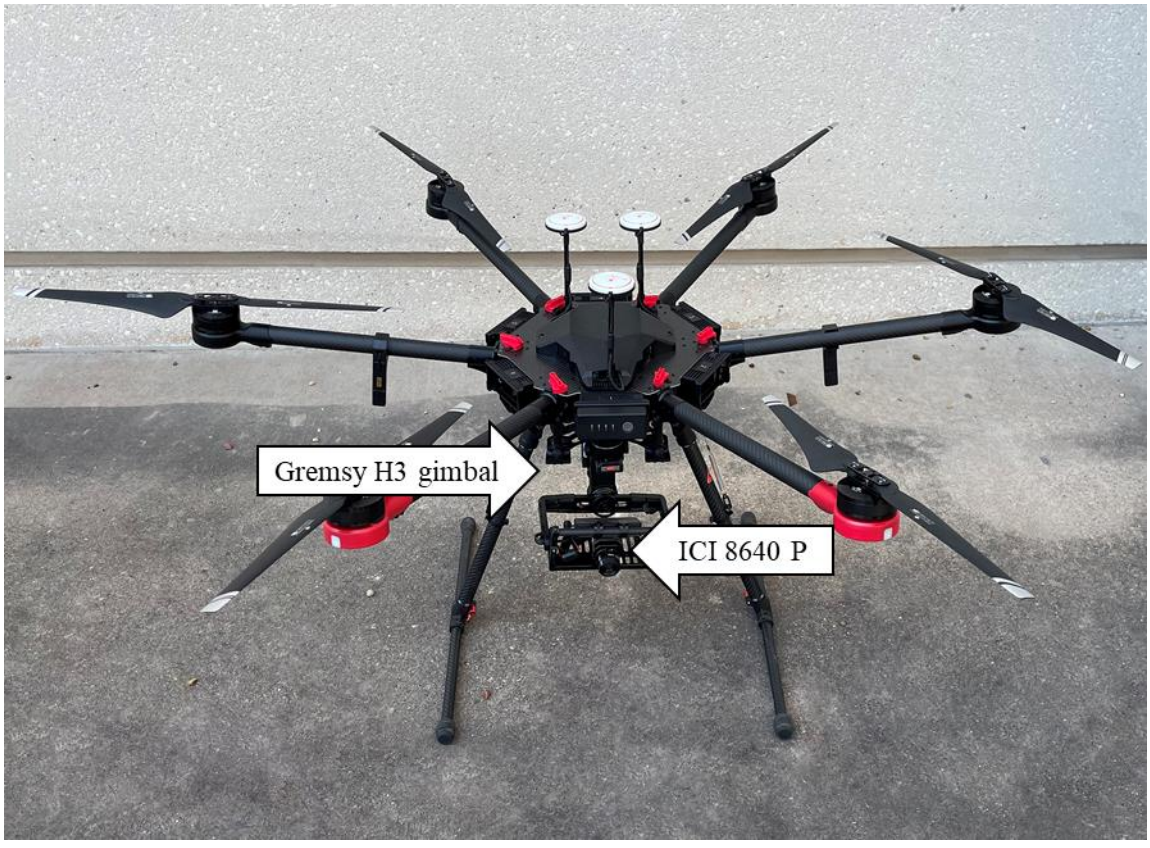

Figure 4.1. Infrared Cameras Incorporated 8640p thermal infrared camera attached to a Gremsy H3 gimbal. The gimbal mount includes a rubber damping system to isolate any vibration produced by the Matrice 600 Pro hexacopter.

Figure 4.2. Photogrammetric targets were used to ensure accurate georeferencing of thermal infrared orthomosaics. Low emissivity aluminum tape ensured a stark contrast for easy target identification in the thermal images. A small hole was drilled in the center of each target to align it over threaded rod in permanent concrete footers.

4.2.5. Image Processing and Analysis

After each flight, raw 16-bit TIFF images were exported from ICI proprietary software. Unnecessary images during pre-flight checks, takeoff, and the landing sequence were removed prior to importing the images and ground control point positions into Pix4Dmapper. Orthorectified mosaics were generated using structure from motion photogrammetry (Pix4D S.A., Prilly, Switzerland). As described in detail by Han et al. (2020), the heated and cooled temperature reference targets were identified in the orthomosaics and paired with their measured temperatures to build a linear regression model relating the thermal image digital numbers to measured temperature references. The equation from this regression was used to apply a radiometric calibration to produce a final orthomosaic with surface temperature in degrees Celsius. A threshold temperature was then selected for each orthomosaic using the bimodal temperature data histogram of all temperatures within the orthomosaic. Canopy temperatures were separated from soil temperatures by identifying the minimum or trough centered between the two local maxima (peaks) in the bimodal distribution. All pixels above this identified temperature threshold, which essentially represented the maximum canopy temperature in the orthomosaic, were set to a null value using ArcMap (ESRI, Redlands, USA). To confirm the threshold was accurate, the new image was displayed over a natural-color composite to ensure it matched the canopy area. This effectively removed soil background from the surface temperature mosaics. Finally, a single canopy temperature for each plot was derived by averaging the temperatures within the plot vector boundaries (Figure 4.3).

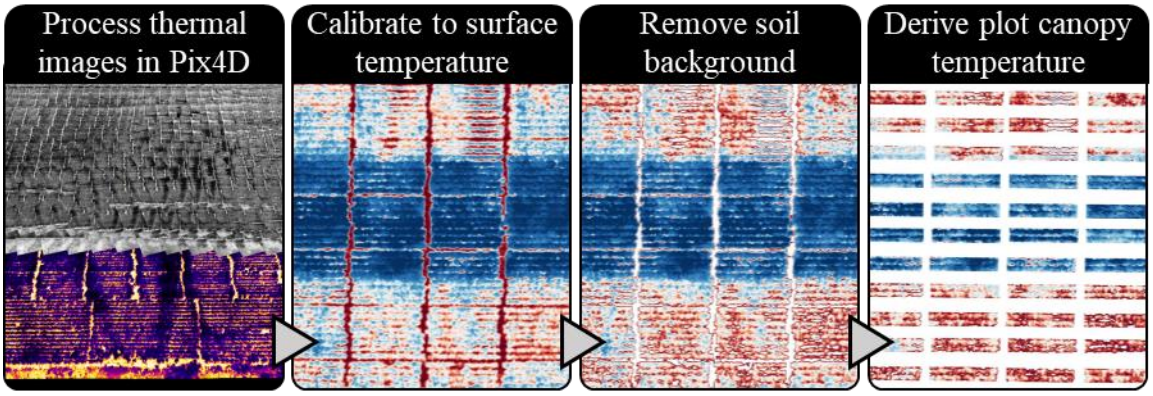

Figure 4.3. Flow chart summarizing steps in the thermal infrared image processing workflow. Cool temperatures are represented by blue colors while red colors indicate warm temperatures.

4.2.6. Data Analysis

Linear regression analysis was conducted in R Studio (R Core Team, 2021) to examine the relationship between canopy temperature and yield and between canopy temperature and soil moisture for 8 UAS flight dates over two years. All available canopy temperature data within each year was also analyzed with multiple regression using the R leaps package (Lumley & Miller, 2020), which returned the model with the highest Adjusted R^2 value. The exhaustive search method included all possible subsets and was configured to select a maximum of 3 predictors. Linear models were evaluated using R^2, root mean squared error (RMSE) and normalized RMSE (NRMSE). NRMSE was calculated by dividing RMSE by mean yield and multiplying by 100. Analysis of variance (ANOVA) of yield and canopy temperature was conducted in R Studio. Post-hoc means comparisons were made using Tukey's Honestly Significant Difference (HSD).

To account for seasonal weather variation and to provide a more universal and physiological basis for analysis, the data was plotted against heat units accumulated after planting rather than by time with R packages ggplot2 and ggpubr (Kassambara, 2021; Wickham,2009). Daily heat units were calculated using on-site ambient temperature and the development threshold temperature of 15.6°C (Oosterhuis, 1990) as in the following equation:

$$Heat\ Units = \frac{Max\ Ambient\ Temperature\ °C\ -\ Min\ Ambient\ Temperature\ °C}{2} - 15.6°C$$

4.3. Results and Discussion

4.3.1. Irrigation Treatment Effects on Canopy Temperature

There were significant differences in yield among irrigation levels in both 2019 and 2020 (Table 4.1). There were also significant differences among irrigation levels for canopy temperature on all flight dates in 2019 and 2020. Pairwise comparisons for mid-season canopy temperature matched yield results (Table 4.2), where all irrigation levels were different. However, in 2020 the 80% ET_c irrigation and 40% ET_c deficit irrigation treatments were not different by canopy temperature earlier in the growing season (July) when less than 1000 heat units had accumulated. In 2019, there was no significant difference between deficit irrigated and dryland at 989 heat units (July 3). This was due to 50 mm rainfall during the previous two weeks largely negating the need for irrigation in the deficit irrigated treatment.

Treatment means comparisons during July always indicated two groups, where irrigated and deficit irrigated treatments were usually not different. All irrigation

treatments were different than the others for the flights conducted in August (as early as 1154 heat units). Irrigated treatments consistently had lower mean canopy temperatures, and dryland cotton had higher canopy temperatures relative to other irrigation levels in each year (Figure 4.4).

Table 4.1. Analysis of variance for cotton yield and corresponding canopy temperature (CT) for all years in the study. Accumulated heat units are presented in parenthesis behind each flight date.

Source of Variation	DF	F-value	Pr > F	F-value	Pr > F
		2019 Yield		**2020 Yield**	
Irrigation	2	41.171	< 0.0001	42.33	< 0.0001
Cultivar	7	8.236	< 0.0001	1.619	0.144
Irrigation x Cultivar	14	0.682	0.785	0.8	0.666
		CT on 7/9/19 (774)		**CT on 7/3/20 (709)**	
Irrigation	2	4.438	0.0152	57.787	< 0.0001
Cultivar	7	2.108	0.0534	1.85	0.092
Irrigation x Cultivar	14	0.684	0.7827	1.105	0.37
		CT on 7/25/19 (989)		**CT on 7/16/20 (897)**	
Irrigation	2	41.054	< 0.0001	211.61	< 0.0001
Cultivar	7	0.94	0.482	0.688	0.681
Irrigation x Cultivar	14	0.661	0.804	0.554	0.89
		CT on 8/12/19 (1237)		**CT on 8/4/20 (1154)**	
Irrigation	2	378.18	< 0.0001	155.674	< 0.0001
Cultivar	7	0.965	0.463	3.999	0.001
Irrigation x Cultivar	14	0.682	0.784	0.296	0.99296
		CT on 8/22/19 (1390)		**CT on 8/18/20 (1356)**	
Irrigation	2	435.168	< 0.0001	68.835	< 0.0001
Cultivar	7	2.018	0.0645	8.051	< 0.0001
Irrigation x Cultivar	14	1.377	0.1876	0.855	0.609

Table 4.2. Tukey's HSD post hoc test results for comparison of treatment means for yield data and canopy temperature for each year. Accumulated heat units are presented in parenthesis behind each flight date.

Treatment	Yield (kg ha^{-1})	Canopy Temperature (°C)			
2019		**7/9/19 (774)**	**7/25/19 (989)**	**8/12/19 (1237)**	**8/22/19 (1390)**
Irrigated	2879.2 a	31.02 a	31.07 a	33.87 a	29.37 a
Deficit Irrigated	2479.2 b	31.25 ab	32.24 b	38.28 b	34.46 b
Dryland	1998.5 c	31.55 b	32.55 b	39.38 c	35.75 c
2020		**7/3/20 (709)**	**7/16/20 (897)**	**8/4/20 (1154)**	**8/18/20 (1356)**
Irrigated	1724.4 a	32.87 a	32.87 a	33.8 a	35.51 a
Deficit Irrigated	1183.1 b	33.27 a	33.27 a	35.5 b	37.43 b
Dryland	866.2 c	35.20 b	35.20 b	37.0 c	38.05 c

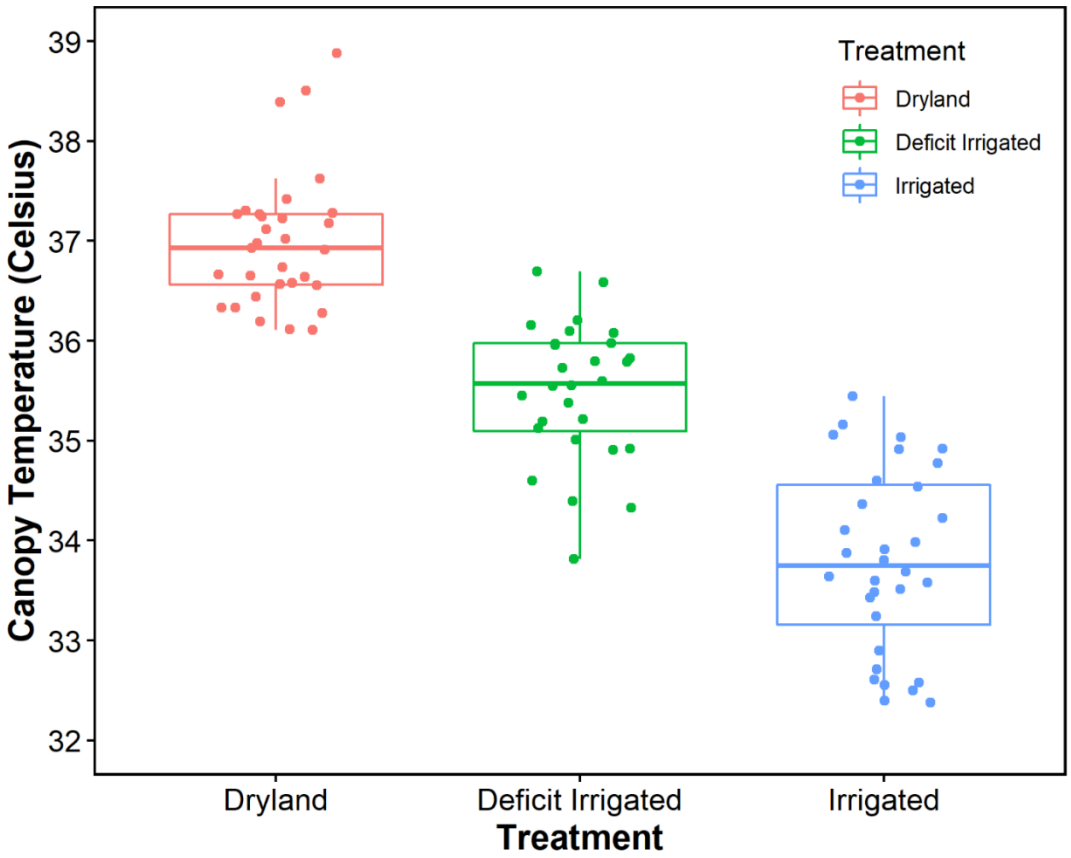

Figure 4.4. Box and whisker plot of cotton canopy temperature separated by Irrigation Treatment for August 4, 2020 at 1154 heat units.

There were not any significant differences in canopy temperatures among cultivars in 2019 for any flight date. However, there were significant differences ($p < 0.05$) in canopy temperatures among cultivars in the August 2020 imagery despite the lack of differences in seed cotton yield. While cultivars with cooler canopy temperatures also generally had higher yields, relative cultivar canopy temperatures were not always consistent with final yield (Table 4.3). This could be related to the ability of each cotton cultivar to recover from water deficit or related heat stress while minimizing yield loss. When screening for traits related to drought tolerance, Thorp et al. (2018) similarly found significant differences in cultivar crop water use efficiency estimates (yield divided by amount of water consumed) derived from UAS multispectral remote sensing and noted that incorporating canopy temperature could improve crop water use efficiency estimates. Results suggest that canopy temperature could be used to target labor-intensive data collection efforts such as plant gas exchange measurements, which are sensitive to the severity of crop drought stress (Baker et al., 2007).

Table 4.3. Tukey's HSD post hoc test results for comparison of cultivar means for yield data and canopy temperature on 8/4/20 at 1154 heat units and on 8/18/20 at 1356 heat units.

Cultivar	2020 Yield (kg ha^{-1})	Canopy Temp. (°C) 8/4/20	Canopy Temp. (°C) 8/18/20
Phytogen 400	1469.3 a	35.3 abc	36.4 ab
Phytogen 580	1456.0 a	34.8 a	35.9 a
NexGen 5711	1265.2 a	35.5 abc	37.3bcd
Stoneville 4550	1255.7 a	35.2 ab	37.5 cd
DeltaPine 1845	1184.7 a	35.0 ab	36.5 abc
NexGen 4936	1182.5 a	36.0 c	36.8 abc

FiberMax 2398	1170.1 a	35.8 abc	37.6 cd
DeltaPine 1646	1079.8 a	35.8 bc	38.1 d

4.3.2. Relationship Between Yield and Canopy Temperature

There were strong negative linear relationships between canopy temperature and yield in 2019 and 2020. Cotton plots with cooler canopy temperatures had higher yields, while plots with hotter temperatures had reduced yields. The linear regression models with canopy temperature from a single date had R^2 values that ranged from 0.39 to 0.72

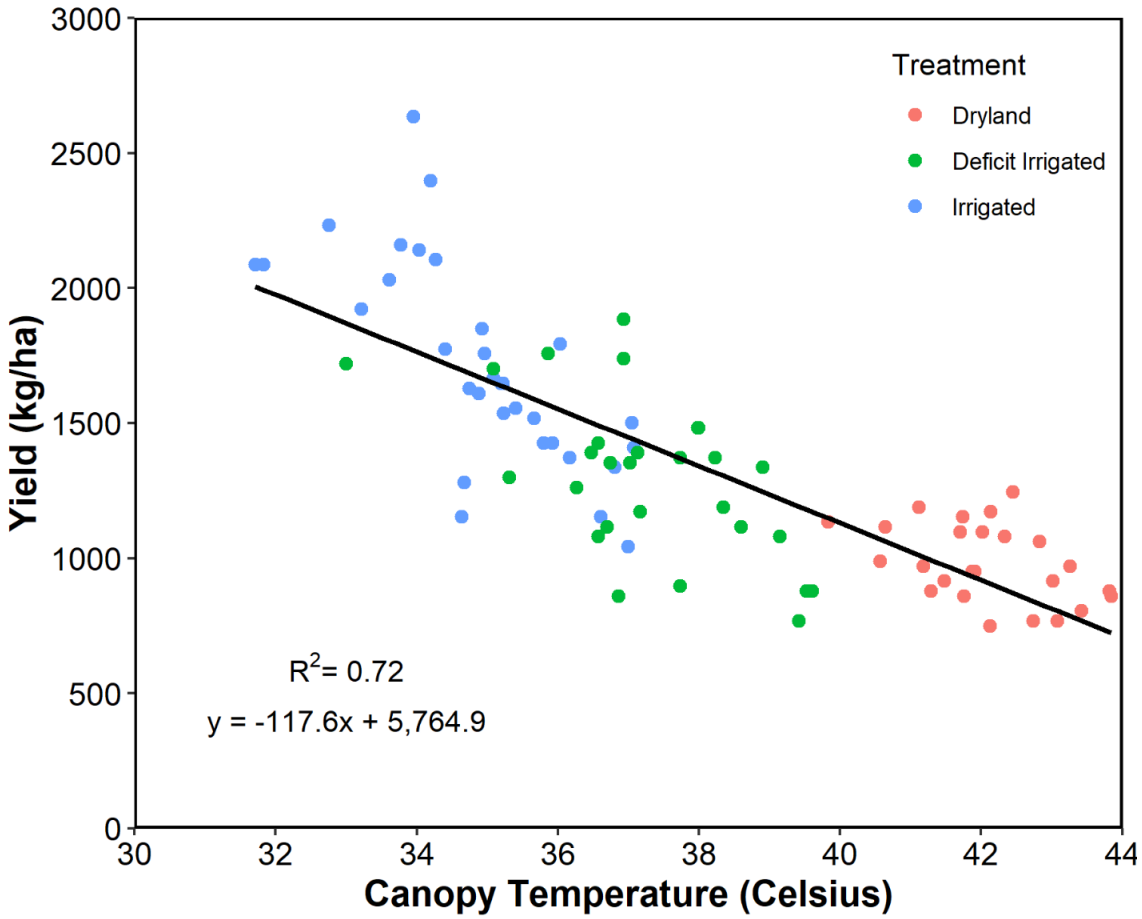

Figure 4.5. Negative linear relationship between seed cotton yield and canopy temperature on July 16, 2020 (897 heat units) represented by black line. Plots with cooler canopy temperatures tended to produce higher yields. Conversely, plots with warmer temperatures tended to yield lower.

(Figure 4.5) with RMSE's of 299.2 and 249.7 kg ha^{-1}, respectively. Thompson et al. (2020) found similarly strong relationships between cotton yield and canopy temperature measured with proximal sensors mounted on a high clearance sprayer. The best subset multiple regression model in 2019 included canopy temperature at 774 heat units (July 9) and 1237 heat units (August 12) and had an adjusted $R^2 = 0.57$ and RMSE of 372.7 kg ha^{-1} (NRMSE = 15.2%). The best subset multiple regression model for 2020 had an adjusted $R^2 = 0.72$ and RMSE of 250.1 kg ha^{-1} (NRMSE = 19.2%) and included canopy temperature from 709 and 897 heat units or July 3 and July 16, respectively. While the error is moderate, these models are early enough in the growing season to adjust management practices in a commercial production setting. Both best subsets models included two independent variables (i.e. canopy temperature from two dates). UAS-derived canopy temperature could be used as timely data to help efficiently distribute irrigation water spatially through variable rate irrigation systems. Furthermore, issues with irrigation systems such as clogged sprinklers and field characteristics such as suboptimal terrain and drainage could be identified in the imagery and further used as part of cost-benefit analysis for weighing mitigation options.

4.3.3. Relationship Between VWC and Canopy Temperature

Canopy temperature from the thermal orthomosaics generally had negative linear relationships with VWC. In 2019, only canopy temperature at 1237 heat units (August 12) had a significant relationship with VWC at 15 cm deep ($R^2 = 0.5$). This was following a period of minimal precipitation and shortly after applying most of the

irrigation (Figure 4.6). The relationship between canopy temperature from the same date with VWC at 30cm deep was much stronger (R^2 = 0.9). VWC at 30 cm was correlated with canopy temperature at 1390 heat units on August 22 (R^2 = 0.37). The quantity of roots at 30 cm and deeper is much greater than roots at 15 cm (Ritchie et al., 2007), so it follows that VWC at 30 cm would be more strongly related to canopy temperature. Although Kamara et al. (1991) previously noted that emitter depth of drip irrigation did not affect cotton root depth or distribution, the 30 cm sensors were also closer to the depth of the drip tape. Out of both years, August 12 in 2019 (1237 heat units) was the

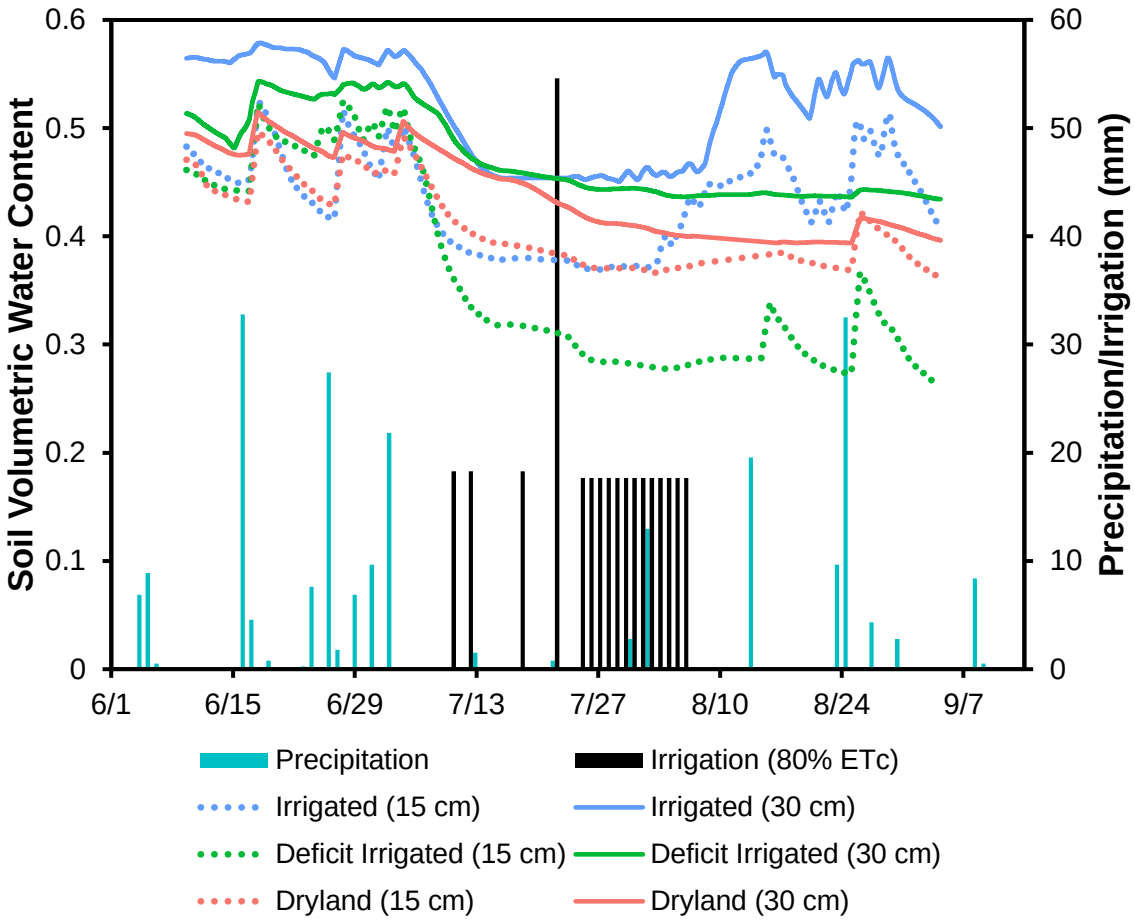

Figure 4.6. Daily precipitation and 80% ET_c irrigation amounts during the 2019 cotton growing season. Lines and dashed lines represent soil volumetric water content within each irrigation treatment.

only image date for which soil VWC also had significant differences among irrigation treatments, which were observed at both 15 cm ($P = 0.04$) and 30 cm ($P = 0.007$) depths. Soil VWC at 30 cm furthermore had a strong relationship with yield on the same date ($R^2 = 0.81$).

In 2020, there was a positive linear relationship ($R^2 = 0.48$) between VWC at 15 cm and canopy temperature at 897 heat units on July 3. There was limited range in VWC (0.41 for 80% ET_c irrigated, 0.37 for 40% ET_c deficit irrigated, and 0.46 for dryland) across irrigation treatments on that date caused by 50 mm rainfall over the previous two weeks (Figure 4.7). The model was not a negative relationship as expected because it was not driven by crop water deficit stress but more likely caused by differences in soil texture near saturated conditions. The relationship was negative at 1356 heat units on August 18 ($R^2 = 0.4$) when the soil was drier and there was a greater range in VWC (0.24 to 0.42). There were not any other significant relationships at 15 cm deep. For VWC at 30 cm, there was only one significant relationship on July 3 ($R^2 = 0.47$), which had a slightly positive regression coefficient. As the model did not have a negative slope as expected, this was not likely related to crop water stress. Results may have been clearer if tensiometers were used as such measurements are tied more directly to plant water stress (Irmak et al., 2000) than VWC and would be sensitive to the effects of soil physical properties such as texture (Sui et al., 2012). However, thermal imagery could likely be paired with soil moisture tension data from wireless sensor networks to better quantify soil moisture and crop water status together.

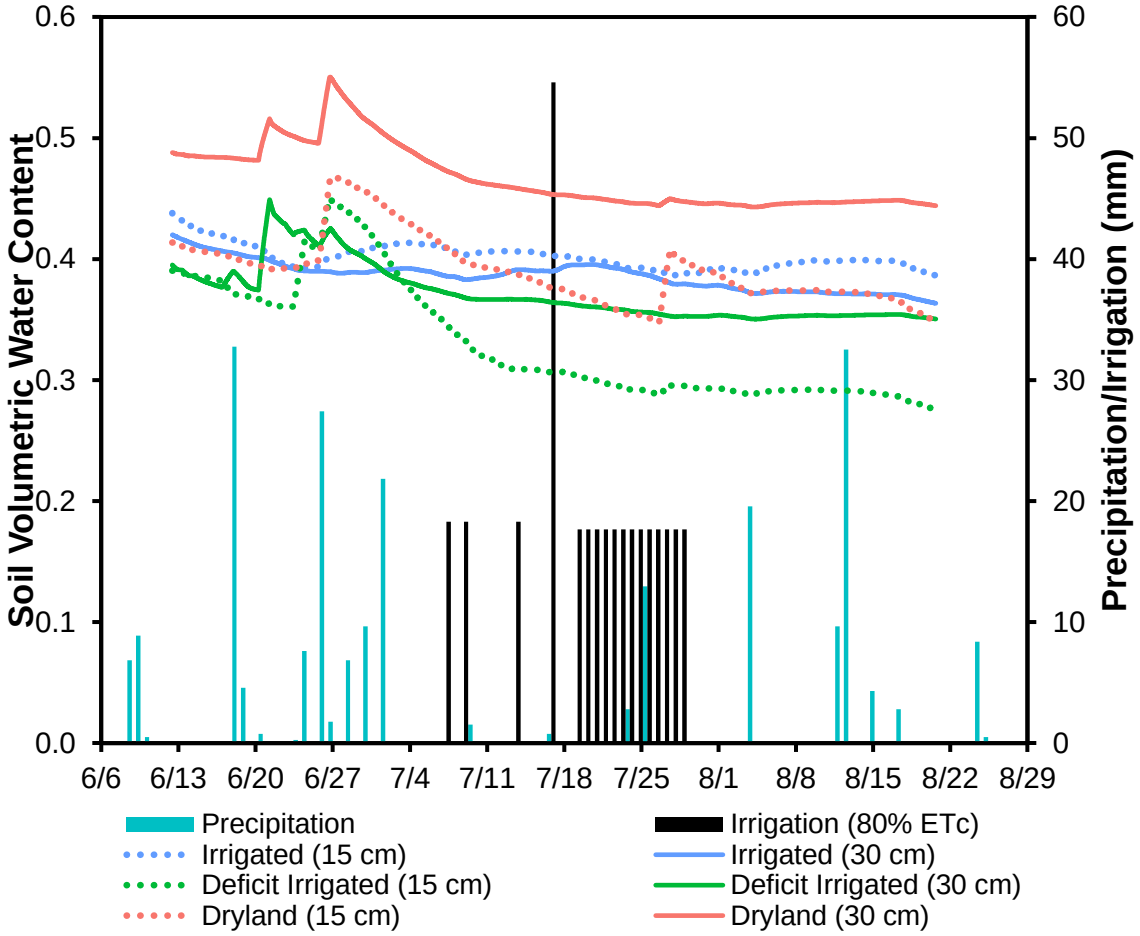

Figure 4.7. Daily precipitation and 80% ET_c irrigation amounts during the 2019 cotton growing season. Lines and dashed lines represent soil volumetric water content within each irrigation treatment.

4.4. Conclusions

Bare soil background was accurately excluded in UAS-derived thermal infrared orthomosaics using a simple threshold method without the need for ancillary imagery, and average canopy temperatures could be calculated for irrigation treatments and cotton cultivars. Canopy temperature was reliable for in-season irrigation treatment mean comparisons, providing similar results to cotton yield data while indicating more subtle

differences between cultivars that could be further explored. For example, labor-intensive data collection such as plant gas exchange measurements could be targeted only for cultivars of interest identified by canopy temperature. Cultivars with lower canopy temperatures generally had higher cotton yields with exceptions likely caused by differences in the cultivar's capacity for recovering from heat or water deficit stress. There was a linear relationship between UAS-derived canopy temperature and seed cotton yield which ranged from weak to strong. Canopy temperature was generally correlated with VWC, but results suggest that single time point VWC measurements are not always representative of crop water status and should not be used alone but rather incorporated into broader irrigation management strategies. For example, thermal imagery could potentially be calibrated using georeferenced wireless soil moisture sensor networks for timely, high-resolution maps of soil moisture and crop water status.

4.5. References

Allen, R. G., Pereira, L. S., Raes, D., & Smith, M. (1998). Crop evapotranspiration-Guidelines for computing crop water requirements-*FAO Irrigation and drainage paper 56.*

Andrade-Sanchez, P., Gore, M. A., Heun, J. T., Thorp, K. R., Carmo-Silva, A. E., French, A. N., Salvucci, M. E., & White, J. W. (2013). Development and evaluation of a field-based high-throughput phenotyping platform. *Functional Plant Biology*, 41(1), 68-79. https://doi.org/https://doi.org/10.1071/FP13126

Bai, G., Blecha, S., Ge, Y., Walia, H., & Phansak, P. (2017). Characterizing Wheat Response to Water Limitation Using Multispectral and Thermal Imaging. *Transactions of the ASABE*, 60(5), 1457-1466. https://doi.org/https://doi.org/10.13031/trans.11967

Bai, G., Ge, Y., Hussain, W., Baenziger, P. S., & Graef, G. (2016). A multi-sensor system for high throughput field phenotyping in soybean and wheat breeding. *Computers and Electronics in Agriculture*, 128, 181-192.

Baker, J. T., Gitz, D. C., Payton, P., Wanjura, D. F., & Upchurch, D. R. (2007). Using Leaf Gas Exchange to Quantify Drought in Cotton Irrigated Based on Canopy Temperature Measurements. *Agronomy Journal*, 99(3), 637-644. https://doi.org/https://doi.org/10.2134/agronj2006.0062

Burke, J. J., & Upchurch, D. R. (1989). Leaf temperature and transpirational control in cotton. *Environmental and experimental botany*, 29(4), 487-492.

Clarke, T. R. (1997). An empirical approach for detecting crop water stress using multispectral airborne sensors. *HortTechnology*, 7(1), 9-16.

Clarke, T. R., Moran, M. S., Barnes, E., Pinter, P., & Qi, J. (2001). Planar domain indices: A method for measuring a quality of a single component in two-component pixels. *IGARSS 2001. Scanning the Present and Resolving the Future. Proceedings. IEEE 2001 International Geoscience and Remote Sensing Symposium* (Cat. No. 01CH37217),

Cohen, Y., Alchanatis, V., Meron, M., Saranga, Y., & Tsipris, J. (2005). Estimation of leaf water potential by thermal imagery and spatial analysis. *J Exp Bot*, 56(417), 1843-1852. https://doi.org/10.1093/jxb/eri174

Colaizzi, P. D., O'Shaughnessy, S. A., Evett, S. R., & Howell, T. A. (2012). Using canopy temperature to improve irrigated crop management. Publications from USDA-ARS / UNL Faculty. https://digitalcommons.unl.edu/usdaarsfacpub/1820

Colaizzi, P. D., O'Shaughnessy, S. A., Evett, S. R., & Mounce, R. B. (2017). Crop evapotranspiration calculation using infrared thermometers aboard center pivots. *Agricultural Water Management*, 187, 173-189. https://doi.org/https://doi.org/10.1016/j.agwat.2017.03.016

Drew, P. L., Sudduth, K. A., Sadler, E. J., & Thompson, A. L. (2019). Development of a multi-band sensor for crop temperature measurement. *Computers and Electronics in Agriculture*, 162, 269-280. https://doi.org/10.1016/j.compag.2019.04.007

Gan, H., Lee, W. S., Alchanatis, V., Ehsani, R., & Schueller, J. K. (2018). Immature green citrus fruit detection using color and thermal images. *Computers and*

Electronics in Agriculture, 152, 117-125. https://doi.org/https://doi.org/10.1016/j.compag.2018.07.011

Ge, Y., Bai, G., Stoerger, V., & Schnable, J. C. (2016). Temporal dynamics of maize plant growth, water use, and leaf water content using automated high throughput RGB and hyperspectral imaging. *Computers and Electronics in Agriculture*, 127, 625-632. https://doi.org/https://doi.org/10.1016/j.compag.2016.07.028

Han, X., Thomasson, J. A., Swaminathan, V., Wang, T., Siegfried, J., Raman, R., Rajan, N., & Neely, H. (2020). Field-Based Calibration of Unmanned Aerial Vehicle Thermal Infrared Imagery with Temperature-Controlled References. *Sensors*, 20(24), 7098. https://www.mdpi.com/1424-8220/20/24/7098

Heilman, J., Heilman, W., & Moore, D. (1981). Remote Sensing of Canopy Temperature at Incomplete Cover. *Agronomy Journal*, 73(3), 403-406.

Huang, J., Scudiero, E., Choo, H., Corwin, D. L., & Triantafilis, J. (2016). Mapping soil moisture across an irrigated field using electromagnetic conductivity imaging. *Agricultural Water Management*, 163, 285-294. https://doi.org/https://doi.org/10.1016/j.agwat.2015.09.003

Ihuoma, S. O., & Madramootoo, C. A. (2017). Recent advances in crop water stress detection. *Computers and Electronics in Agriculture*, 141, 267-275. https://doi.org/10.1016/j.compag.2017.07.026

Irmak, S., Haman, D. Z., & Bastug, R. (2000). Determination of crop water stress index for irrigation timing and yield estimation of corn. *Agronomy Journal*, 92(6), 1221-1227.

Ishimwe, R., Abutaleb, K., & Ahmed, F. (2014). Applications of Thermal Imaging in Agriculture—A Review. *Advances in Remote Sensing*, 03(03), 128-140. https://doi.org/10.4236/ars.2014.33011

Jackson, R. D., Idso, S., Reginato, R., & Pinter Jr, P. (1981). Canopy temperature as a crop water stress indicator. *Water resources research*, 17(4), 1133-1138.

Kamara, L., Zartman, R., & Ramsey, R. (1991). Cotton-root distribution as a function of trickle irrigation emitter depth. *Irrigation Science*, 12(3), 141-144.

Kassambara, A. (2021). ggpubr: 'ggplot2' Based Publication Ready Plots. In https://CRAN.R-project.org/package=ggpubr

Khanal, S., Fulton, J., & Shearer, S. (2017). An overview of current and potential applications of thermal remote sensing in precision agriculture. *Computers and Electronics in Agriculture*, 139, 22-32. https://doi.org/10.1016/j.compag.2017.05.001

Lumley, T., & Miller, A. (2020). leaps: Regression Subset Selection. In https://CRAN.R-project.org/package=leaps

McBratney, A. B., Minasny, B., & Whelan, B. M. (2005). Obtaining 'useful'high-resolution soil data from proximally-sensed electrical conductivity/resistivity (PSEC/R) surveys. *Precision Agriculture*, 5, 503-510.

Menefee, D., Rajan, N., Cui, S., Bagavathiannan, M., Schnell, R., & West, J. (2020). Carbon exchange of a dryland cotton field and its relationship with PlanetScope remote sensing data. *Agricultural and Forest Meteorology*, 294. https://doi.org/10.1016/j.agrformet.2020.108130

Moran, M., Clarke, T., Inoue, Y., & Vidal, A. (1994). Estimating crop water deficit using the relation between surface-air temperature and spectral vegetation index. *Remote sensing of environment*, 49(3), 246-263.

Nielsen-Gammon, J. W., Banner, J. L., Cook, B. I., Tremaine, D. M., Wong, C. I., Mace, R. E., Gao, H., Yang, Z. L., Gonzalez, M. F., Hoffpauir, R., Gooch, T., & Kloesel, K. (2020). Unprecedented Drought Challenges for Texas Water Resources in a Changing Climate: What Do Researchers and Stakeholders Need to Know? *Earth's Future*, 8(8). https://doi.org/10.1029/2020ef001552

O'Shaughnessy, S. A., & Evett, S. R. (2010). Canopy temperature based system effectively schedules and controls center pivot irrigation of cotton. *Agricultural Water Management*, 97(9), 1310-1316. https://doi.org/https://doi.org/10.1016/j.agwat.2010.03.012

O'Shaughnessy, S. A., Evett, S. R., Colaizzi, P. D., & Howell, T. A. (2011). Using radiation thermography and thermometry to evaluate crop water stress in soybean and cotton. *Agricultural Water Management*, 98(10), 1523-1535. https://doi.org/10.1016/j.agwat.2011.05.005

O'Shaughnessy, S. A., Evett, S. R., Colaizzi, P. D., & Howell, T. A. (2012). A crop water stress index and time threshold for automatic irrigation scheduling of grain sorghum. *Agricultural Water Management*, 107, 122-132. https://doi.org/https://doi.org/10.1016/j.agwat.2012.01.018

Oosterhuis, D. M. (1990). Growth and Development of a Cotton Plant (W. N. Miley & D. M. Oosterhuis, Eds.). https://doi.org/https://doi.org/10.2134/1990.nitrogennutritionofcotton.c1

Padhi, J., Misra, R. K., & Payero, J. O. (2012). Estimation of soil water deficit in an irrigated cotton field with infrared thermography. *Field crops research*, 126, 45-55. https://doi.org/10.1016/j.fcr.2011.09.015

Pinter, J. P. J., Hatfield, J. L., Schepers, J. S., Barnes, E. M., Moran, M. S., Daughtry, C. S. T., & Upchurch, D. R. (2003). Remote Sensing for Crop Management. *Photogrammetric Engineering & Remote Sensing*, 69(6), 647-664. https://doi.org/10.14358/PERS.69.6.647

R Core Team. (2021). R: A Language and Environment for Statistical Computing. In R Foundation for Statistical Computing. https://www.R-project.org/

Ritchie, G. L., Bednarz, C. W., Jost, P. H., & Brown, S. M. (2007). Cotton growth and development.

Soil Survey Staff. (2021). Soil Survey Geographic (SSURGO) Database. Natural Resources Conservation Service, United States Department of Agriculture.

Sudduth, K. A., Drummond, S. T., & Kitchen, N. R. (2001). Accuracy issues in electromagnetic induction sensing of soil electrical conductivity for precision agriculture. *Computers and Electronics in Agriculture*, 31(3), 239-264. https://doi.org/https://doi.org/10.1016/S0168-1699(00)00185-X

Sui, R., K. Fisher, D., & M. Barnes, E. (2012). Soil Moisture and Plant Canopy Temperature Sensing for Irrigation Application in Cotton. *Journal of Agricultural Science*, 4(12). https://doi.org/10.5539/jas.v4n12p93

Sullivan, D., Fulton, J., Shaw, J., & Bland, G. (2007). Evaluating the sensitivity of an unmanned thermal infrared aerial system to detect water stress in a cotton canopy. *Transactions of the ASABE*, 50(6), 1963-1969.

Taiz, L., Zeiger, E., Moller, I. M., & Murphy, A. (2015). Plant Physiology and Development (6 ed.). Sinauer Associates, Inc.

Thompson, C. N., Mills, C., Pabuayon, I. L. B., & Ritchie, G. L. (2020). Time-based remote sensing yield estimates of cotton in water-limiting environments. *Agronomy Journal*, 112(2), 975-984. https://doi.org/10.1002/agj2.20126

Thorp, K., Thompson, A., Harders, S., French, A., & Ward, R. (2018). High-Throughput Phenotyping of Crop Water Use Efficiency via Multispectral Drone Imagery and a Daily Soil Water Balance Model. *Remote Sensing*, *10*(11). https://doi.org/10.3390/rs10111682

Virnodkar, S. S., Pachghare, V. K., Patil, V. C., & Jha, S. K. (2020). Remote sensing and machine learning for crop water stress determination in various crops: a critical review. *Precision Agriculture*, 21(5), 1121-1155. https://doi.org/10.1007/s11119-020-09711-9

Wanjura, D., Kelly, C., Wendt, C., & Hatfield, J. (1984). Canopy temperature and water stress of cotton crops with complete and partial ground cover. *Irrigation Science*, 5(1), 37-46.

Wickham, H. (2009). ggplot2: Elegant Graphics for Data Analysis. In Springer-Verlag New York. http://ggplot2.org

5. CONCLUSIONS

The relationship between UAS-derived vegetation indices and cotton yield across irrigation treatments was explored over time and accumulated heat units were investigated as a physiological basis for optimal timing of UAS flights for in-season yield predictions. There were strong positive linear relationships between vegetation indices and yield. NDVI produced better linear regression models than NDRE for all years except 2017, which suggests that NDVI is more suitable for quantifying yield in cotton. Except for the dryland treatment, models split by irrigation level were weaker than when pooled across irrigation levels. Results indicated that the optimal in-season timing was during the bloom period around 1200 accumulated heat units. Dryland yield for 2020 was estimated with fair accuracy from the previous two years of NDVI data captured closest to 1200 heat units. Furthermore, NDVI was sufficient for irrigation treatment comparisons with statistical results that were comparable to observed yield. UAS-derived NDVI could be useful during beginning stages of pedigree selection as a simple tool for cotton breeders to eliminate lines with poor performance ahead of labor-intensive data collection efforts such as boll sampling and fiber quality analysis. NDVI could also act as a reserve dataset for potential yield based on historical data for insurance claims when crop losses occur.

Boll Area index, which was derived from a pixel-based classification of cotton bolls in multispectral imagery, was sufficient for comparison of irrigation treatment means, delivering statistical results similar to observed cotton yield. BAI had strong

positive linear relationships with cotton yield. Incorporating BAI, vegetation indices, and canopy temperature in multiple linear regression models for yield estimation considerably reduced error. Yield for 2020 was estimated with fair accuracy using the multiple regression model generated from the previous two years of BAI combined with NDVI data captured during the bloom period. This methodology has potential to save time for cotton breeders during early stages of pedigree selection by excluding the worst performing lines before harvest and other labor-intensive data collection endeavors. Nevertheless, results suggest that it may not provide adequate accuracy for assessment of advanced lines later in the selection process. Multispectral UAS imagery from just two flight dates, one timed during bloom and another after defoliation, together provided better yield estimates than previous work which relied on RGB imagery after defoliation.

Unmanned aerial infrared thermography was evaluated for comparing crop water deficit stress across irrigation treatments and commercial cotton cultivars, the relationship between cotton yield and canopy temperature derived from UAS was explored, and the relationship between canopy temperature and soil volumetric water content was examined. Accurately removing bare soil background from the high spatial resolution thermal orthomosaics was possible without secondary multispectral or RGB imagery. Average canopy temperature could be derived for both irrigation treatments and cotton cultivars for in-season pairwise mean comparisons, and it produced statistical results comparable to observed yield data. Canopy temperature also indicated potential differences between cultivars that could warrant further exploration, and such results could help constrain labor-intensive data collection efforts such as plant gas exchange

measurements only to cultivars identified as important by canopy temperature. The linear relationship between cotton yield and canopy temperature ranged from weak to strong. Soil volumetric water content did not have consistently strong relationships with canopy temperature. Results suggest that volumetric water content observations alone are not always indicative of water deficit stress and ideally should be considered alongside data such soil moisture tension which would be more representative of crop water status.

Overall, UAS remote sensing has demonstrated potential as an efficient source for collection of multispectral and thermal infrared imagery, which are valuable for quantifying variability of crop yield and other important traits for high-throughput phenotyping purposes and precision agriculture analytics. Further investigation is warranted to determine the most economical UAS flight heights for collecting imagery intended for crop research and production purposes. Finally, scientists and agronomists should continue to improve the methodologies for analyzing and leveraging such imagery to its full potential as a means for improving crop production efficiency.